Oxidised Cellulose Gels and Films for Encapsulation and Release

Celebi, Duygu

Award date:
2015

Awarding institution:
University of Bath

Oxidised Cellulose Gels and Films for Encapsulation and Release

Duygu Çelebi

A thesis submitted for the degree of Doctor of Philosophy

University of Bath Chemistry Department

May 2015

Babaanneme ve anneanneme..

Acknowledgement

Firstly, I would like to thank all my supervisors Prof. Karen J. Edler, Dr Janet L. Scott, Prof. Richard Guy and Dr Gianfranco Unali in Unilever for their support throughout these years. Undertaking this PhD has truly been an unforgettable experience in my life and thanks to the people around me, I now came to the end of this journey. Prof Karen J. Edler, thank you for all your support and trust in me. I admired the fact you were always available if I had any questions and always tried to create time to meet up. Your input in this thesis has been invaluable. Dr Janet L. Scott you were always encouraging me and the other DTC students to try new techniques, learn new skills and visit different countries- if there was a conference, even better! Thank you for teaching us to be open minded. You were always honest and constructive with your comments for which am grateful. Prof Richard H. Guy, thank you for teaching me more about drug delivery which was a new subject for me. I always enjoyed our insightful discussions. You were always positive and encouraging. Dr. Gianfranco Unali, I spent a month in the Unilever research facilities with you. The experience opened my eyes for the industrial environment which also now shaped my future career. Thank you for the great advice and mentoring during my internship and throughout my studies.

My PhD has been a remarkable part of my life. I matured and learned a lot during these last four years both academically and personally. I also met my soul mate and future husband here in Bath, Jose Fernandez who never stopped believing in me and supported me all the way, put up with all my grumpiness throughout these years. Thank you canim. Dr Gavin Hazell, your friendship was invaluable throughout this journey. We had our ups and downs together but managed to stay positive. I made a friend for life. Dr Ilaria Idini, you have always been there to pick me up when I was down. You were always so thoughtful, so kind to everyone else in our group. Everyone needs a friend like you. Dr Amani El Fagui, we made the connection the moment we met. I don't think we ever had a conversation without a laugh. You have been so supportive throughout my PhD and gave me constructive advice. Cecillia, you are the most positive person I have ever met in my life. Always stay this way.

Also to the special women I met during my PhD: Tulay Gulsen, Begum Kurkcu and Viviana Ramirez. Thank you all for putting up with me and being such amazing friends. We had a great time together and I will deeply miss those days.

Last but not least, mum, you never stopped believing in me. Your love was always there whenever I needed it. Dad, you always wanted me to become a doctor and wear those funny graduations gowns, so here you go! Brother, you were always there to listen my moaning and make me laugh. I love you all and am ever so grateful for all your moral support throughout these years.

Abstract

Aqueous formulations are essential components of personal care products such as shampoos, creams and gels for pharmaceutical products and paints and drilling lubricants.[1] The majority of these products mainly contain polymeric thickeners or additives such as surfactants to modify their rheology. These materials are however derived from non-renewable resources. TEMPO-oxidised cellulose nanofibrils (TOCN) could provide a desired alternative for such thickeners. TOCN is a non-toxic, renewable and non-irritating material which gels aqueous and alcohol based formulations and forms films on surfaces, such as skin. This also offers opportunities in delivery of active pharmaceutical compounds via the skin. The previous studies suggested that even at low concentrations of additives (surfactants and salts) TOCN could form shear thinning gels. However, this mechanism is not fully understood. It is thought that it is mainly due to the charge shielding effect and depletion flocculation mechanism. The aim of this work was to further our understanding on this mechanism.

TOCN gels in the presence of low molecular weight alcohols (methanol, ethanol and propan-1-ol) and TOCN films were developed in an attempt to understand the interaction between these additives and TOCN in a formulation and once applied to the skin. The work included many advanced techniques including small angle X-ray and neutron scattering and reflectivity. The transdermal delivery of ibuprofen across the skin/membrane from TOCN gels as well as the commercial gels was investigated for the final part of this study. This work involved determining the amount of drug penetrated across the skin/membrane using Franz diffusion cells and tape-stripping method.

Overall, the thesis has provided an insight on the changes of the fibril aggregation in different alcohol systems and the interaction of TOCN with the surfactants and salts. Due to its ability to thicken formulations, TOCN may be of use in many applications including personal care products and alcohol sanitisers. This role could also be extended for use in pharmaceutical gel formulations for transdermal drug delivery.

Table of Contents

List of Figures

List of Tables

Abbreviations

Symbol	Definition
AFM	Atomic Force MicroscopyActive Pharmaceutical Ingredient
APS	Active Pharmaceutical Ingredient
CAC	Critical Aggregation Concentration
CB	Cellulose Beads
$C_{12}E_6$	Hexaethylene monododecyl ether
CMC	Critical Micelle Concentration
C_{16}TAB	Hexadecyl trimethyl ammonium bromide
D_2O	Deuterated water
DTAB	Dodecyltrimethylammonium bromide
GI	Gastrointestinal
HPLC	High-Performance Liquid Chromatography
H_2SO_4	Sulfuric acid
IBU	Ibuprofen
ILL	Institut Laue-Langevin, Grenoble, France
I07	X-ray Reflectometer, Diamond, UK
LB	Langmuir-Blodget
LOQ	SANS Instrument, ISIS, UK
MFC	Microfibrillated Cellulose
MTM	Montmorillonite
NaBr	Sodium bromide
NaCl	Sodium chloride
NaClO	Sodium hypochlorite
NFC	Nanofibrillated Cellulose
NR	Neutron Reflectivity
OFFSPEC	Neutron Reflectometer, ISIS, UK
PAM	Poly(acrylamide)
PVA	Poly(vinyl alcohol)
SANS	Small Angle Neutron Scattering
SAXS	Small Angle X-ray Scattering
SC	Stratum Corneum
SDS	Sodium dodecyl sulfate
SEM	Scanning Electron Microscope
SLS	Sodium lauryl sulfate
TDS	Trandermal Drug Delivery
TEM	Transmission Electron Microscopy
TEMPO	2,2,6,6-tetramethylpiperidine-1-oxy radical
TEWL	Transepidermal Water Loss
TMSC	Trimethylsilyl cellulose
TOCN	TEMPO-Oxidised Cellulose Nanofibril
VE	Viable Epidermis
XRR	X-ray Reflectivity

1. Introduction

The work presented in this chapter gives an overview of nanocellulose (TOCN in specific) and its applications based on the current literature. The theory behind the fundamental colloid science and techniques will also be discussed.

The second chapter comprises theory of scattering techniques, the method followed to create formulations of hydroalcoholic TOCN gels with and without sodium dodecyl sulfate (SDS) and sodium chloride (NaCl). The changes in fibrillar aggregation were examined by means of small angle X-ray and neutron scattering (SAXS, SANS). The physical changes of the gels were characterised by gravimetric analysis and rheology.

The third chapter focuses on understanding the interactions of the same additives from the perspective of films formed by TOCN which resembles the thin film formed once the formulation is applied to the skin. The techniques used for this part of the thesis include X-ray and neutron reflectivity (XRR, NR) and the pre-characterisation of the films were done by atomic force microscopy (AFM). The first two results chapters were part of product development and characterisation of TOCN gels and films.

The final and the third chapter of the results was on the application of hydroalcoholic TOCN gels to the skin. The selected hydroalcoholic TOCN gels were loaded with ibuprofen. The ability of these formulations to deliver the active ingredient across the skin both *in-vivo* (human volunteers) and *in-vitro* (abdominal pig skin, silicone membrane) experiments were investigated. The TOCN gels were compared to commercial gels available in the market. Franz diffusion cells and tape-stripping were the methods used to obtain the results. The analytical technique used was high-performance liquid chromatography (HPLC).

Overall, the project began with formulation, followed by optimisation and in the end was completed with the application of the formulation to the skin.

1.1 Cellulose

Cellulose which was first isolated by Payen[2], is the most abundant polymer on Earth found in plant-based materials such as wood, cotton but also synthesised by algae, tunicate and bacteria.[3–6] It is a polysaccharide made from repeated units of D-glucopyranose units linked by 1,4-β glycoside bonds (Figure 1).[7,8]

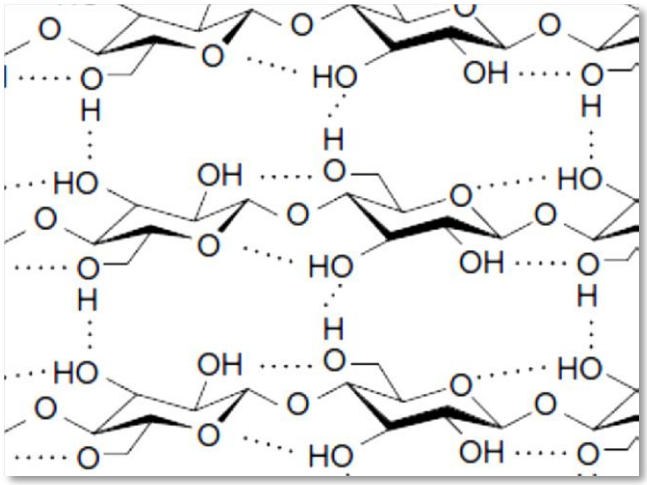

Figure 1: Structure of cellulose, adapted from reference 8.

Cellulose is the main component of a plant cell wall and is a system of fibrils. A single plant fibre is similar to microscopic tube with a length from 1 to 50 mm and diameter around 10-50 µm.[8] The fibre has lamellae in the middle and surrounded by a secondary wall which has three layers. The cell walls are made up of semi-crystalline microfibrils embedded in them.[9] Figure 2 illustrates the arrangement of the plant cell wall and the microfibrillar system.

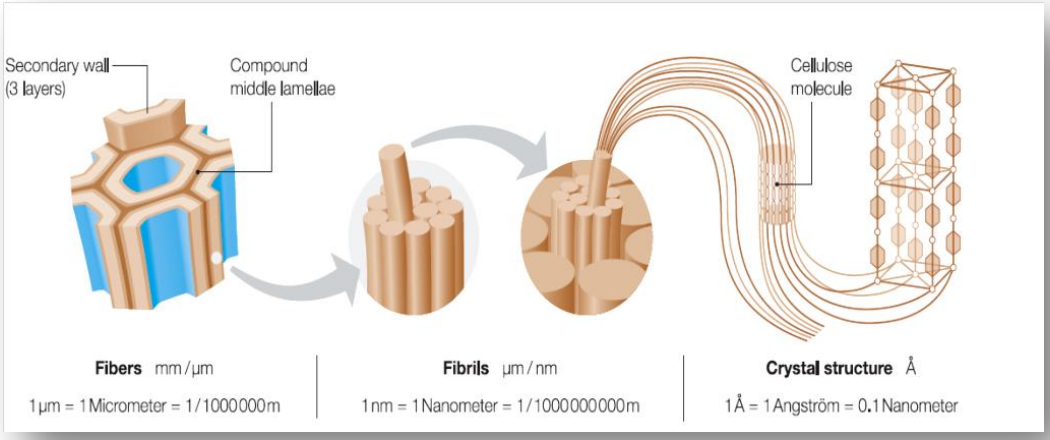

Figure 2: A diagram showing the components of a cell wall and arrangements of microfibrils cellulose, reproduced with permission from reference 9.

The cellulose fibres consist of amorphous and crystalline domains and the latter depends on the origins of the material. The cellulosic resources comprise cotton, wood pulp, agricultural by-products (e.g. soy hulls, corncob, rice husk) and animal sources, including tunicates and bacteria.[10] The crystallinity is a consequence of hydrogen bonding between the cellulosic chains. The fibres have many hydroxyl groups for interaction with water by hydrogen bonding and this is not limited at the surface, but also true in bulk. All the hydroxyl groups of amorphous phase interact with water, however only a small amount of water is in contact with the hydroxyl groups on the surface of crystalline phase.[11]

1.2 Fibrillated Cellulose

In order to maximise the potential use of the fibrils and hence to increase the surface area, it is essential to break down the bigger fragmentation of the cellulose fibres into individual fibrils.[9] This is often referred as *fibrillation* which enhances the interaction between the fibres as well as the contact with other compounds and therefore facilitates their use in wide range of applications.

The extraction of nanofiber from wood was first demonstrated by Herrick *et al*. and Turbak *et al.* in 1983 [12,13] when they used a cyclic mechanical treatment with high-pressure homogeniser to produce microfibrilliated cellulose (MFC). MFC consists of

nanofibrils as well as fibres and fibre fragments, hence the fibrils tend to be much bigger in size in comparison to nanofibrillated cellulose (NFC) which in turn affects the application of different cellulose fibrils.[14] The energy consumption by mechanical disintegration of the fibres often requires high energy when used on its own however, this could be overcome if combined with chemical or enzymatic pre-treatments and therefore enabling its application in films, nanofibre-reinforced composites, gas-barrier films, cosmetics, flame resistant and high-tech materials.[4,15]

The production of NFC and their potential application in composite materials has considerably increased in the recent years due their high strength, low weight and biodegradability.[4] Moreover, materials made from nanocellulose are especially of commercial interest as they can often be obtained from waste produced from pulp and paper industry, therefore not a threat for food supplies.[1]

The chemistry assisted fibrillation of cellulose can be categorised as [16] : (1) cellulose nanocrystals or cellulose nanowhiskers prepared by acid hydrolysis of native celluloses and successive mechanical agitation [17–20]; (2) microfibrillated cellulose (MFC) prepared by mechanical disintegration of cellulose/water slurries by partial carboxymethylation[6,12,13,21,22]; (3) cellulose nanofibrils prepared by 2,2,6,6-tetramethylpiperidine-1-oxy radical (TEMPO)-mediated oxidation of native celluloses followed by mechanical disintegration of the oxidised cellulose in water .[15,23–26] In comparison to other types of nanocellulose, TEMPO-oxidised cellulose fibrils (TOCN) has the advantage of having the most uniform fibril widths of 3-4 nm and ability to be dispersed in organic media as individual fibrils due the functionalised surface groups. The morphology and the properties of the cellulose fibrils depend on the original source of the cellulose as well as the extraction technique and the conditions.

1.3 TEMPO- Oxidised Cellulose Nanofibrils (TOCN)

1.3.1 Chemistry and Mechanism

A high energy input is often necessary to convert bulk fibres to nanofibres owing to inter-fibrillar hydrogen bonds.[15] One alternative to minimise the energy consumption is the pre-treatment of cellulose. One of the most common chemical treatments of cellulose is the introduction of groups by acid hydrolysis with 64% H_2SO_4, at 45℃ for 1-4 hours.[15] The TEMPO oxidation of cellulose fibres is a selective process rather than full oxidation of the cellulose, since when all the primary alcohol groups in cellulose are oxidised, it becomes soluble in aqueous media. The oxidation of all the primary groups is also relatively energy intensive and therefore a costly process, hence the selective oxidation is the preferred method for the fibrillation.[27]

The selective oxidation of polysaccharides has been a subject of research since early 1940s.[8,9] However, the traditional technique of using nitrite in phosphoric acid was reviewed and improved by de Nooy *et al*.[30] He and his group reported the oxidation of polysaccharides by the stable TEMPO radical and hypochlorite as the main oxidant. They concluded that selectivity of the oxidation of the primary hydroxyl groups was around 98%. This method was mainly used for water soluble polysaccharides such as starch, pullulan, amylopectin, chitosan, but was later implemented for water-insoluble compounds such as cellulose, chitin and amylase.[25,31–34]

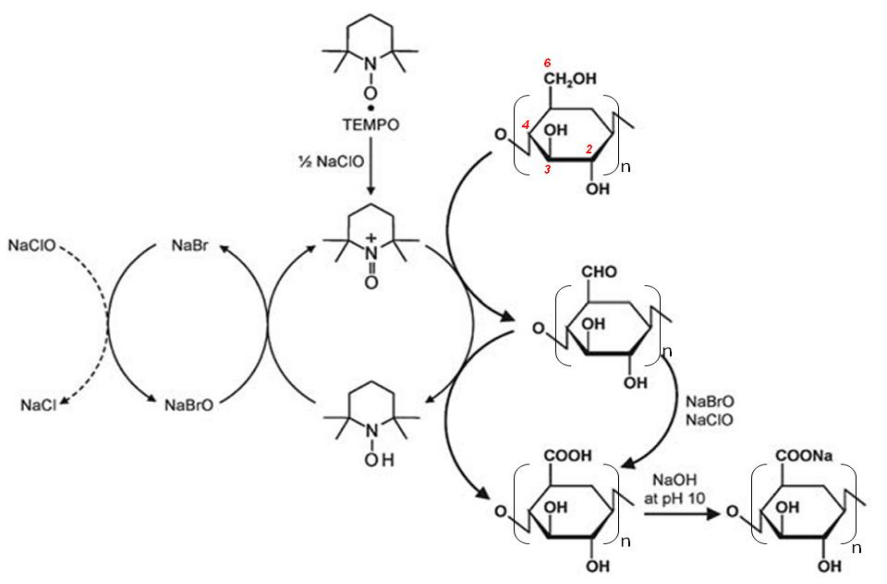

Figure 3: TEMPO-mediated oxidation of cellulose, reproduced with permission from reference 15.

Isogai *et al.*[15] performed this reaction by using catalytic amounts of TEMPO and NaBr which were dissolved at pH 10-11 and the oxidation commenced by addition of NaClO solution as the primary oxidant. This resulted in oxidation of C6 primary hydroxyl groups to carboxylate groups. The level of oxidation was monitored by following the NaOH consumption which was used to keep the pH level at 10 during the oxidation, although care had to be taken as this method followed decomposition of NaClO and so may result in overestimation of the degree of oxidation if unproductive decomposition of NaClO occurs.[15] Figure 3 shows the mechanism for the TEMPO-mediated oxidation of cellulose. This chemical pre-treatment also enhances separation of individual microfibrils by the addition of negatively charged COO^- groups on the surface of the fibrils causing repulsion of the fibrils.[31]

Saito *et al.*[31] reported that native cellulose fibres were successfully disintegrated by TEMPO mediated oxidation when never-dried cellulose was used.

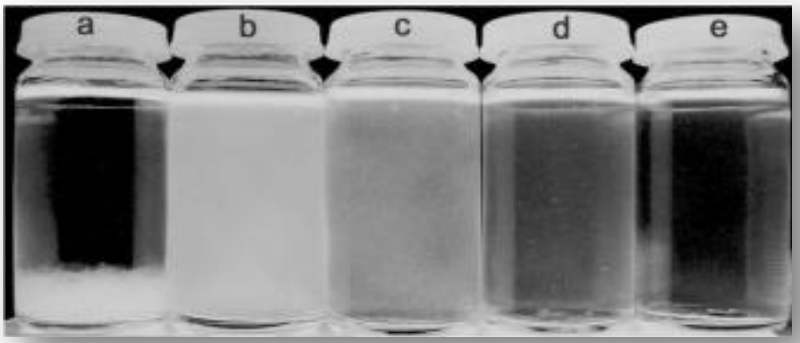

Figure 4: Photograph of 0.1% bleached sulfite wood pulp suspensions after TEMPO-mediated oxidation with various concentrations of NaClO per gram of cellulose: a) 0, b) 1.3, c) 2.5, and d) 3.8 mmol e) supernatant of suspension c) after centrifugation at 12 000 rpm for 30 min, reproduced with permission from reference 31.

Figure 4 shows the cellulose suspensions resulting from pulps subjected to different degrees of oxidation and the supernatant after centrifugation. More light scattering is observed when the wavelength is closer to the diameter of the particles in the suspension. When suspended fibrils or rods have cross-sectional diameter less than the wavelength of the incident light, the light scattering is directly proportional to the mass/length ratio of the fibrils or the cross section area.[31,35] Therefore, as the fibrils are further oxidised resulting in reduction in fibril sizes, the suspension becomes more and more transparent. Saito *et al.*[31] showed that unoxidised microfibrils did not disintegrate if only mechanically treated; therefore the TEMPO-mediated oxidation evidently enhanced the separation of microfibrils. The weakening of the adhesion between the microfibrils and electrostatic repulsion were suggested as the reason for this behaviour. The long length of the fibrils enables them to form networked structures which have the same crystallinity as the original cellulose and able to form stable dispersions.[24] The individual fibrils of TOCN can be seen in Figure 5.

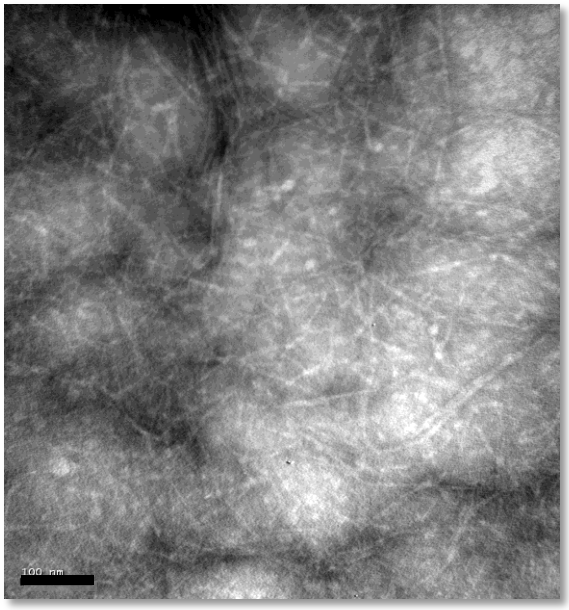

Figure 5: Transmission electron microscopy (TEM) images of individual TOCN fibrils, scale bar is 100 nm.

1.3.2 Industrial Applications of TOCN

The chemical modification of cellulose via oxidation creates value-added products which can be tailored for use in many applications. [36] It can find use in medical applications commonly as a hemostatic scaffolding material to stop bleeding during surgery.[37–40] The other applications include use in personal care products, pharmaceutical products and as a carrier in agricultural products.[15,24,41] The oxidised cellulose fibers also act as blood clotting agents.[42] TOCN play an important role in paper pulp industry where they can increase the strength properties of the paper.[43,44] Crawford *et al.* also suggested the specific use of TOCN in aqueous formulations as an alternative to polymeric thickener.[1]

1.4 Colloids and Surface Chemistry

TEMPO-oxidised cellulose nanofibrils form a colloidal system when dispersed in a medium. Colloids have one component or more between macroscopic particles and this colloidal system can vary in size from 1 µm to 1 nm. They have very large surface area and therefore the surface effects are extremely important for colloidal dispersions. The dispersions of solid particles can be stabilised in a medium by making changes to the surface chemistry. This can be done by charging the surface or adsorbing molecules on to it.[45] When the continuous phase, the *suspending medium*, is liquid they do not readily sediment and cannot move through dialysis membrane. [46] Colloids systems are used in products of everyday life such as gels, emulsions, foods and coatings. The specific examples of such systems could be listed as milk, ink, paints, blood and mayonnaise. The terms used for colloids are often referred as dispersion, suspension or solution. Dispersion will be used throughout this work where colloids in a medium are accepted as a type of mixture. Suspensions often used for mixtures where dispersed phase particles are bigger than colloidal in size, whereas solution refers to a molecular mixture. [47]

The colloid particles move by Brownian motion, thus they are in contact with each other and ultimately, the balance between the attractive and repulsive forces determines the stability of the dispersion. If the repulsive charges balance the attractive van der Waals forces, then the suspension is stable. On the other, if there are no forces preventing the components of colloids to separate from each other then, they aggregate. If the aggregation is reversible it is called *flocculation*, if not, then it is described as *coagulation*.[45]

The stability of colloids can be better understood by the Derjaguin-Landau-Verwey-Overbeek (DLVO) theory.[45,48,49] The van der Waals forces and electrostatic forces form the basis of this theory. It is possible to determine the stability of suspensions or possibility of flocculation or coagulation that would take place.

Many colloids display charged surfaces from anionic or cationic functional groups which defines their role in specific applications. Natural fibers have negative charges on their surfaces because of the carboxylic acid groups of hemicelluloses and cellulose. Many other polymers used in colloidal systems also bear charges. These

charges could be positive due to cationic groups from polymers with amine groups or metal cations or negative from phosphate , carboxylate groups or sulfate group to name a few. The magnitude and the type of the surface charges are therefore critical to the stability and solubility properties of colloids. The kind and amount of electrolytes, pH and temperature are also key factors in solution properties of charged colloids.

1.4.1 Van der Waals Forces

One of the most important applications of van der Waals forces theory used in colloidal science is to see the effect of ions from an electrolyte solution.[50] Van der Waals forces are product of attractions between electric dipoles of molecules. The interaction between colloidal particles is estimated based on the assumption that the total potential is equal to the sum of the potentials; furthermore, the company of other molecules will not directly affect the interaction between the pairs of molecules.[45]

By integrating the pair potential of molecules in volume dV_1 on particle 1 and dV_2 in particle 2 over the volumes of particles, the interparticle forces between colloids can be calculated (Figure 6).

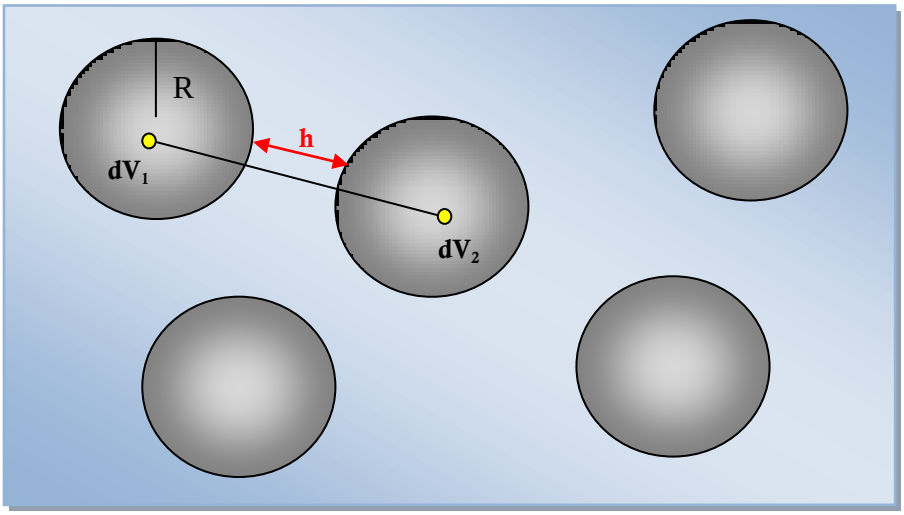

Figure 6: The model for calculating interparticle forces between colloids. dV of particle pairs is integrated, the image was redrawn from reference 45.

Equation (1) defines the potential based on two flat surfaces having *h* distance between them, where A_H is the *Hamaker constant*, which signifies the strength of van der Waals interaction between the particles. This equation is only valid *in vacuum*, therefore if the particles are present in liquid, then the *Hamaker constant* is replaced with a calculated value suggested by Lifshitz *et al.* which is the geometrical average of the *Hamaker constant* for the particle and the medium surrounding it. [45,51]

$$V = \frac{A_H}{12\pi h^2} \quad (1)$$

1.4.2 Electrical Double-Layer Forces

TOCN, like many other colloid particles carry a charge which attracts the ions in the medium they are in. This results in the ions to form a double layer which carry the exact opposite charge to the particle they surround with. The extent of the double layer is given by *1/*κ where κ is the quantity in $(\text{length})^{-1}$ from Debye-Hückel theory and it only depends on the temperature and the concentration of the electrolyte. [52]

*1/*κ is a function of the dielectric constant, *ε*; the universal gas constant, *R*; temperature, *T;* Faraday's constant, F; and the concentration of each ionic species, (*i*) of valence *z* in mol L^{-1} defined as :

$$\frac{1}{\kappa} = \left(\frac{\varepsilon RT}{F^2 \sum c_i z_i}\right)^{1/2} \quad (2)$$

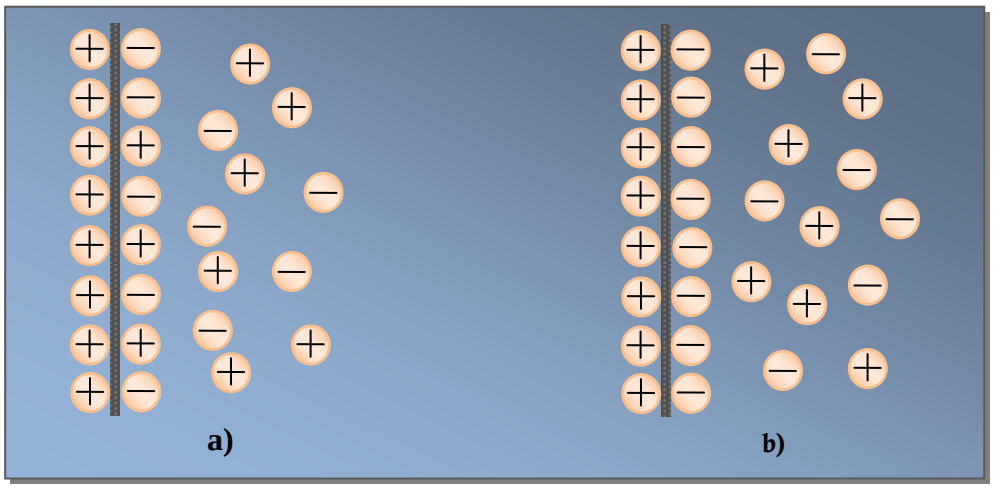

Figure 7: Models for ionic double layer, a) diffuse double layer, b) Stern model, image redrawn from reference 45.

In the diffuse double layer model, closer to the particles, the counterions outweigh due to the electrostatic forces (Figure 7-a). Further away from the particles however, they assemble in a more distributed way as a result of random thermal motion. In the Stern model on the other hand, there is a sharp attraction between the counterions and the particles (Figure 7-b).

The diffuse double layer is explained by the Poisson-Boltzmann equation which connects the electrical potential of particles to the concentration and distribution of the charged particles where the electrical potential is Φ and the concentrations of positive and negative ions can be described as:

$$c_{\mp} = c_0 exp\left(\frac{\mp ze\Phi}{k_B T}\right) \tag{3}$$

where; c_0 is the number density (molar concentration=c_0/N_A) of individual ionic species, z is valence of these ions and e is the basic charge. Subsequently, the excess charge density is:

$$\rho = ze(c_+ - c_-) \tag{4}$$

When this is inserted into Poisson's equation, it is possible to link the potential as a function of distance, *x*, from the charged surface. The *Poisson equation* therefore is:

$$\frac{d^2\Phi}{dx^2} = \frac{\rho}{\varepsilon_r \varepsilon_0} \quad (5)$$

Where, ε_r is the relative permittivity and $\varepsilon_0$is permittivity of the vacuum. The surfaces with similar charges display a repulsive force because of the overlap of the electrical double layers.

1.5 Gel and Film Structure

1.5.1 TOCN Gels

TOCN form clear, shear thinning gels and act as a rheology modifier.[1] The ability to control the rheology of a colloidal system is one of the most important parts of formulation across sectors including personal care and cosmetic, paint, pharmaceutical and agrochemical products. The rheology can be modified to achieve the desired product which would require minimum mixing (minimum use of energy), display stability over a long period of time (no sedimentation) and tuning for ease of application.[53]

The gels formed by polymers can usually absorb the medium they are in and become considerably swollen up to some point. The gels will absorb the water for example by osmotic effect. The water can diffuse into the network of polymers but the polymer network cannot diffuse out. This way, the network acts as a semi-permeable membrane. If the gel is strong enough, then the internal pressure inside the gel is equal to osmotic pressure. If the initial gel formed is not stable, the polymer chains may prefer to form a more stable structure. This leads to increased pressure which gives rise to slow release of the water in the gel, which is known as *syneresis*. This is observed when high concentration of salts is added to the TOCN dispersions.[45] Transparent TOCN gels could be obtained by addition of small concentration of salts or anionic surfactants (Figure 8).[1]

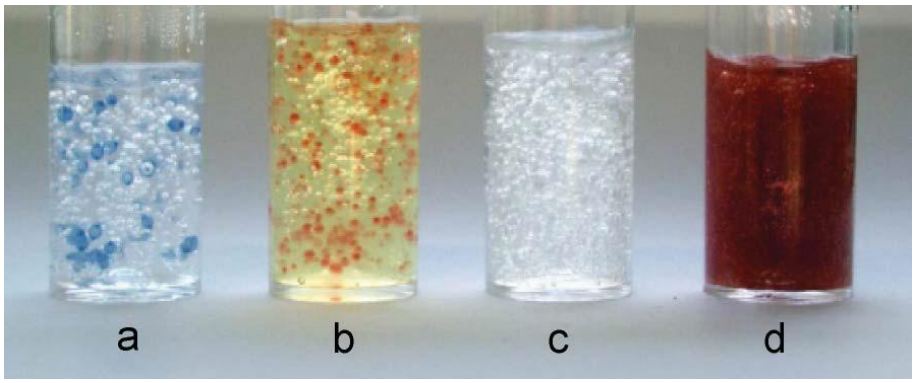

Figure 8: Different formulations of stable surfactant-oxidised cellulose gels prepared with sodium lauryl ether sulfate (SLES) (5 wt%) in an aqueous dispersion of oxidised cellulose (1.3 wt %), first two gels contain microcapsules, a) blue empty and b) orange with perfume; and c) suspended bubbles, and d) red glitter particles, reprinted with permission from reference 1.

Electrostatic repulsion caused by anionic carboxylate groups between the TEMPO-oxidised cellulose fibrils avoids the many interfibrillar hydrogen bonds otherwise present in the wood cell walls. The TOCN gels display excellent characteristics for use in cosmetic formulations. The gels are non-irritant to the skin and have a smooth texture to the touch. Since they are highly shear thinning in nature, they can be applied as sprays and they are also stable at room temperature.[27] It was also suggested that the formation of gels was enhanced by the addition of simple alcohols such as ethanol and propanol.[1]

1.5.1.1 Influence of Surfactants and Salts on TOCN Gels

Salts are found in many products including pharmaceuticals. In fact, many of the pharmaceutically active ingredients (APIs) are simple salts. Hence, it is in our interest to investigate their relationship with TOCN as it was reported that at low salt concentrations (0.05-0.3M), optically clear and continuous gels were formed.[1] Their interaction is another incentive for my research. Fukuzumi *et al.*[54] has recently published work on the effect of electrolytes on TOCN dispersions. They have seen no significant change in the pH of the dispersions ranging from 0-400 mM. The salt had an impact on the TOCN dispersion stability where the nanodispersion of the fibrils was only achieved at concentrations lower than 50 mM (fluidity was lost with

an increase in salt concentration and gels were formed) and over 200 mM aggregates of gel particles started to form. The viscosity of the dispersions was also affected by the increase in the NaCl concentration (Figure 9).

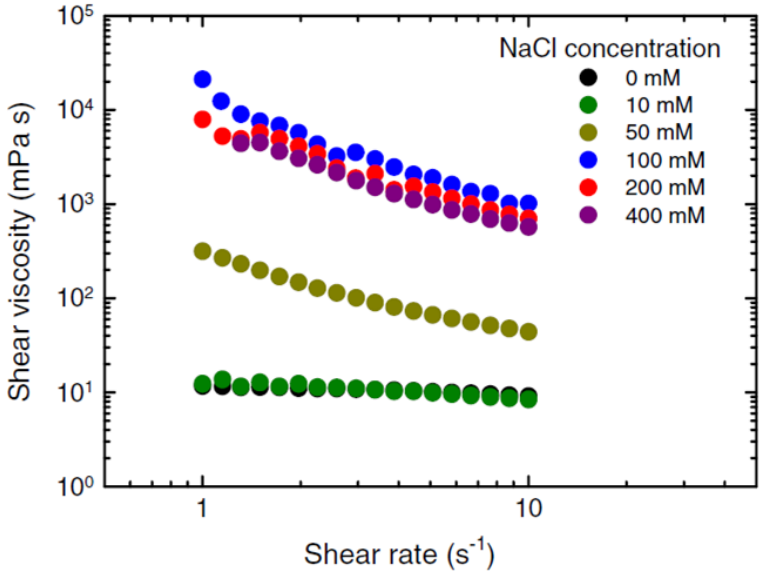

Figure 9: Effect of salt concentration on TOCN dispersion viscosity, reprinted with permission from reference 54.

Polymer/surfactant mixtures found use in a wide range of commercial applications including detergents, paints and paper coatings as well as in food and pharmacy. Such formulations often incorporate low molecular weight surfactant and polymer to contribute to the stability, modify rheology for a specific role. It is therefore important to understand the polymer-surfactant interaction to create the desired formulation.

Surfactants are one of the key components of many formulations and the driving force for them to adsorb at an interface is to lower the free energy of that phase boundary.[55,56] Sodium dodecyl sulfate (SDS), an anionic surfactant, is amongst the most widely used surfactants in such formulations, especially in soaps (Figure 10).The anionic surfactant group is the most popular of all the surfactants used in the industry with production estimated at 10 million tons per year, hence cover 60 % of all the surfactants. The driving force behind such high volume of production is a direct result of ease and low cost manufacture. [56]

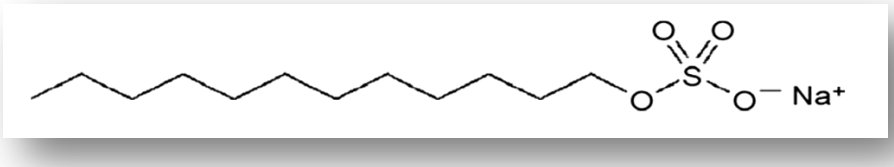

Figure 10: Structure of sodium dodecyl sulfate (SDS)

SDS and similar surfactants can be found in a wide spectrum of personal care and household products including shampoos, skin creams, pharmaceuticals and paint. Although, they enhance viscosity of products, surfactants are generally not derived from environmentally friendly resources. Therefore, it is essential to offer a new alternative thickener derived from a renewable resource which moreover, should not be a threat to food production. TOCN could offer this and be an alternative green thickener for water-based formulations.

When SDS or a similar anionic surfactant, sodium lauryl ether sulfate (SLES) was added to fibril containing aqueous phases, gelation took place at very low concentrations of surfactant, 1-10 wt%, and 2wt% TOCN. [1] This is the ideal combination for a formulation with a lower surfactant yet still able to meet the expectations for a gelled or thickened product. SDS is used in many formulations as an emulsifier, solubilising and stabilising agent. It is also known to increase the permeability of drugs. As an anionic surfactant it interacts with the skin strongly and changes the skin barrier properties.[57] However, it is also known to be a skin irritant. A study carried out by Tsang *et al.*[58] suggested the SDS present in the aqueous cream BP (a popular skin cream used for eczema) is responsible for thickness reduction of the stratum corneum (outermost layer of skin) and increased permeability leading to water loss; hence its use in drug formulations for damaged skin should be reconsidered. It is possible to use less of the surfactant or lessen its side effects by adding the TOCN into similar formulations. It is therefore important to understand the interaction between the surfactants and TOCN.

1.5.1.2 Influence of Alcohols on TOCN Gels

The effect of alcohols on TOCN has been briefly discussed in the literature.[59,60] A study by Crawford *et al.*[1] suggested that addition of simple alcohols such as ethanol or propanol increases the gel weight % of TOCN-surfactant formulations by 10 %. The cellulose nanofibrils have many uses one of which is addition into nano-composites and plastics. The individual cellulose nanofibrils have high aspect ratio (ratio of length to diameter of the fibre) and the aggregation of these fibrils reduces this ratio. [15] Therefore, in order to corporate the hydrophilic nanofibrils in hydrophobic plastics and minimise the use of aggregation, organic solvents where the plastics are soluble in may be utilised. Fujisawa *et. al.*[61] introduced aliphatic amine salts to TEMPO oxidised cellulose (TOCN) fibrils in the presence of isopropyl alcohol/water mixture. The surfaces of the hydrophilic fibrils were covered with hydrophobic long-alkyl chains via amine salt formation which resulted in stable dispersion of TEMPO oxidised cellulose in isopropyl alcohol. However, they also reported that the amine salt formation hindered the inter-fibrillar hydrogen bonds which resulted in lower tensile strengths and elimination of the oxygen barrier properties of thin films of TOCN-C_{12} amine salts.

1.5.2 TOCN Films

The dispersed nanofibrillated cellulose display high crystallinities, Young's modulus, tensile strengths, surface areas and form network structures in aqueous medium and they also form self-standing films, coating layers, foams and composites which have great mechanical strength, optical transparency, thermal stability and gas barrier functionality. [6,62–66]

The behaviour of cellulose surfaces in different medium as well as their interaction with different substituent is of great importance in their use in many applications. The adhesion cannot be explained by theory but as a sum of mechanical, physical and chemical forces and involves electrostatic forces as they relate to electronegativities of adhering materials, intermolecular forces which is related to wetting properties and weak hydrogen bonding or van der Waals forces.[67] In order to improve the interaction of cellulose with solvents surfactant may be added or the

cellulose surface may chemically be modified. This attraction of cellulose to other additives depends on its structure. The highly ordered hydrogen-bonded lattice must be modified by swelling or dissolution. The C-6 primary hydroxyl is the most reactive position for esterification reactions.

Smooth cellulose surfaces have been used to study the adhesion on cellulose. Model surfaces of cellulose have been generated by spin coating processes on wafer surfaces. [68,69] Plastic films can also be created with thin TOCN layers surfaces-hydrophilised plastic base films. TOCN films have been studied for optical, mechanical, thermal and gas-barrier properties.[15,16,66,70,71] The TOCN display particularly high oxygen-barrier properties in dry conditions. In general, the degree of polymerisation of nanocellulose plays an important role in the optical and mechanical properties of cellulose, but in the case of TOCN, fibril length could be the deciding factor.

Kurihara *et al.*[65] combined TEMPO-oxidised TOCN with poly(acrylamide) (PAM) which is a water soluble polymer and have abundant C=O and NH_2 groups forming hydrogen bonds with cellulose fibers. PAM molecules are used to enhance the mechanical properties of the TOCN films. Another study by Zhao *et al.*[22] investigated the characteristics of edible film materials formed by cellulose nanofibrils and glucomannan (an analogue to cellulose with mannose and glucose monomers) where a mixture of 50-50% of composite film produced great mechanical properties. Cellulose hydrogels were generated in NaOH/urea solvent media and upon evaporation of the hydrogels and diecasting, 3D ordered structure of cellulose sheets were formed by Yuan *et al.*[72] A mixture of enzymatically treated cellulose and microfibrillated cellulose were created by Saarikoski[73] and the plasticity of the films were investigated. The non-toxic and biodegradable nature of cellulose further leads to use in food packaging as an edible raw material. Gelatin, a protein obtained from animal is also widely used in food industries as gelling agent. Films made from corn starch, glycerol, cellulose nanocrystals and gelation which displayed good mechanical properties was recently developed by Alves *et al.*[18]. A recent study by Ong *et al.*[74] demonstrated use of cellulose ester in seawater desalination and water re-use of seawater. They achieved this by constructing a membrane support for flat sheet thin film composites.

Isogai [75] and his colleagues reported nanofibre films prepared from TEMPO-oxidised softwood and hardwood cellulose exhibiting tensile strengths and elastic moduli higher than cellophane films, which are made from cellulose xanthate solution (Figure 11).

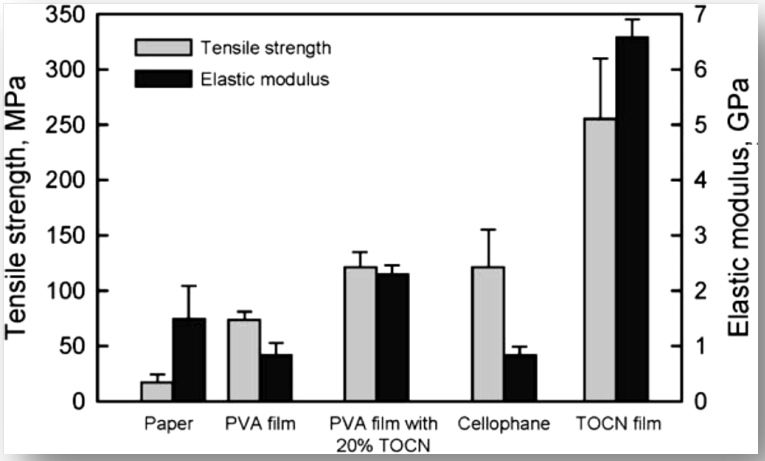

Figure 11: Tensile strength and elastic modulus of TOCN film and other types of films, reprinted with permission from reference 15.

The same authors also reported 20 % increase in tensile strength and elastic modulus of poly(vinyl alcohol) (PVA) films, upon addition of TOCN. They suggested that carboxylate groups present in the TOCN may hinder the hydrogen bonding on the surface. They also reported that if the films were prepared under more acidic conditions (at pH 6.8), rather than at pH 10, the tensile strength has improved considerably.[15]

A number of potential applications for TOCN films have been suggested, as these films display low thermal expansion (a result of high crystallinity) and high transparency, which are ideal for flexible panels and electronic devices.[66] These films also showed considerable oxygen barrier properties suggesting opportunities for use in biodegradable packaging. A study carried out by Wu *et al.* also suggested that the mechanical and the oxygen barrier properties of TOCN films could be improved by adding <10 wt % montmorillonite (MTM) nanoplates (Figure 12). [71]

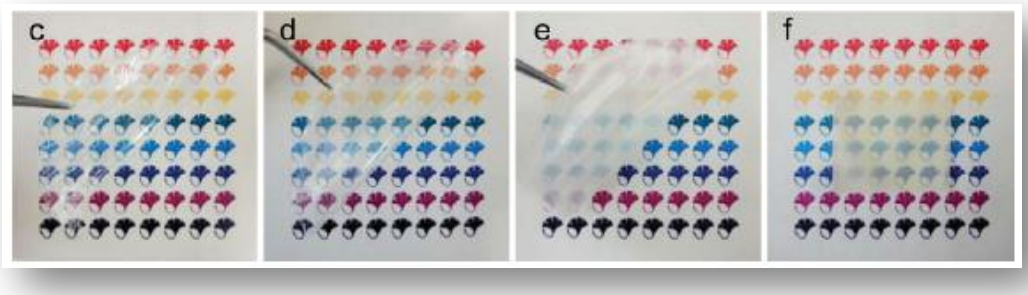

Figure 12: Photographs of TOCN/MTM composite films with different MTM contents. c) TOCN only, d) 5 % MTM, e) 50% MTM. The thickness of the films were between 5-7.7 µm, f) MTM film 35 µm in thickness, reprinted with permission from reference 71.

The different techniques used for cellulose film casting in general and their advantages and disadvantages are shown in Table 1which is used as a guideline for the TOCN film casting in this project.

Table 1: Advantages and disadvantages of methods available for preparation of cellulose film, redrawn from reference 76.

Surface	Advantage	Disadvantage	References
Cast-coated films	Simple Simple equipment required	Non-defined thickness Thick & rough surface	Hishikawa *et al.*[24]
Langmuir-Blodgett films	Well-defined Prepared at a certain surface pressure	Time consuming Desilylation needs more research Detach in water-tenside solutions	Holmberg *et al.*[25] Neuman *et al.*[77]
Spin-coated films	Relatively simple Controllable thickness Simple equipment needed Relatively well defined	Adjustment of thickness difficult for thin surfaces Polymers attaching the cellulose film not trivial	Holmberg *et al.*[78]
Cast-coated cellulose I	Relatively simple	Smoothness undefined No controlled thickness Raw material	Grey, D.

A recent study by Homma *et al.*[79] investigate the effects of carboxyl-group counter-ion of TEMPO-oxidised cellulose fibers (TOCs) and nanofilms on biodegration behaviours. They introduced various carboxyl-group counter-ions including Na^+, H^+, Ca^{2+}, NH_4^+, Cu^{2+}, K^+ and Cs^+ into TOCN films. The group suggested that there is a significant difference in the degradation behaviour of the films based on these ions which are influenced by the swelling behaviour of the TOCs in distilled water (the higher the degree of swelling, the higher the degradation efficiency). Therefore they stated that the order of the degradation level was $Na^+ \approx NH_4^+ \approx K^+ \approx Cs^+ \gg Ca^{2+} > H^+ > Cu^{2+}$.

1.5.2.1 Interaction of Cellulose Films with Surfactants

Interaction between polymer-surfactant systems and surfactant adsorption can be studied using hydrophilic and hydrophobic cellulose model films.[80–82] Such studies of model surfaces could be used to resemble hair cuticle, the stratum corneum of the skin and fabrics.[80] Although information on this interaction can be obtained from methods focusing on aggregates, a more sensitive technique could be an alternative to study the individual components of the system. The interactions between polymer/surfactant can be the result of either of the two forces: (1) strong electrostatic attraction between oppositely charged polyelectrolytes and surfactant head groups, often supported by hydrophobic forces, (2) weak interactions between hydrophobic groups in polymer chains and surfactant head groups. The complex formation between polyelectrolyte and oppositely charged surfactant takes place at critical aggregation concentration (CAC) of the surfactant which is much lower than the critical micelle concentration (CMC).[83,84] Mixed layered structures at the solid-liquid, liquid-liquid and liquid-air interfaces are generated which are building blocks for applications including colloidal stabilisation, wettability, adhesion and emulsion formation.[85] It is known that beyond the CMC (when surfactant molecules form aggregates called micelles), the spherical ionic micelles transform into structures such as ellipsoids, rods or disks.[86] Alila *et al.*[87] proposed a correlation between the higher number of carboxyl groups on TEMPO-oxidised cellulose resulting in better surfactant adsorption on the surface. In a system of cellulose/surfactant/solute, they

showed that the surfactant concentration (up to CMC) increases the solute adsorption and the solute solubility also plays an important role.

Surface tension measurements of the mixed system can often produce variable results as it is difficult to determine if the surface is at equilibrium or not and imaging techniques such as atomic force microscopy (AFM) may not be a sufficient technique to study the interaction on its own, however neutron scattering techniques can overcome this problem. Neutron reflectivity (NR) is often chosen to study this aspect by revealing information on the adsorption at interface. Small angle scattering could also be used to study these systems for interfacial properties in foam stability, spreading, adhesion and coating, but reflectivity can offer more for mixed systems to study thin layers at solid-liquid and air-liquid interfaces.[88] Penfold *et al.*[81] used reflectivity to study surfactant adsorptions with different approaches onto model hydrophobic and hydrophilic cellulose surfaces.[80,89–93] The cellulose films were assembled by Langmuir-Blodgett deposition of trimethylsilycellulose onto silanted silicon surface with a thickness of 50-120 Å.[94] Tucker *et al.*[80] demonstrated adsorption of non-ionic surfactant hexaethylene monododecyl ether, $C_{12}E_6$, and the mixed nonionic/cationic surfactants $C_{12}E_6$ and hexadecyl trimethyl ammonium bromide, C_{16}TAB, onto the hydrophilic and hydrophobic surfaces of thin cellulose films by Langmuir-Blodget (LB) deposition, have using neutron reflectivity. They showed that the presence of non-ionic surfactant enhanced the hydrophilic and hydrophobic cellulose film penetration.

1.5.2.2 Interaction of Cellulose Films with Salts

Wagberg *et al.*[95] showed that the type of salt has an impact in the electrostatic repulsion between fibrils of carboxylated microfibrilliated cellulose (MFC) in a multilayer film. A slight increase in NaCl concentration has only minor effect on the colloidal stability of the material as the dissociation of the charged groups is considerably increased with the increased salt concentration increase which inhibits the decline in surface potential caused by the addition of salt. Native cellulose model films with amorphous and crystalline cellulose I were arranged by spin-coating aqueous cellulose nanofibrils dispersions onto silica substrates by another study.[96] They showed that addition of 1 mM of NaCl solution does not influence the swelling

of the films whereas 10 Mm NaCl results in deswelling of films. Therefore the small changes in the swelling can be attributed to bulk effects i.e. the change in density and viscosity of the electrolyte solution. At high electrolyte concentration, the effect of steric forces starts to take place. Tucker *et al* [82] measured the interaction of sodium dodecyl sulfate (SDS, anionic surfactant) with trimethylsilyl-cellulose (TMSC, hydrophilic cellulose) in the presence of electrolyte (0.1 M NaCl) by various techniques including reflectivity. The films were deposited on the silica surfaces by Langmuir-Blodgett (LB) method where a trough spreads smooth monolayer of TMSC with thickness of ~100 Å. They demonstrated that addition of NaCl would facilitate the ability to control the adsorption of the surfactant onto the cellulose surface and the extent of penetration into the cellulose film. The same group also studied[97] the effect of SDS adsorption on the hydrophobic cellulose surface where the greater SDS penetration was observed in the presence of NaCl.

1.6 Drug Delivery

1.6.1 Structure and Anatomy of Skin

Skin is the largest organ with the function of protecting the body against chemicals/drugs and water while acting as the primary barrier for diffusion.[98] This barrier function is accomplished by its multilayered structure. The skin is divided into three layers including: epidermis (the most outer layer), dermis (tissue supporting the skin) and hypodermis (the thickest and most inner layer) (Figure 13). The uppermost layer of skin is called "stratum corneum" (SC). It could be described with a "brick and mortar" model where the dead cells (mainly proteins) would represent the bricks and the lipid matrix signify the mortar part of the SC model.[99] The stratum corneum consists of 10-30 cell layers with a thickness of 5-20 µm.[100]

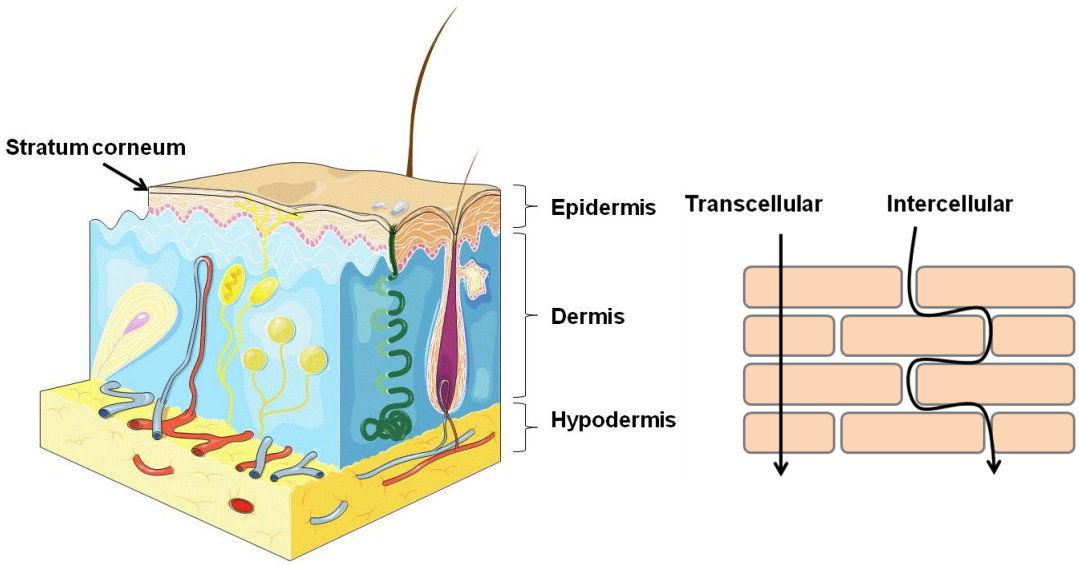

Figure 13: Anatomy of skin (left) and the "brick and mortar" structure of stratum corneum. The image (left) was redesigned using Servier Medical Art from reference 301.

The pathway of a drug molecule could be via the transepidermal route or the appendages (hair follicles and glands). The route of the appendages often not considered of importance, (approximately 0.1% of the total skin surface).[101] For the interest of our study we will focus on the transepidermal transport of a drug molecule which can take place through the intercellular and transcellular pathway (Figure 13).[102] The intercellular lipid pathway is the direct pathway through SC; therefore it has a great impact on the diffusion rate of a drug molecule across the skin. This pathway is the principal reason of the skin's barrier function. Therefore, the SC demonstrates selective permeability and has affiliation towards the lipophilic molecules and the only way of drug delivery is achieved via passive diffusion.[103] Even though, the intracellular structure formed by lipophilic lamellae is convoluted, it can still offer a continuous pathway to the deeper epidermis right from the surface. The permeability of the drug molecule can be improved by extraction of the lipids or agitating their lamellar structure by introducing solvents for example. In addition, the diffusion via the aqueous part of the interlamellar water can be also enhanced by dehydrating the skin surface by occlusive application of drugs or use of moisturisers for instance. [104]

1.6.2 Transdermal Delivery

Drugs can be administered into the body via various pathways. These routes may include systems such as gastrointestinal (oral, rectal), parenteral (injection via various routes), transmucosal (drug application at sites where mucous membrane present), transnasal (nasal delivery of the drug), pulmonary (drug delivery by inhalation) and transdermal (delivery of drug through skin).[105] In the interest of this project, we will only focus on the transdermal delivery system (TDS).

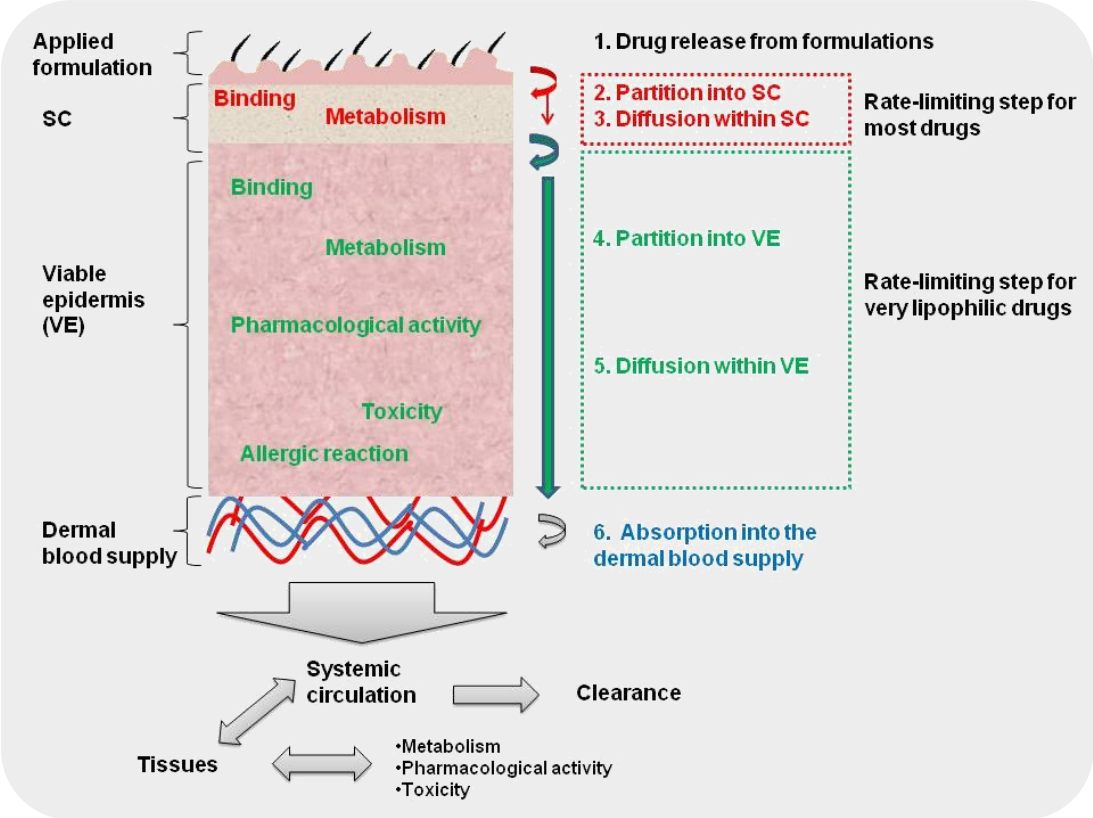

Figure 14: A schematic diagram of the process may occur after the application of a topical formulation, image redrawn from reference 106.

When a formulation is applied to the skin, the route it may follow is depicted in Figure 14. The active drug released from the vehicle and partitions into the SC. Due to the concentration gradient, the molecules will move through SC and the partitioning into epidermis and diffusion will be followed into dermis will. The drug will be cleared from the skin once it reaches the vasculature and lymphatic vessels. Based on the lipophilicity of the molecules they can travel through different layers of the skin therefore the absorption is restricted. The binding of the molecules to specific sites could yield a physiological response such as therapeutic activity or allergic reaction. [106]

There are various approaches for the transdermal delivery of a drug via the skin and these include transdermal gels, penetration enhancers, drug carriers (nano particles etc.), transdermal patches, transdermal electrotransport and needle-free injections. For a drug to penetrate through the skin via passively, it should have the suitable lipophilicity and generally have a molecular weight less than 500Da. These two requirements can be overcome by optimising a formulation or drug carrying vehicle in order to enhance the permeability. However, this passive delivery may not be as successful for drugs with molecular weights > 500 Da. Therefore, the delivery enhancement could be achieved by active methods such as iontophoresis, electroporation, ultrasound and needleless injection.[105]

The variation in the transdermal delivery across species or diverse application sites in the same model are essentially because of the differences in the SC thickness, the content of the intercellular lipid matrix, the presence of free fatty acids and triglycerides and the density of hair follicles in the skin area studied.[98,107] The transdermal delivery has many advantages including [108–114]:

- The avoidance of first-pass metabolism related to GI tract , pH for example
- Controlled and maintained drug delivery over a prolonged period of time
- Improved patient compliance
- Reduction of side-effects related to systematic toxicity
- Direct treatment of the target area
- Non-destructive and painless drug administration

However, like many other delivery systems, this path of delivery also has limitations which can be listed as [115–119]:

- The molecular weight of the molecule should be <500 Da for passive delivery
- Suitable water and lipid solubility, a log P (octanol/water) between 1-5 is required for the molecule to go through the SC and the aqueous environment lying underneath that
- Skin irritation or sensitisation may occur

The SC is a predominantly lipophilic barrier which reduces the transepidermal water loss and known to be the main obstacle for percutaneous absorption (process of absorption of molecules through the skin from topical applications). Transdermal delivery of small molecules therefore can be explained in terms of interfacial portioning and molecular diffusion through this barrier. [120] *In-vitro* experiments involve use of Franz diffusion cells which has a donor and receptor compartment separated by skin (or artificial membrane). The donor chamber contains the drug formulation from which the drug molecules permeate through the skin and travels into the receptor solution. The passive diffusion of a non-electrolyte in the absence of any bulk flow can be defined by Fick's first law of diffusion[120]:

$$J = -D\frac{\partial C}{\partial x} \tag{6}$$

Where J is the diffusion flux (amount per unit area per unit time), D is the diffusion coefficient of drug in SC, $\frac{\partial C}{\partial x}$ is the concentration gradient over a distance of x. Equation (6) can be used to explain the skin permeation of drugs but the concentration gradient can only be estimated by the product of permeability coefficient, k_p and drug concentration in the vehicle, C_v.

The steady-state flux, J_{ss}, through the skin barrier therefore can be shown as:

$$J_{ss} = k_P C_v \tag{7}$$

where permeability coefficient, k_p is defined by:

$$k_p = K\frac{D}{h} \tag{8}$$

And SC/vehicle partition coefficient, *K* and the thickness of the skin, *h* is considered. The cumulative amount of drug permeating through the skin, Q_t is given as:

$$Q_t = K \cdot D \cdot \frac{C_s}{h\left(t - \frac{h^2}{6D}\right)} \quad (9)$$

where C_s is the saturated reservoir concentration when a sink condition is achieved in the receptor solution. It is often used in *in-vitro* experiments with an indefinite dosing technique where the skin is separated by an infinite reservoir of drug on donor compartment and a perfect sink condition supplied in the receptor part using Franz diffusion cells.

1.6.3 Animal skin versus Human Skin

The transdermal delivery of a molecule is best described by human skin which can be obtained from cosmetic surgery and amputations for *in vitro* studies. However , it serves a challenge to have human skin required for such experiments hence animal skins with similar anatomy to human skin is often used. These animals may include primates, pig, mouse, rat, guinea pig and snake. Nevertheless, since use of primates is very restricted for research studies, the most relevant model adapted for *in vitro* studies often uses pig skin. The porcine ear skin is commonly used for permeation studies for example. The studies have demonstrated that the SC thickness of pig ear skin is around 21-26 µm which is in resemblance to human skin.[121–123] The follicular structure of pig skin is also similar to human skin where on average 20 hairs are present per 1 cm^2 of pig ear skin compared to 14-32 hairs in humans. [98,122]

Herkenne *et al.*[124] for instance showed the estimated steady-state fluxes across human skin *in vivo* were close to those measured across pig ear skin *in vitro* for four different ibuprofen formulations (Figure 15).

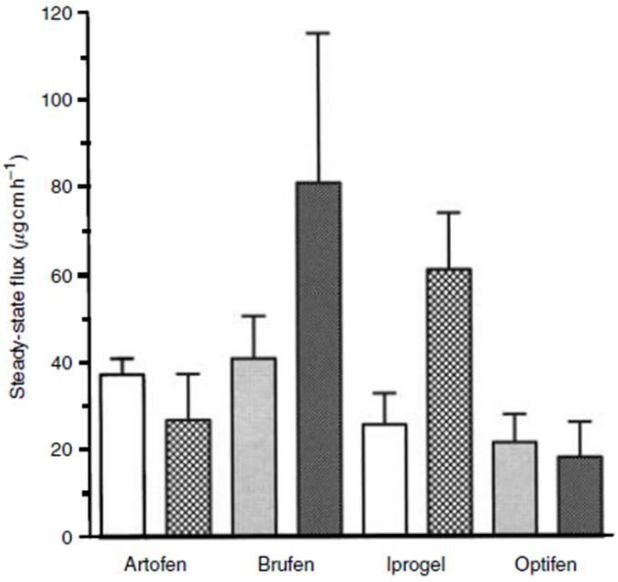

Figure 15: Ibuprofen flux across porcine (hatched bars) and human skin (open bars), from different ibuprofen formulations, reproduced with permission from reference 124.

1.6.4 Delivery of ibuprofen to the skin

Ibuprofen (α-methyl-4-(2-methylpropyl)benzeneacetic acid) is a non-steroidal small drug (MW 206) with log *P* (octanol-water partition coefficient) value of 4 which is often used as anti-inflammatory treatment (Figure 16). [124,125]

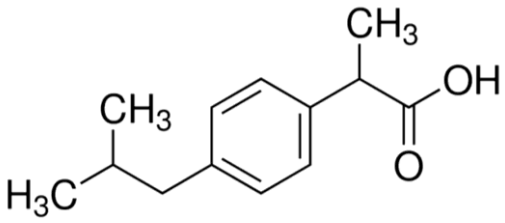

Figure 16: The chemical structure of ibuprofen

The delivery of ibuprofen is positively correlated with the dosage and the more the drug permeates the skin via passive diffusion, the greater the therapeutic effect. As a consequence, the formulation becomes an important factor in the topical drug

delivery. Ibuprofen is a lipophilic molecule which ionise at physiological pH values (4-7.4).[125]

The permeability of ibuprofen across skin has been studied extensively.[125–130] IBU is a carboxylic acid; hence the pK_a value of the molecule is an important factor in ionisation and in turn permeation. The effect of pH on IBU permeation has also been studied previously.[126] The findings of this research indicated that there is a high permeation of the ionised drugs through the lipophilic pathway which may be a result of ion pairing. Their study also showed that the maximum flux (the product of the permeability coefficient and the solubility) through the skin may occur at a pH is where ibuprofen ionisation is high which is a consequence of the aqueous solubility of the ionised material being much higher than the unionized one. As a result, the optimum topical formulation may not be for the free acid.[126]

When the pH increases, the solubility also increases along with the degree of ionisation, however this has the negative effect on the permeability. Table 2 shows the solubility and the permeability profile of ibuprofen at different pH.[131] The pK_a value of ibuprofen is 4.45 and the values for the permeabilities correspond to unionised and ionised drug at the extreme side of the pH range. [126,132]

Table 2: The solubility and permeability properties of ibuprofen as a function of pH [131]

pH	*2.2*	*2.3*	*4.0*	*5.0*	*6.0*	*7.0*	*9.0*	*9.2*
Solubility (mg/ml)	0.024	0.027	0.029	0.096	0.52	3.7	7.83	14.8
Permeability coefficient (cm/h)	0.06	0.053	0.045	0.036	0.019	0.0066	0.0024	0.0012

A study by Herkenne *et.al* [124] compared ibuprofen transport across skin both in *in vivo* and *in vitro* (silicone membrane and pig skin) from four different ibuprofen gel formulations from the market. The formulation Artofen contains 10% w/w ibuprofen whereas the rest of the formulations had 5% w/w. Figure 17 shows the differences in the amount of ibuprofen permeated across pig skin *in vitro* over an eight hour period.

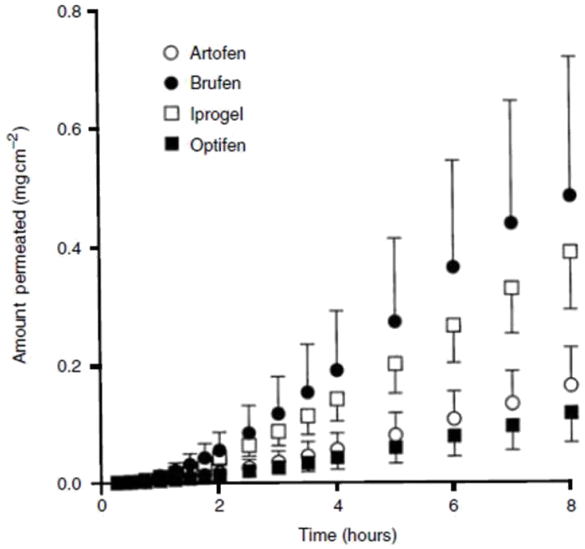

Figure 17: The delivery of ibuprofen from different formulations across porcine skin *in vitro*, reproduced with permission from reference 124.

1.6.5 The effect of permeation enhancers

Passive skin permeation can be enhanced by two major approaches including changing the drug's thermodynamic activity in formulation (supersaturation) or using skin penetration enhancers in the formulation. Supersaturation condition is met where the drug is formulated at a concentration higher than the solubility limit. This is often done by changing the drug solubility unexpectedly by manipulating the reliance of the solubility with pH, temperature and solvent used during the formulation. The advantages of this state includes increase in flux hence the driving force of the drug across SC and not using external enhancers.[125]

Skin penetration enhancers are molecules which interact with the SC constituents to improve drug partitioning into the membrane or diffusion through the membrane or both with the purpose of enhancement on drug delivery.[106,125] These molecules include co-solvents such as ethanol, propylene glycol, Transcutol®, simple chain alcohols as well as surfactants, amides, esters, fatty acids, sulphoxides and terpenes.[106,115,133–136] They are added to formulations in order to increase the drug flux.

Although there are many keen candidates for the permeation enhancement role, unfortunately there is no ideal penetration enhancer for human and animal skin to-date. The ideal enhancers should have the following characteristics [133,137]:

- They should be non-toxic, non-irritant and non-allergenic.
- They should have a nice "skin-feel".
- They should work fast so that the extent of effect can be predictable and reproducible.
- They should have no pharmacological activity within the body.
- They should not interfere with the therapeutic agents diffusion into the skin.
- Once removed from the skin, the barrier properties of the skin should rapidly be restored.
- They should be compatible to both excipients and drugs and be used in diverse topical preparations.

Not surprisingly, it has been a challenge to discover a material that could satisfy all these points. However, there are some enhancers that show many characteristics of those listed and some of them which are of relevance to this study mentioned here:

Water: An established method to improve the transdermal and topical delivery of molecules is to use water. The SC contains 15-20% water of the tissue dry weight. Soaking the tissue in water, exposing the membrane to high humidity, or as of a more common method of occluding the tissue to stop any transepidermal water loss can enable SC to reach equilibrium with the epidermal cells underneath. The occlusion method can bring up the water content of the outer layer to 400 % of the tissue dry weight. It is applied in products such as patches.[133]

Short chain alcohols: Use of alcohols in formulations as an enhancers has been a topic of interest for many decades.[134,136,138,139] Ethanol is commonly used as a co-solvent in formulations to provide sink conditions during in vitro permeation experiments. It permeates through human skin with a steady state flux of approximately 1 mg cm^2/h.[140] It can increase the solubility of the drug in the vehicle and change the solubility properties of the tissue with an enhancement for drug partitioning. [141] Ethanol can also be used to increase the solubility of the permeant

likely to depletion in the donor compartment. [142] The rapid evaporation of ethanol can generate a supersatured state for the drug and enhance the permeation. A study by Meshali *et al.*[143] demonstrated the effect of ethanol as a co-solvent in ibuprofen formulations where the percentage drug permeated across rabbit skin was considerably higher for formulations prepared with ethanol.

Surfactants: Surfactants are found in many existing formulations in therapeutic, cosmetic and agro-chemical products. In general, they are added to the formulation in the light of their ability to solubilise lipophilic active ingredients and consequently the lipids within the stratum corneum. Anionic and non-ionic surfactants are the common ones used in such formulations. Examples of anionic surfactants include sodium dodecyl sulfate (SDS) and sodium lauryl sulfate (SLS). The anionic and cationic surfactants are found to damage the skin and swell the stratum corneum and interact with intercellular keratin.[144] Non-ionic surfactants tend to be widely regarded as safe.[133] Despite being commonly used in many consumer products, surprisingly SLS and SDS have been found to be well-known irritants to the skin. [57,58,135,145–147] SLS, also an emulsifier, is suggested to change the effectiveness of the skin barrier.[58] It is also reported that SDS-induced skin barrier disruption is dose-dependent and that it increases with an increase in the SDS concentration above the CMC of SDS which is the case for the many formulations.[148]

1.6.6 The effect of formulation type and rheology

Ibuprofen could be incorporated into many formulation vehicles such as sprays, gels, microemulsions and creams.[149–152] Stahl *et al.*[152] presented the difference in the ibuprofen permeation from three different formulation vehicles all containing 5% w/w drug (Figure 18). Although the highest amount of drug permeation was achieved from the cream formulation, the values for apparent permeability coefficients (a quantitative measure of membrane permeability) were not significantly different between the formulations. However, after 28 hours, the amount of ibuprofen found in the skin was considerably higher for the solution and the gel formulations. The group suggested that this could be of advantage where long term application is required as the skin would continuously supply the body with ibuprofen. It was also interesting

to see the ibuprofen solution they used as a control performed in the middle of the commercial products which lacked permeation enhancers such as 2-propanol. [152]

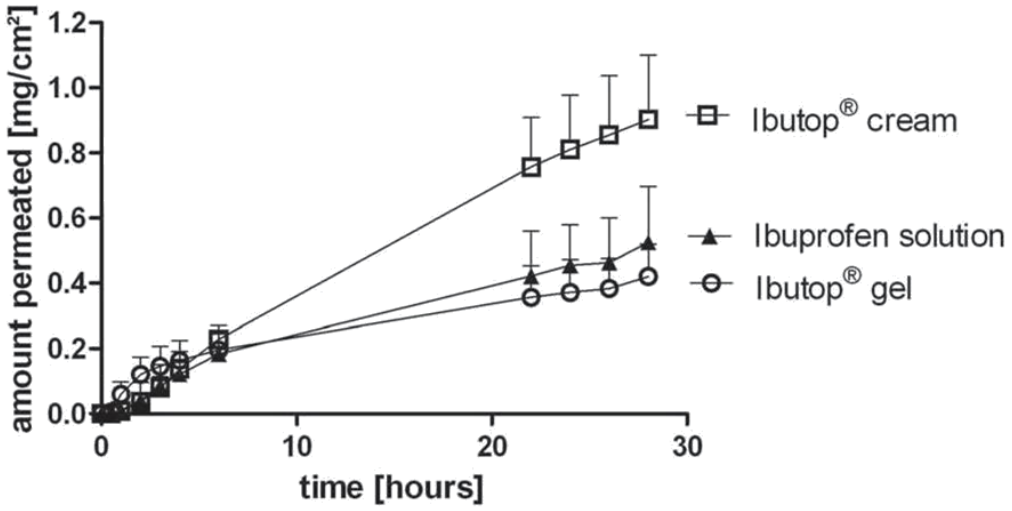

Figure 18: Bovine udder skin permeation in vitro following applications of different ibuprofen formulations (5 % w/w), reproduced with permission from reference 152.

The drug release profiles of a formulation could also be influenced by the rheological properties of the systems. [151,153–155] Although the drug-vehicle interactions determine the drug release profiles, the formulation should also be easy to apply and stay in the treatment site for the necessary time period. The apparent viscosity or macroviscosity could affect the diffusion of particles in the formulation. The drug molecules however are more affected by the microviscosity and hence by the physical properties of the bigger structures such as polymer in the formulation. [155] Welin-Berger *et al.*[155] used various topical creams with and without gelling polymers and one of the formulations with the gelling polymer contained carboxypolymethylene (C934). The permeation rate of the model compound was lower for C 934 concentrations above 0.5 % w/w which had higher viscosities (Figure 19). The release of the active compound was affected negatively due to reduced droplet diffusion at higher concentrations.

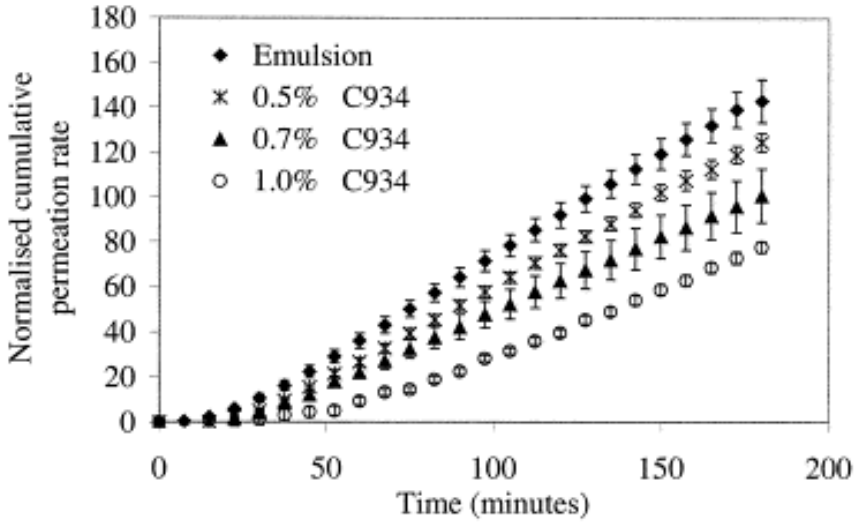

Figure 19: Normalised cumulative permeatition rate of model compound (amino diether, AD) through guinea-pig skin, reprinted with permission from reference 155.

1.6.7 Application of cellulose in drug formulation

A great number of polymers are used in pharmaceutical industry as suspending and emulsifying agents, flocculating agents, adhesives, packaging and coating materials and increasingly as components of controlled and site-specific drug delivery systems.

Cellulose derived polymers has been used in many topical delivery formulations mainly by partial methylation or carboxylmethylation. This is done in order to convert the naturally insoluble cellulose into soluble cellulose. *Ethylcellulose* (insoluble in water but soluble in alcohol) is an ethyl ether of cellulose and contains 44-51% of ethoxyl groups. *Methylcellulose* samples contain methylated groups scattered around which are not evenly distributed throughout the chains. It is a methyl ether of cellulose holding around 29 % methoxyl groups and it becomes slowly soluble in water upon heating. *Ethylhydroxyethylcellulose* is an ether of cellulose and it swells in water to generate a clear viscous colloidal solution. *Hydroxyethylcellulose* is soluble in water however it does not gel and it found use in ophthalmic solutions. Sodium carboxymethylcellulose is also soluble in water and

due to its carboxylate group it is more prone to changes in pH of the formulation where its viscosity is reduces considerably below pH 5. [156]

Zhu *et al.*[157] showed that the partially neutralised oxidised cellulose dispersions readily form ionic complexes with primary amines which allows high-drug load into the polymer matrix. Oxidised cellulose also found use as hemostatic agent (brand name Surgicel)[158] and adhesion barrier as well as being used as an matrix holder for drugs, enzymes and proteins. [159,160] Avicel® PH101 (microcrystalline cellulose) is another commercial brand available in the market which has the main purpose of aiding the formulation of tablets of poorly compressible and soluble drugs. [161] Cellulose beads (CB) have recently gained some attention in the pharmaceutical industry as their biocompatible, non-toxic, highly porous, large specific surface area, mucoadhesivity, hydrophilic characteristics found great use. [162–164] CB generated by dropping a solvent mixture of dissolved cellulose into a bath where cellulose beads are formed by precipitation.[165–168] The effects of carboxylation of C-6 hydroxyl group on the chemical properties of cellulose beads were also investigated.[169] The contributions of the carboxyl groups included adding properties such as swelling, water retention and pore size distribution. Biodegradable cellulose mesh was also used as a membrane after periodontal surgery for tissue healing.[170] Nerurkar *et al.* [171] blended a mixture of cellulose ethers and carrageenans as tablets and used them for sustained delivery of ibuprofen for 10-12 hours. They suggested that the anionic polymers had ionic interactions with the non-ionic polymers which favoured the water uptake capacity and gel viscosity which yields improved control over the release of ibuprofen. The hydration led to porous structure of the polymer which created routes for the drug delivery. Bacterial cellulose was also utilised for wound dressing material.[129,172,173] Shimotoyodome *et al.*[174] administered TEMPO-oxidised cellulose with glucose to mice and seen a reduction in the postprandial blood glucose, plasma insulin and triglyceride concentrations.

1.7 Summary

In this current chapter the recent developments in cellulose research with a focus on TEMPO-oxidised cellulose was described. The structure and applications of TOCN have been explained. Cellulose gels and films formed by other cellulose derivatives as well as TOCN have also been discussed. There have been many studies involving different types of cellulose which are often water soluble but the studies with TOCN were limited.

The following chapters include an introduction, materials, method, results and discussion sections. The theory of the each technique was discussed individually however; some common methods and techniques were only described once to avoid repetition.

In Chapter 2, the interaction of TOCN in low molecular weight alcohols in the presence of additives such as surfactants and salts using X-ray and neutron scattering techniques has been introduced. The formulation of hydroalcoholic gels containing TOCN and these additives were also described.

In Chapter 3, the focus was on the TOCN films which are formed when applied to the surfaces such as skin. Therefore, the interaction of the fibrils with the additives was investigated by means of X-ray and neutron reflectivity.

In Chapter 4, the drug delivery aspect of the hydroalcoholic gels similar to those in Chapter 2 were discussed. The active ingredient was ibuprofen which was loaded into these gels and the delivery of the drug across the membrane/skin was studied.

2. Effect of alcohol on gelation behaviour of TEMPO-oxidised cellulose nanofibrils (TOCNs) in the presence of anionic surfactant and salt

Overview:

The effect of small chain alcohols (methanol, ethanol and propan-1-ol) on the structure of TEMPO oxidised cellulose dispersions has been studied as a function of concentration of sodium dodecyl sulfate (SDS) and sodium chloride (NaCl) by means of small angle x-ray scattering (SAXS) and small angle neutron scattering (SANS) .The results show that an increase in the alcohol content has an impact on the structure of the oxidised cellulose gels causing the fibrils to aggregate; generating sheet like structures which was further supported by scanning electron microscope (SEM) images. The higher concentration of alcohols yielded scattering patterns where the model required to fit the small angle scattering data changed from an elliptical cylinder model for the fibrils to a lamellar model. The effect of alcohol concentration was not limited to changes in the fibril aggregation but also caused changes in the micellization of the SDS molecules where the micelle formation was inhibited by the higher concentrations of alcohol. Rheology studies were also completed where the storage modulus (G′), loss modulus (G″) and complex viscosity (|η*|) were measured for the TOCN-alcohol gels. The results revealed that the complex viscosities of the gels were considerably higher in the presence of the alcohols compared to aqueous dispersions. The storage and loss modulus values were higher for gels with salt (NaCl) compared to surfactant (SDS) at the same alcohol concentrations or in the absence of salt or surfactant. The alcohol with the longest chain (propan-1-ol) formed the thickest gels compared to methanol and ethanol.

2.1 Introduction

Aqueous formulations play an important role in our daily lives as they are used in many personal products such as shampoos, shower gels and creams as well as in paints, coatings and drilling lubricants. These formulations predominantly depend on polymer-based thickeners to modify their viscosity.[1] However, these rheology modifiers are mainly obtained from non-renewable resources and they might have other undesired effects such as damaging the skin or drying the hair as well as changing the physical properties of the skin[58,135,145]. These factors contributed to a search for alternative thickeners which are obtained from renewable resources and do not cause skin irritation. TEMPO-oxidised cellulose could prove to be such an alternative as it forms clear shear thinning gels with or without the addition of surfactants or salts.[1] Cellulose fibrils found in plant walls are held together by hydrogen bonds and therefore are difficult to separate down to individual fibrils by only mechanical or chemical treatment. Modification of the surface of the fibrils is necessary to reduce the effect of these strong hydrogen bonds. Oxidised cellulose nanofibres obtained by regioselective conversion of α-cellulose fibres by TEMPO-mediated oxidation, followed by mechanical treatment in water under mild conditions yields individual nanofibres 3-4nm in width and a few microns in length. [15,24] This was achieved by oxidation of C6 primary hydroxyl groups of cellulose by TEMPO radicals and NaBr/NaClO oxidation in water at pH 10-11. If this oxidation was taken to completion, it would have resulted in poly(glucoronic acid), however for the cellulose used in this study, the oxidation was kept at 20-25% by limiting the amount of oxidant used.[1,15] In this way, individual cellulose fibrils were obtained rather than cellulose bundles or whiskers which makes them ideal for formulations. Oxidised cellulose is already extensively used as a hemostatic material for surgical applications and as a carrier material in cosmetic and pharmaceutical applications.[36,41,75,175,176] There have been previous studies on dispersion of TEMPO-oxidised cellulose in low boiling point alcohols such isopropyl alcohol as it is difficult to nano-disperse them in these organic solvents. [61,177] Crawford *et al* [1] reported that the gelation of oxidised cellulose gels with surfactants was not hindered by the addition of short chain alcohols and that the formulations could hold up at least 10 % by weight alcohols such as ethanol which would widen the opportunities for it to be used in different personal care product formulations.

Surfactants are common additives to these formulations and their application is not limited to personal care products as they are also used in lubrication, foaming, emulsification and detergency.[178–180] They are often employed in the presence of co-surfactants, most commonly low concentration alcohols, in order to manipulate the interfacial properties. [180] The surfactant-alcohol systems are also used to produce microemulsions which are utilised in tertiary oil recovery and therefore are of great importance.[181] There have been many publications focused on the effect of alcohol on the properties of surfactant micellar systems.[60,178,181–192] The hydrophilic/hydrophobic nature of the alcohol has an impact on the activity of the micelles. The alcohols methanol, ethanol and propanol are more hydrophilic compared to longer chain alcohols and they are known to be thermodynamically destabilising to the micelles, hence contributing to destruction of the aggregates. These short chain alcohols dissolve in the aqueous solution (hence altering the solvent properties), unlike the longer chain alcohols which take part in the actual micellisation process.[193] The studies revealed that addition of long chain alcohols decreases the critical micelle concentration (CMC), whereas the shorter chain alcohols such as methanol are too small to have such an effect. [178] This is due to the penetration of alcohol molecules into the micelle core and this effect is seen less in non-ionic surfactants compared to anionic surfactants.[187] Forland *et al.*[193] reported that increasing the concentration of the propanol, yielded a decrease in the minor radius of SDS micelles and promoted the breakdown of the micellar system based on the results obtained from SANS studies. The shape of the micelles change from ellipsoidal to spherical, when the concentration of propanol is increased to 1.5 M. It was also suggested that a longer chain alcohol such as pentanol caused an increase in the micellar size and generate wormlike aggregates.[193]

However, no previous work has been reported on the effects of methanol, ethanol and propan-1-ol on the structures of thickened liquids/gels formed by TEMPO-oxidised cellulose fibrils. In this study, we have used SAXS to understand how different alcohols and their concentrations might affect the structures formed in the gelled formulations containing oxidised cellulose fibrils. In particular, we investigated the effect of SDS and NaCl in these oxidised cellulose-alcohol gels. The understanding of the relationship between oxidised cellulose, alcohols, surfactants and salts gives us the ability to modify personal care products and create

formulations using renewable materials like TOCN to create products such as alcohol hand sanitisers. The research is supported by gravimetric analysis of the alcohol-oxidised cellulose gels and rheological experiments were carried out to highlight the physical changes in the gel properties. Analysis of SAXS data indicates a change in the shape of the fibril aggregates where a transition from a network of cylindrical shaped individual fibrils to more sheet-like structures of aggregated fibrils occurred with an increase in the alcohol concentration. These changes were also imaged using a scanning electron microscope (SEM).

2.2 Materials and Methods

2.2.1 Chemicals

For gravimetric analysis and SAXS experiments

Sodium dodecyl sulfate (ACS reagent, ≥99.0%), sodium chloride (BioXtra, ≥99.5%), dialysis tubing cellulose membrane (average flat width 16 mm, MWCO 14000), absolute ethanol (CHROMASOLV®, for HPLC, ≥99.8%), methanol (CHROMASOLV®, for HPLC, ≥99.9%), propan-1-ol (CHROMASOLV®, for HPLC, ≥99.9%) were purchased from Sigma Aldrich. Ultrapure water (18.2 MΩ cm) was used for the preparation of all dispersions. Dispersions of oxidised cellulose fibrils were prepared by sonication using a Vibra Cell Sonicator and the tip used was an ultra-high intensity tip (tip diameter 3 mm) purchased from Sigma Aldrich.

For SANS experiments

Deuterated sodium dodecyl sulfate (D25, 98 %) was obtained from Sigma Aldrich. Ethanol (D6, 99%), ethanol (D1, 99 %), methanol (D4, 99.8 %), methanol (D1, 98 %) and deuterium oxide (D, 99.8 % at.) were purchased from Goss Scientific UK.

TEMPO-Oxidised Cellulose Nanofibrils

TOCN dispersed in deionised water was kindly provided by Unilever (Port Sunlight, UK). The degree of oxidation was limited to ~ 20-25 %. It was freeze-dried and stored at 4 ℃ for further use. TEMPO-oxidised cellulose nanofibres were developed from softwood waste α-cellulose fibres by TEMPO)mediated NaOCl/NaBr oxidation process in water, followed by mechanical dispersion as described elsewhere.[15,31] These conditions resulted in breakdown of large fibres in the starting material through partial removal of amorphous cellulose, followed by sonication, yielding fibrils the surface of the fibres functionalised with acid (-COOH) and small amount of aldehyde groups(-CHO).[1]

2.2.2 Preparation of aqueous TOCN dispersions

Prior to use, TEMPO oxidised cellulose was purified by redispersion in water and dialysed using dialysis membrane (MWCO 12000, diameter 16 mm, Sigma Aldrich, Gillingham, UK) in deionised water for a week (changing the water three times a day). The dialysed cellulose was then freeze-dried and dispersed in deionised water at desired concentrations. 2.0 g of oxidised cellulose was weighed out and dispersed in 98.0 g of water and was stirred overnight at room temperature. This was used as the stock solution (pH 6.5). Ultrapure water (18.2 MΩ cm) was used for the preparation of the dispersions. The dispersion was then sonicated in 20 g batches for 30 minutes under the following conditions: 1 second on and 1 second off mode at a power of 2 W cm^{-2}. Sodium chloride (*0.20 M*) and the sodium dodecyl sulfate (*0.04 M*) were added to the dispersions after the sonication where required.

2.2.3 Preparation of Oxidised cellulose-alcohol gels

For gravimetric analysis and SAXS experiments

The stock dispersions (2 wt %) were diluted to 0.8 wt%. A hole was drilled in the lid of an eppendorf tube (1.5 mL) and weighed quantities of cellulose dispersions in water were placed inside the tubes. A piece of dialysis tubing was placed between the

tube and the lid. The small eppendorf tube was placed inside a centrifuge tube (50 mL) filled with alcohol (methanol, ethanol or propanol) in different concentrations 10-100 wt % in water for all the alcohol gels prepared and stirred overnight (Figure 20). The alcohol solution was changed frequently and three repeats were completed for each alcohol concentration.

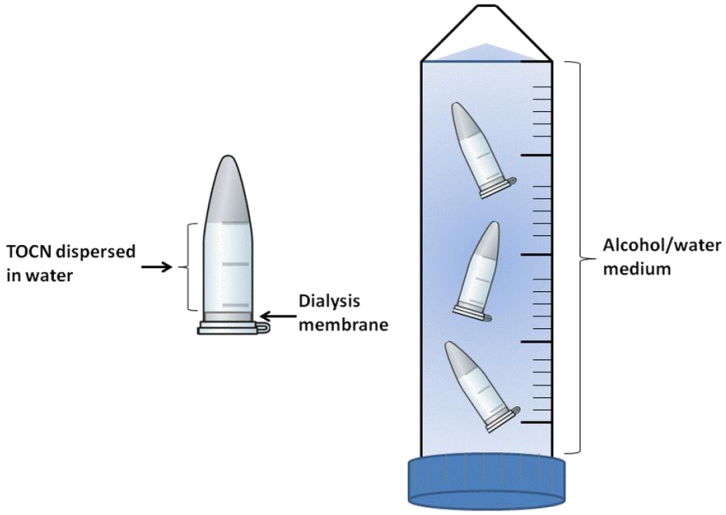

Figure 20: A schematic diagram of the process of alcohol-oxidised cellulose gel formation using dialysis membrane to carry out solvent exchange

Once solvent equilibrium was completed, the small eppendorf tubes were placed in a centrifuge at 11000 rpm for 10 minutes, any syneresis fluid present was decanted and the individual gel weights were recorded for the gravimetric analysis. The recovered gels were retained for use in the SAXS experiments.

For SANS experiments

The same procedure as described above was followed for the gels used in SANS experiments with the following modifications: the concentration of TOCN was also set to 0.8 wt % but it was dispersed in deuterium oxide (D_2O) instead of ultrapure water. The deuterated alcohols were 50:50 (w/w) mixtures for ethanol (d_1-ethanol:d_6-ethanol) and methanol (d_1-methanol:d_4-methanol). The selected hydrogenated solvents were d_1-methanol and d_1-ethanol which are partially deuterated.

For rheology measurements

For the purpose of rheology studies, at least 10 g of each gel was required therefore dialysis membrane tubes were filled with 0.8 wt% of cellulose dispersions (approximately 20 g) which were then placed in a larger container for solvent exchange with different alcohol concentrations of 10-100 wt % in water. The dialysis tubes were left to stir overnight, the alcohol/water medium was changed three times and the resultant gel was collected by centrifugation at 11000 rpm for 10 minutes and used for rheometric measurements.

2.3 Instrument Analysis

Small Angle X-ray Scattering (SAXS)

The SAXS experiments were carried out using an in-house Anton Parr SAXSess instrument in the University of Bath. The X-ray source for the in-house SAXS was a copper tube (40Kv/50mA, =0.1542 nm) on a PANalytical generator (PW 3830). The q range was 0.07-27 nm^{-1}. The cellulose gels were placed in a sample holder designed for gels where the gel is spread through the compartment of the sample holder which has clear windows to protect the sample from the vacuum. There are no other windows between the source and the detector. The measurements were completed in 4 hours at 25 ℃ for both the samples and the background (the medium the sample was in i.e. alcohol/water mix). The data obtained from SAXS measurements were reduced by electronic subtraction of the background and desmearing of the data with the software package. The NIST SANS Analysis package within IGOR PRO 6.2 was used to fit the model to the data.[194] The two models used for fitting the data were a cylinder with elliptical cross section[195] or a dilute lamellar form factor[196] . No structure factor was used for either of these model fittings due to the dilute nature of the samples. The SLD of oxidised cellulose was set and fixed to 1.35 x 10^{-5} $Å^2$ for both models. The SLDs of the solvents were calculated and also fixed during the fitting. For the cylinder with an elliptical cross section model, the length of the cellulose fibrils was set to 2000 Å since the length of the fibrils are several microns in size which is bigger than the range accessible using the SAXSess instrument and the minor radius was set to 18 Å for all the fittings. The

data was fitted to find the major/minor radius value and the scale. The polydispersity of the thickness was set to 0.3 for all the fitting using lamellar form factor model. The SLDs of the bilayer (cellulose) (the model was originally derived for fitting bilayer structures) and the solvent (alcohol or water) were also fixed during the fitting. The layer thickness and the scale were obtained from these fittings.

Small Angle Neutron Scattering (SANS)

SANS experiments were performed on the LOQ instrument[197] at the pulsed neutron spallation source ISIS at the Rutherford Appleton Laboratories, Didcot, UK. LOQ is a fixed geometry time of flight instrument with a q-range of 0.006–0.24 $Å^{-1}$ normally operating at 25 Hz, with a wavelength between 2.2-10 $Å^{-1}$. D_2O, deuterated ethanol (d_1:d_6) and deuterated methanol (d_1:d_4) were used to prepare the samples, providing the necessary contrast which was achieved by using either deuterated /hydrogenated alcohols or deuterated/hydrogenated SDS. For example, in the presence of h-SDS, d-alcohol was used to highlight the changes on the fibrils as well as to observe the effect of alcohol on the surfactant micelles. The oxidised cellulose was not deuterated. Samples were placed in clean 1 cm wide and 1 mm path length Hellma quartz cuvettes. The SANS data were normalized for transmission and subtraction of the empty cell and solvent background. IGOR PRO 6.2 was used to fit the models for the data. The same models for SAXS were also applied for the interpretation of SANS data. The neutron SLD of cellulose was calculated and kept constant at 1.5 x 10^{-6} $Å^{-2}$. The calculated SLDs were 3.2 x 10^{-6} $Å^{-2}$, 3.4 x 10^{-6} $Å^{-2}$, for the deuterated ethanol and methanol, respectively.

Rheology

The rheology measurements on the alcohol gels were conducted with a Discovery Hybrid Rheometer (Model HR-3) equipped with a small angle cone (2º gap) in the Unilever R&D labs at Port Sunlight. Oscillatory tests were carried out to evaluate storage modulus (*G′*), loss modulus (*G″*) and loss tangent (*tanδ)* as a function of frequency (*ω)* at 0.1 to 100 Hz. Each sample was transferred onto the rheometer plate

with the aid of a spatula and excess material was wiped off. All the measurements were carried out at 25 °C. The samples were covered by metal caps to prevent evaporation during measurements. Prior to the measurements, the linear viscoelastic region (LVR) for the cellulose-alcohol gel samples was determined by performing strain sweep measurements (0.01-100%) at constant frequency (1 Hz). Frequency sweep tests at a constant strain in the LVR region were carried out to determine the viscoelastic nature of the gels and the oscillatory sweep test was carried out within this region.

Scanning Electron Microscopy

Aqueous TOCN dispersion (0.8 wt %) was freeze-dried and immobilised on sticky carbon tape and gold sputter-coated prior to imaging. The TOCN-alcohol gels in ethanol (100 %) or methanol (100 %) were sliced into squares (2 x 2 cm) and critical point dried from CO_2 and also sputter coated with gold prior to imaging. The samples were imaged on a JEOL JSM6480LV scanning electron microscope at 10 kV in the imaging suite at the University of Bath.

2.4 Theory of Techniques

2.4.1 Scattering experiments

SAXS and SANS are powerful techniques for analysis of structures and structural changes of nanoparticles in solution. These techniques require small amounts of purified material. The scattering process takes places when X-rays or neutrons interact with the irradiated volume and cause scattering. The interaction of X-rays and neutrons are with different parts of the atom where X-rays interact mainly with electrons, neutrons interact with the nuclei and spin.[198] The measurement of scattering of a sample is often followed by the scattering measurement of the solvent the sample was in which is later subtracted to eliminate any scattering from the solvent and background scattering from the instrument. Therefore the scattering intensity from the sample (after the solvent subtraction) can be defined as:[199]

$$I(q) = P(q)\, x\, S(q) \qquad (10)$$

The form factor, *P(q)*, represents the scattering from individual particles and gives information about their structure whereas the structure factor, *S(q)*, is a result of interference of scattered waves emitted by different particles and contains information about the interparticle interactions and the structure of the solution. The structure factor was ignored in this study since the solutions were dilute and thus the interaction was at too long a length scale in the TOCN gels to be measured.

There are two types of scattering when an X-ray or neutron hits matter which are elastic and inelastic scattering. For this study, we will only focus on elastic scattering of X-rays and neutrons where the wavelength (λ) of incidence and scattered radiation is equal and no energy is lost during the process. The relationship between energy E and wavelength λ can be described as $E=hc/\lambda$, where X-rays photons with energy E have a wavelength $\lambda=h/mv$ and for the case of neutrons, $E= m_n v^2/2$ where v is the velocity and m_n is the mass of a neutron. When an object is illuminated by a monochromatic wave with modulus $k =|k|= 2\pi/\lambda$, atoms interacting with the incident radiation generate sources of waves. For elastic scattering (also known as Rayleigh or coherent scattering), the modulus of the scattered wave is $k' = |k'| = k$. In inelastic scattering (also known as incoherent or Compton scattering), the energy from incident radiation and the scattered radiation are not equal to each other.[199] Inelastic scattering occurs when a photon hits an electron and the scattered photons lose energy in comparison to incoming photons. Elastic scattering relies on momentum transfer $q= k' - k$ and is commonly used to study soft matter.

The scattering process is a result of change from the "real" space of lab coordinates, r, where the structure of the scattering object is defined, to "reciprocal" space of scattering vectors, q, in which scattered radiation is measured. In the Born approximation, this procedure is achieved by Fourier transformation. The Fourier transform generates reciprocal relationship between sizes in real and reciprocal spaces given that the smaller the real size, the larger the reciprocal size. This approximation then enables us to sum the contributions from all N atoms in the sample and find the net scattered wave from individual centres which is defined as *the scattering length* (units in cm). Based on this approximation, anything unrelated to atom x is not included in the summation and the scattered intensity only depends on $q= k' - k$ [200] (Figure 21).

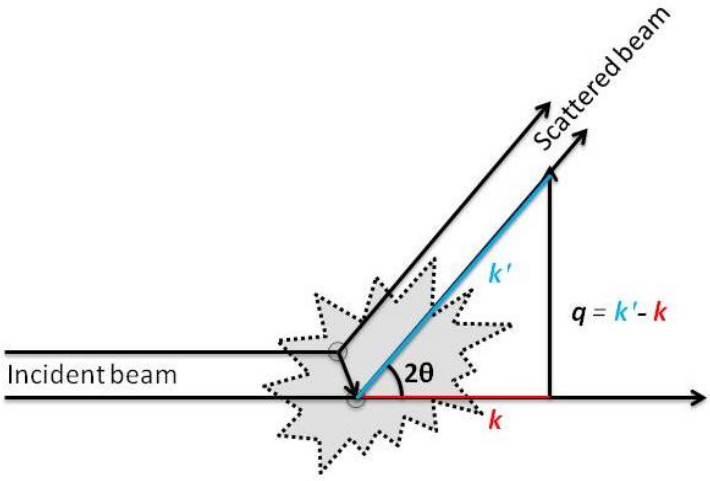

Figure 21 : A schematic diagram of elastic scattering where the incident beam is scattered through the angle 2θ by two individual scattering centres, separated by *r*, where $|q|$ = q = $(4\pi \sin\theta)/\lambda$. Figure redrawn from reference 198

In SAS the angle θ (scattering angle is 2θ) is less than 5º and the scattering vector q is defined as the difference between the incident and the diffracted wavevector. These wavevectors are equal to each other for elastic scattering and therefore the magnitude of wavevector is, $|\boldsymbol{q}|$, is equal to

$$q = |q| = \frac{4\pi sin\theta}{\lambda} \qquad (11)$$

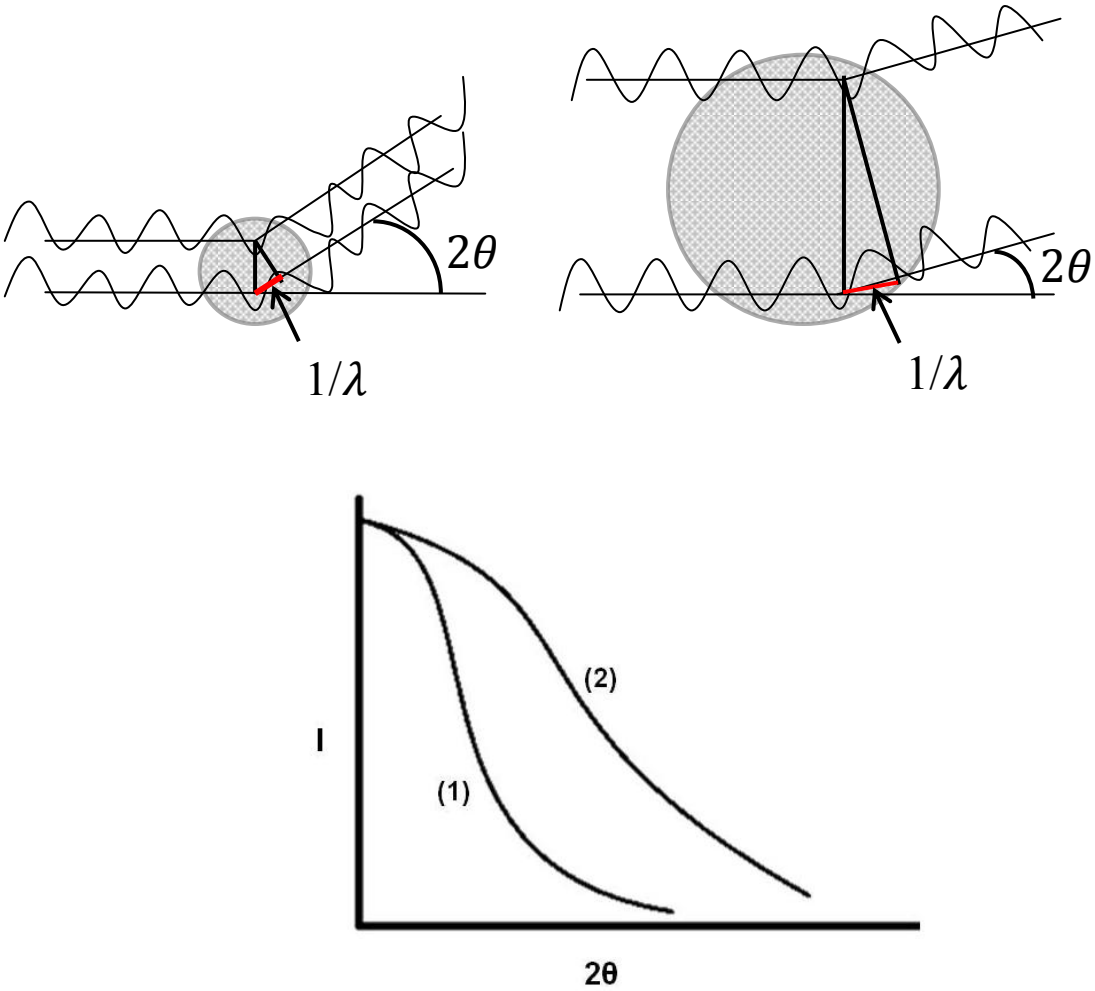

Figure 22: A diagram of scattering from particles with different sizes (top) and scattering curve from smaller (2) and larger sphere (1) (below). Image redrawn from reference 302.

As previously mentioned, the scattering experiments define matter in reciprocal space, therefore small objects will give large *q* values while large objects will result in small q values. The focus of this study has been on the analysis of low q regions. It is assumed that waves scattered from two points with an angle of 2θ will have a path length difference of $1/\lambda$ (Figure 22). The larger sphere will produce a narrower scattering curve that is closer to lower q regions.

X-rays interact with the electron cloud of a sample and therefore the scattering is dependent on the electron density of the sample. The position of individual atoms are unknown and in order to resolve this problem, the sample is considered as a particle with average material properties and the scattering can therefore be defined in terms

of the scattering length, as Zr_e, where Z is the atomic number of the atoms within the material and r_e is the electron radius equal to 2.81 x 10^{-13} cm.[201] On the other hand, for neutrons interacting with the nuclei, the scattering length is described as b_i and this value is previously measured for different atoms.[202] The scattering length of X-rays is linearly correlated to the atomic number whereas this is rather random for neutrons. The tabulated scattering lengths can be used to calculate the *scattering length density*,ρ, which is a key parameter especially for neutron scattering experiments. Scattering length density is defined as the ratio of the scattering length per molecule and the molecular volume.[203]

$$\rho = \frac{\sum_{i=1}^{n} b_i}{v_m} \tag{12}$$

Equation (12) shows the coherent scattering length, b_i, of the i^{th} of n atoms in the molecule (which is already calculated for all the atoms) and v_m is the molecular volume of that molecule. When X-rays are considered, b_i can be replaced with $Z_i r_e$ where Z_i is the atomic number of the i^{th} of n atoms and r_e is the radius of the electron. The molecular volume v is defined in terms of density d and molar mass m for a molecule and Avogadro's number (N_{av} 6.022 x 10^{23} mol^{-1}) as:

$$v_m = \frac{m}{N_{av} d} \tag{13}$$

Although X-ray and neutron scattering are different techniques, the theory and data analysis are very similar. The main difference is that X-ray scattering is sensitive to heavier atoms since they have more electrons and hence greater electron density. On the other hand, neutron scattering is related to the nuclear structure and has no correlation with the number of electrons. SANS is a much more gentle technique which does not induce radiation damage on the sample, however the main advantage of SANS is its sensitivity to isotopic composition of the samples, especially the difference in the scattering of hydrogen and deuterium. The contrast variation resulting from partially or fully deuterated materials can highlight parts of the molecule,or material, and reveal structural information about separate sections. The main issue with the X-ray radiation in this study was the damage they caused on the cellulose films. The disadvantage of SANS is that it is not available for use in individual laboratories unlike SAXS and it generates strong background noise due to

incoherent scattering when hydrogen is present. However, these advantages and disadvantages make these two techniques complementary to each other. [198]

2.4.2 Small Angle X-ray Scattering (SAXS)

X-rays are electromagnetic waves like visible light but have much smaller wavelengths than light, characteristically around 0.1 nm. X-ray scattering can be used to investigate structures of small particles.[45]

There are two main types of X-ray sources; X-ray tubes used in the lab instruments (continuous sources) and powerful synchrotron sources (pulsed sources using magnets). The SAXS measurements for this study were carried out on a laboratory instrument (SAXSess system). This instrument performs at a fixed wavelength of 0.154 nm, achieve q min values of 9 x 10^{-2} nm^{-1} and fluxes at the sample of 10^{8}-10^{9} photons s^{-1} mm^{-2} using a block collimator. [204]

The main components of a SAXS instrument consist of a source, collimation system, beam stop and a detection system which collects the data. The source illuminates the sample and the detector measures the radiation scattered from the sample in a certain range of angles. The collimation system (based on the type of collimation) makes the beam narrow and defines a zero angle position. The beam stop inhibits the intense incident beam hitting the detector which could damage the detector. The X-ray source for this system is an X-ray tube which has a filament (wire) and an anode (target) in a vacuum environment. When the electrical current heats up the wire, the electrons are emitted. Once a voltage of 40kV is achieved, this enables the electrons to move towards the anode. Deceleration takes place when the electrons hit the anode and cause the emission of the X-rays, which is called Bremsstrahlung.[204] A portion of the electrons that hit the atoms of the anode will remove electrons from these atoms and lead to emission of characteristic radiation of copper anode. The intensity of the X-ray tube (number of photons) is restrained by the power of the electrons that hit the anode. The electrons then collide with atoms in the sample and are scattered. Although, most of the energy is lost as heat, some is dissipated as a continuous spectrum of X-rays (which adds to the background). Because of the energy loss and weak electron source, the experiment for one sample takes much longer than at the synchrotron sources. The intensity of the scattering depends on the electron density dissimilarity of the sample.

One important facet of SAXS is the collimation system, which is required to keep the divergence of the incoming beam small so that scattering pattern can be easily identified. In order to achieve this, a collimation is put in place which consists of a system of slits or pinholes for the beam to permeate through (Figure 23). These systems need to be very narrow with the purpose of collimating the beam, an unfortunate side effect is that they also lower the intensity considerably.

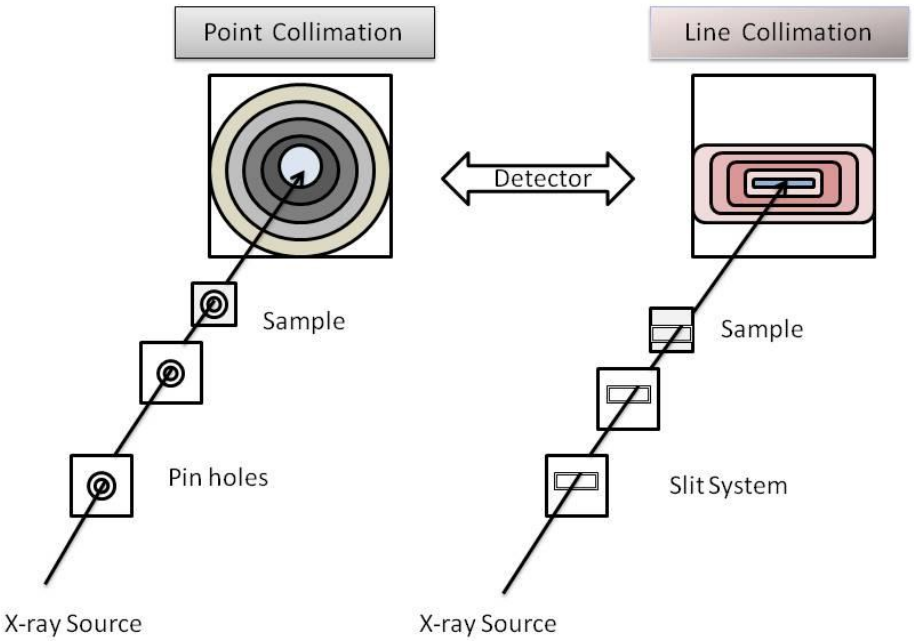

Figure 23: A diagram showing SAXS collimation types; point or line collimation. Image redrawn from reference 204.

The point-collimation system shapes the beam into small circular spots. Since only a small section of the sample is illuminated, the resolution is often very poor and it takes a long time (hours to days) to measure a scattering intensity of the sample. On the contrary, line-collimation system restricts the beam only in one dimension and this creates a long but narrow beam profile. Therefore the intensity of the scattering is much higher than the point-collimation system as more of the beam passes through this collimation system. The large sample volume however, brings the problem of significant signal broadening. Broadening (wavelength smearing) may also be attributed to scattering of photons from different wavelengths. Consequently, the beam profiles are measured first and using mathematical programs the broadening effect is eradicated. The treatment of data by these programs is called “desmearing” of the data. In this study, line-collimation was used for the SAXS measurements.

Another important part of the SAXS system consists of a beam stopper which is made from a transparent material to attenuate the beam for safe intensity before it reaches the detector. This has the advantage of measuring of the zero position of the beam at the time of the experiment. The detector used in SAXSess measurement was an imaging plate. These are made of a material that stores the X-ray energy by exciting the electrons of the material into so-called F-traps and the electrons can be restored by illumination with visible light. This in turn generates visible fluorescence radiation which is measured with an ordinary photo-multiplier. Imaging plates are flexible white sheets which are exposed like photographic films and are scanned by a device.[204]

Anything that is placed in the path of an X-ray beam including air produces scattering. Hence, the sample-to-detector distance is kept in vacuum. One downside of the vacuum system is that many samples need to be kept at ambient conditions as these may change when they are exposed to vacuum (e.g. by solvent evaporation). Therefore special sample holders are essential to meet the requirements of the samples and the sample thickness is typically smaller than or equal to 1 mm. The scattered intensity of a sample is proportional to product of $D\ exp(-\mu D)$, where D is the thickness of the sample and μ is the linear absorption coefficient of the material. This function reaches at maximum when $D=1/\mu$ which is equal to optimum thickness of the sample. In the case of X-rays, this is very close to 1 mm for a water sample at the photon energy of 8 keV, hence most X-ray sample cells have 1 mm path length.[198]

2.4.3 Small Angle Neutron Scattering (SANS)

SANS is a complimentary technique to SAXS, neutron scattering has many advantageous characteristics over X-ray scattering. These include sensitivity to elements and their isotopes, high penetration without damaging the sample and ability to label isotopes without affecting the structure.[205,206] It is a popular technique as: (1) the particle constituent does not have to be deuterated but instead the solvent can be deuterated in order to reduce the strong contribution from the incoherent scattering from the hydrogenated components, (2) the labelling can be selective, for example the path, chains or cross-links of a molecule can be highlighted by contrast

variation, and (3) due to the flexibility of sample holder types, one can observe swelling and elongation. [205,207,208]

LOQ was the main instrument used for the neutron scattering experiments (Figure 24). There are two main neutron sources: continuous reactors and pulsed sources. LOQ is on a pulsed neutron source, using time-of-flight (TOF) analysis to separate neutrons of different wavelengths, which presents a very wide *q* range coupled to good q resolution.[197] TOF is the time it takes a neutron to travel from a pulsed source to a detector.[209] The continuous reactors measure "some selected neutrons all of the time" while with pulsed sources, one measures "all of the neutrons at some selected time".[210] The main advantage pulsed sources is the use of a wide range of scattering vectors, and therefore sizes of scattering object, that can be measured in a single measurement, compared with using a fixed incidence wavelength in a conventional system. TOF SANS instrument includes some of the main features (collimation, sample chamber, flight paths, area detector etc.) but also in addition, (1) a source chopper is used to define the starting neutron pulse, (2) the area detector is synchronized to the source chopper so that a number of wavelength frames are recorded for each pulse, (3) no monochromator is required , and (4) a super-mirror bender can be used (for LOQ) to eliminate short wavelengths and let the instrument get out of the direct line of view from the source and this bender is used to substitute the filter. A frame overlap mirror removes the wavelengths higher than 12 Å. The sample is positioned 11.1 m from the moderator and an aperture is used to define the beam size. The sample transmissions are measured by placing a monitor after the sample and decreasing the beam diameter between the sample and the monitor to 1 mm.[211]

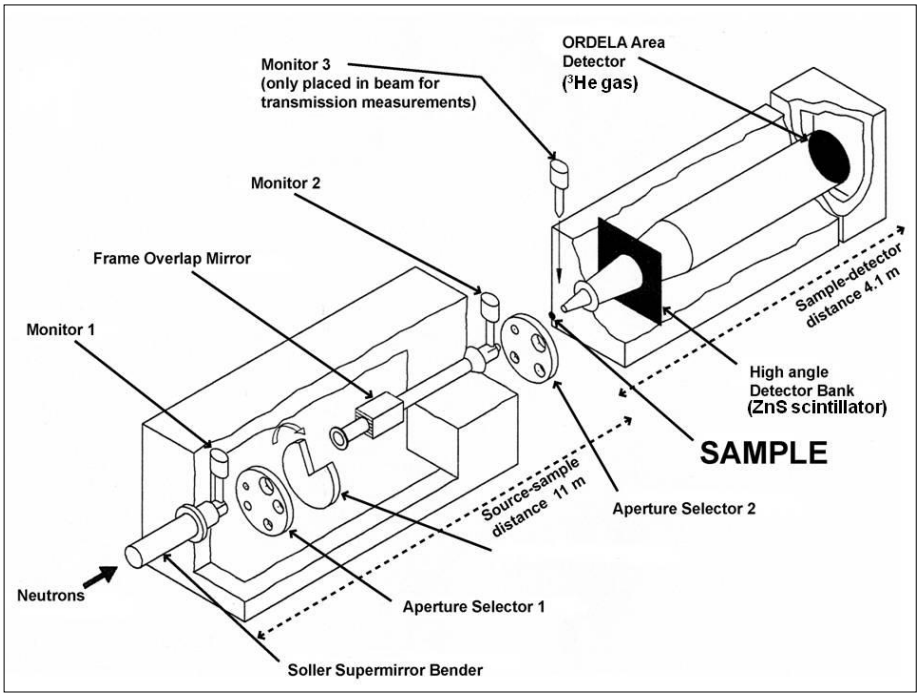

Figure 24: LOQ instrument, reproduced from reference 303.

In a spallation source, a pulsed neutron beam is formed by collision of high-energy protons (generated by a particle accelerator) with heavy metal atoms such as tungsten or uranium which forces the neutrons out from nuclei of the atom. The neutrons arrive in pulses and not continuously as they do if generated by fission in a reactor and no monochromatic beam is required, therefore all neutrons could be used instead of selecting the ones based on a narrow energy band. The beam of highly energetic spallation neutrons is then attenuated by a moderator.[209] The most common detectors for neutron scattering instruments are filled with ^{3}He gas as the detection medium and CF_4 as stopping gas. When a neutron is absorbed by helium gas, a fission reaction occurs which is followed by emission of two charged particles (one tritium and one proton) in opposite directions inducing the primary ionisation in gas.[211] The data reduction is more complex for time of flight instruments as the corrections are wavelength dependent but overall they have the advantage of measuring a wide q-range at once.[210]

2.4.4 Contrast variation

The small angle scattering arises from changes in electron density (for X-rays) or scattering length density (for neutrons) in solutions.[198] The difference between the electron densities or scattering length densities of particles, polymers, proteins or micelles in solution and the solvent they are surrounded by is called *the contrast.* It is an important parameter in scattering experiments and without contrast it is not possible to distinguish the signals arising from the sample from those arising from the solvent it is in. The method of changing the contrast of one part of the sample in order to highlight or hide that section of the system and extract the required information is defined as the *contrast variation method.*[199] This is the most valuable feature of neutron scattering. In SAXS, differences in the electron densities can be achieved by using salts or heavy-metal ions. However, this may affect the structure of the system; therefore contrast variation with X-rays is a limited method and makes neutron scattering more advantageous. In SANS, the contrast variation is resolved by exchanging hydrogen for its heavy isotope deuterium without much alteration to the physical structure of the sample. Because hydrogen is not a good coherent scattering atom, its use in neutron scattering has been limited and changed to deuterium where possible. The neutron scattering length densities vary significantly between these atoms hence enabling us to highlight different parts of the structure due to different scattering (Figure 25). For example, the SLD for H_2O is -0.562 x 10^{-6} $Å^{-2}$ and for D_2O 6.33 x 10^{-6} $Å^{-2}$. There are two approaches to create this contrast variation. One is achieved by solvent exchange via dialysis (24 hours is adequate) in order to enable the solution and the buffer to be in the same H/D equilibrium and hence to calculate the SLD accurately. The other option is to selectively label a part of the structure where it is specifically perdeuterated. In this study, this was achieved by purchasing the desired deuterated product where possible. It is also possible to completely hide certain parts of a sample by mixing H_2O and D_2O at specific volumes in order to give a scattering length density that is identical to the part of the sample to be hidden. Figure 25 shows a schematic illustration of a sample of polymer/surfactant mixture in a solvent. By deuteration of certain parts of the compound, we can then highlight the structures we are interested in.

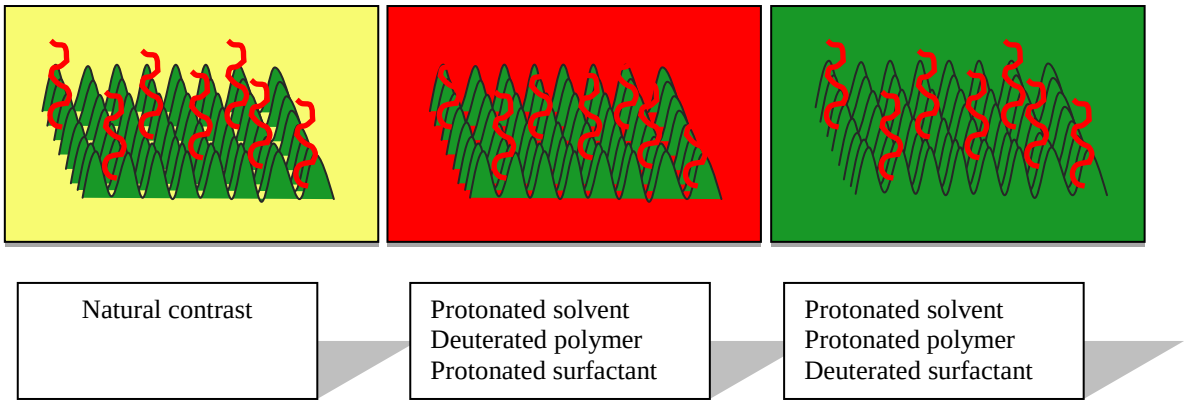

Figure 25: Schematic illustration shows selective deuteration by contrast variation, where the specific areas in the structure can be highlighted.

A protonated structure has a high incoherent scattering length and very small coherent scattering length and for this reason the scattering from the compounds with hydrogen will be strong but overshadowed by the high incoherent signal which gives rise to the high background often seen in SANS measurements. Meanwhile, a deuterated structure has a small incoherent scattering length and often a large positive coherent scattering length, hence the scattering from deuterated compounds is dominated by coherent scattering which occurs from two particle correlations, and therefore contains detailed structural information making it an excellent technique to employ.

2.5 Models used for scattering experiments

The scattering data obtained both from SAXS and SANS experiments were fitted using various models in the NIST SANS analysis package written within IGOR™ Pro 6 (Wavemetrics).[194] The models used include a cylinder with elliptical cross section, lamellar sheets and a cylinder with elliptical cross section combined with sphere (for TOCN formulations containing high surfactant concentrations).

2.5.1 Cylinder with elliptical cross section:

This model calculates the form factor for a cylinder with uniform scattering length density and an elliptical cross section. The form factor is averaged over all possible orientations before being normalised by the particle volume such that P(q) = contrast*scale*<f^2>/Vol + bkg, where < > denotes an average of over all possible orientations of the cylinder.[194]

The scattered intensity function calculated is:

$$I(q) = scale \cdot \int_0^1 \Psi_{ec}\left[q, a(1-x^2)^{\frac{1}{2}}\right] S^2\left(\frac{qHx}{2}\right) dx \; + bkg \qquad (14)$$

With the functions:

$$\Psi_{ec}(q,a) = \frac{1}{\pi}\int_0^{\pi} \Lambda_1^2 \left[qa\left(\frac{1+v^2}{2} + \frac{1-v^2}{2}\cos(y)\right)^{1/2}\right] dy \qquad (15)$$

Where:

$$\Lambda_1 = 2J_1(t)/t \qquad (16)$$

The angle Ψ is the rotational angle around its own long *c*-axis against the *q* plane.[212] For example when the minor axis is parallel to the x-axis of the detector then, the angle Ψ, equals = 0. $J_1(x)$ is the first order Bessel function (used to calculate cylindrical coordinate systems). The fitted intensity value is in units of [cm^{-1}], on absolute scale. The elliptical cylinder is shown in Figure 26 with a total length *H*, minor radius *a*, and major radius *va*.

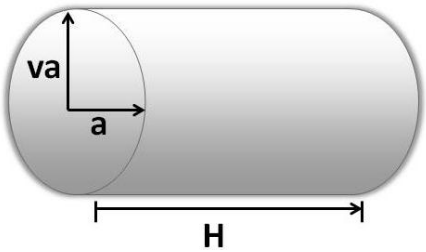

Figure 26: Elliptical cylinder model

The ellipticity, *v* is defined as $v=r_{major}/r_{minor} \geq 1$. The volume of the cylinder is given by:

$$V = \pi v a^2 H \quad (17)$$

The parameters of this model are scale, minor radius (Å), major/minor radius (Å), length (Å), SLD of cylinder (cellulose), SLD of solvent ($Å^{-2}$) and background.

2.5.1.1 Dilute lamellar form factor

This model calculates the form factor from a lyotropic lamellar phase which resembles the thin sheet of cellulose fibrils. The intensity calculated is for lamellae of uniform scattering length density that are randomly distributed in solution. The thicknesses of the lamellae are polydisperse and no interlamellar structure factor is calculated.[194]

The model calculates the scattered intensity *I(q)* in units of cm^{-1} as [196]:

$$I(q) = \frac{2\pi P(q)}{\delta q^2} \quad (18)$$

Where the form factor is given by:

$$P(q) = \frac{2\Delta\rho^2}{q^2}\left[1 - \cos(q\delta)e^{-q^2\sigma^2/2}\right] \quad (19)$$

Where δ is layer thickness and σ is variation in layer thickness (polydispersity). The fitting parameters of this model are scale, layer thickness (Å), polydispersity of thickness, SLD of layer ($Å^{-2}$) and SLD of solvent ($Å^{-2}$).

2.5.1.2 Sphere

This model was combined with the elliptical cylinder model to fit the data of high concentration sodium dodecyl sulfate samples to approximate the micelle scattering added to that of the cellulose fibrils. It calculates the form factor, *P(q)*, for a monodisperse spherical particle with uniform scattering length density. The fitting variables for this model is radius (Å) (for SDS molecule), SLD of sphere (for SDS

molecule) and SLD of solvent (for alcohol or water). The form factor is normalized by the particle volume and calculated by [194,213] :

$$P(q) = \frac{scale}{V}\frac{[3V(\Delta\rho)(\sin(qr) - qrcos(qr)]^{2}}{[(qr)^{3}]} + bkg \qquad (20)$$

Where the *scale* is equal to scale factor* volume fraction, V is the volume of the material, r is the radius of the sphere, bkg is the background level and $\Delta\rho$ is scattering contrast i.e. SLD (micelle core) - SLD (solvent).

In the systems with no inter particle interaction, the form factor can be related to the intensity by Φ, the particle volume fraction :

$$I(q) = \Phi P(q) \qquad (21)$$

2.5.2 Rheology

Brockel *et al.*[214] define rheology as the science of deformation and flow of matter. The rheological behaviour of the material can be described as Newtonian viscous liquids (liquids with small molecules or non-interacting particles) or Hookean elastic solids (such as rubber). However, the rheology of a material is often defined by both viscous and elastic characteristics.

According to Newton's law the relationship between $\sigma$the shear stress, $\dot{\gamma}$ the shear rate and $\eta$the viscosity, is given by:

$$\eta = \sigma/\dot{\gamma} \qquad (22)$$

where $\sigma = F/A$ is the shear stress and $\dot{\gamma} = v/h$ is the shear rate. A is defined as the surface area on which the shear force F is acting and h is the volume it moves with v velocity from minimum to maximum.[214]

A fluid that follows this pattern is called *Newtonian* and its viscosity is independent of the shear rate applied. Examples of such fluids include glycerine, water and mineral oil. Materials used in personal care products, or combined in such

formulations, often display *non-Newtonian* behaviour as the viscosity can decrease with the increasing shear rate and therefore, they present a shear thinning characteristics. Shear thickening compounds (dilatants) display an increase in viscosity as the shear rate increases.

On the other hand, Hooke's law is used to describe the elastic behaviour of solids states that the stress is directly proportional to strain given by:

$$\sigma = \gamma \, G \tag{23}$$

where γ is the deformation and G is the shear modulus describing the stiffness of the material. When a stress is applied to a material, deformation occurs and this deformation per unit length is defined in relative terms by strain. The shear strain is formed by the application of a shear stress which is shown in Figure 27.

$$\text{Stress } \sigma = \frac{F}{xy}$$

$$\text{Strain } \gamma = \frac{\Delta x}{z} \cong \alpha$$

$$\text{Shear modulus } G = \frac{d\sigma}{d\gamma}$$

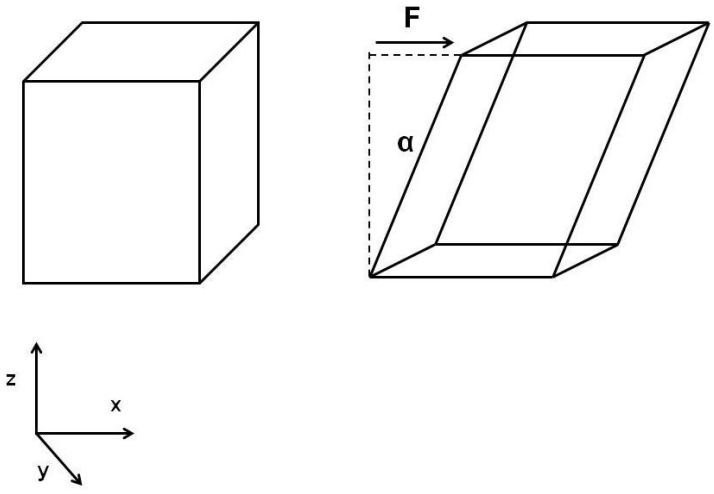

Figure 27: The relationship between the shear strain and shear stress, redrawn from 215.

The shear modulus of an ideal elastic material is independent of the shear stress and the time it takes for shear load. The viscoelastic materials, at constant deformation, relax steadily over time. When this stress relaxation is proportional to strain, this is called linear viscoelastic regime (LVR). Beyond a critical strain, the shear modulus begins to be dependant on the strain and this is referred as non-linear viscoelastic

regime. The linear viscoelastic behaviour of material can be determined by oscillatory shear tests where it is possible to measure viscous and elastic behaviour of the material at the same time. [215].

Cone and plate rheometers can be used to carry out this test where the sample is placed between the plates and while one rotates the other remains stationary.[216] The essence of the oscillatory test is applying sinusoidal shear strain with amplitude,γ_0, and measuring the stress response determined by angular frequency ω and the deformation $\gamma(t)$:

$$\gamma(t) = \gamma_0 \sin(\omega t) \tag{24}$$

where t represents the time. A linear viscoelastic liquid behave with sinusoidal wave of shear stress $\sigma(t)$ with amplitude σ_0 and angular frequency ω and a phase shift by an angle δ will be observed (Figure 28):

$$\sigma(t) = \sigma_0 \sin(\omega t + \delta) \tag{25}$$

Based on the type of the material, the phase shift angle δ takes place between 0° and 90° (Figure 28). If the material is elastic then the phase shift vanishes ($\delta = 0°$) whereas for ideal viscous liquids phase shift is δ =90°.

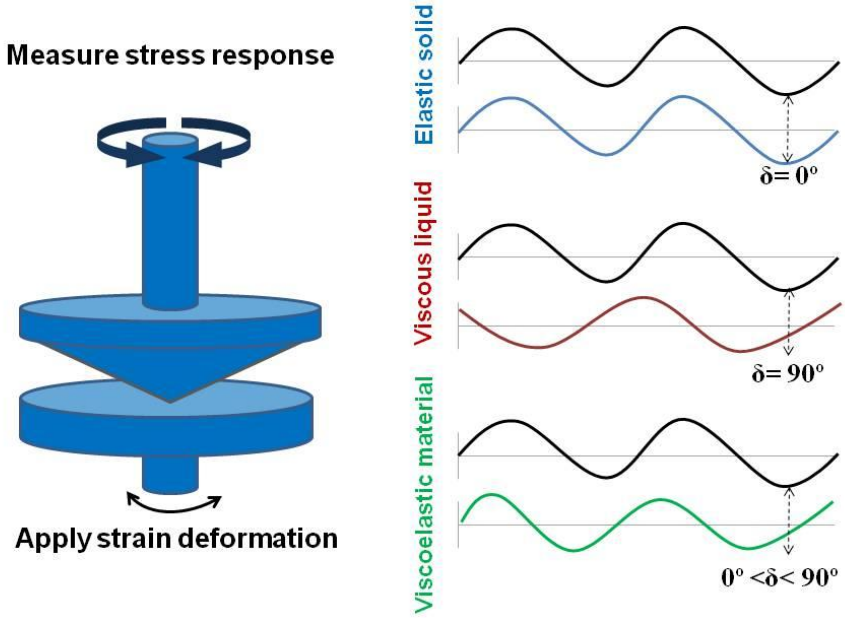

Figure 28: Cone & plate rheometer used for oscillatory test (left) and the stress response of different materials at constant strain, redrawn from 216.

The shear modulus can be defined as:

$$G^*(\omega) = G'(\omega) + iG''(\omega) \tag{26}$$

where G' is the storage modulus which quantifies the energy stored during the deformation by constant strain and signifies elastic behaviour of the material, on the other hand $G''$is the loss modulus that is the energy lost as heat during the shear cycle and signifies the viscous behaviour of the material. The G' and G''can be conveyed in terms of sine and cosine function of the phase shift angle δ:

$$G'(\omega) = \frac{\sigma}{\gamma} cos\delta \tag{27}$$

$$G''(\omega) = \frac{\sigma}{\gamma} sin\delta \tag{28}$$

Therefore the tangent of the phase shift would give the ratio of loss modulus to storage modulus:

$$tan\delta = \frac{G''(\omega)}{G'(\omega)} \tag{29}$$

And the complex viscosity is defined as

$$\eta^*(\omega) = \frac{\sigma(t)}{\dot{\gamma}(t)} = \eta'(\omega) + i\eta''(\omega) \tag{30}$$

The viscoelastic nature of the material can be measured by oscillatory measurements by performing frequency and amplitude sweep. This test was done for the cellulose alcohol gels and the shear rate tests were carried out for the ibuprofen loaded cellulose alcohol gels. Figure 29 shows the frequency response of oxidised cellulose-ethanol gel by oscillatory measurement. The viscoelastic behaviour of oxidised cellulose in ethanol was dominated by the elastic component, G′ (storage modulus), which is an indication of solid-like behaviour.

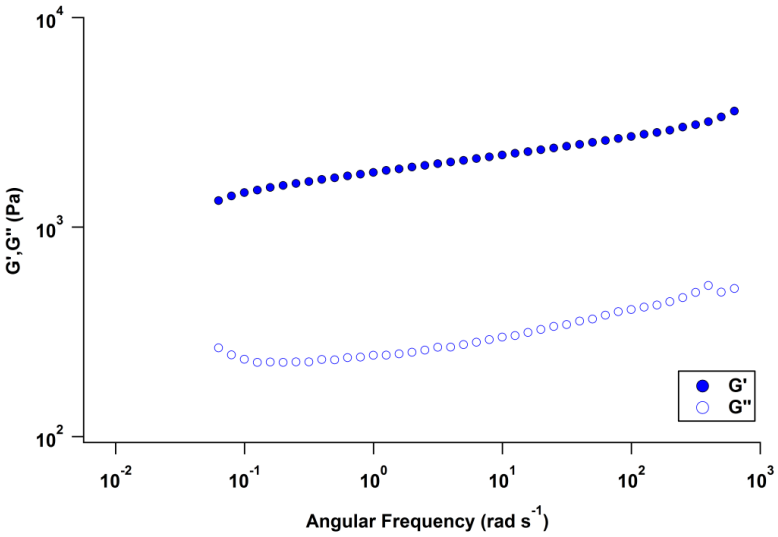

Figure 29: An example of frequency response of oxidised cellulose-ethanol (60 wt %) gel, representing storage (G') and loss (G") modulus

2.5.3 Scanning electron microscopy (SEM)

The scanning electron microscope is the most popular type of electron microscopes. SEM allows analysis of the microscopic structures at great resolution and better depth of field than transmission electron microscopy (TEM). An SEM image is observed when a focused electron beam scans over the surface area of the sample and the image is a three dimensional due to the large depth of field feature of the instrument which enables one to measure up to tens of micrometers at 10^3 x magnification.[217] A scanning electron microscope contains an electron gun (the source of electrons is often a tungsten filament), various electromagnetic lenses (including condenser lenses and one objective lens) and apertures. The electron beam emitted from an electron gun moves to a fine probe which scans the surface of the specimen. The signal electrons emitted from the sample are then collected by the detector and used to generate a 3-D image. One major advantage of SEM over TEM is the ease of sample preparation where the sample is not required to be too thin. On the other hand, if the specimen is not conducting, then the specimen could undergo electrostatic charging when exposed to electron probe. This charging can be prevented by coating the surface of the specimen with a thing film of metal (such as

gold) or conducting carbon. The coating is done in vacuum by an evaporation, or sublimation technique and a coated film of thickness 10-20 nm will prevent charging of most specimens. This thickness allows the scanning electron signal to come from the coating directly rather the sample itself since it is greater than the scanning electron escape depth.[218]

2.6 Results and Discussion

The aim of this chapter is to determine the effect of low molecular weight (LMW) alcohols and sodium dodecyl sulfate on TOCN gels, with and without sodium chloride. The changes in the TOCN-alcohol gels are first shown by gravimetric analysis and effect on gel rheology. This is then followed by description of the results of SAXS and SANS experiments, showing the changes in the fibril aggregate sizes as well as the impact the LMW alcohol has on micellization.

2.6.1 Gravimetric analysis of cellulose-alcohol gels

A previous study by Crawford et al.[1] reported that dispersed TEMPO-oxidised cellulose fibrils formed shear thinning gels in the presence of surfactants and salts. The gelation of TEMPO-oxidised cellulose-surfactant dispersion is not hindered by the addition of low MW alcohols. The effect of surfactant and salts on oxidised cellulose-alcohol gels can be seen in Figure 30.

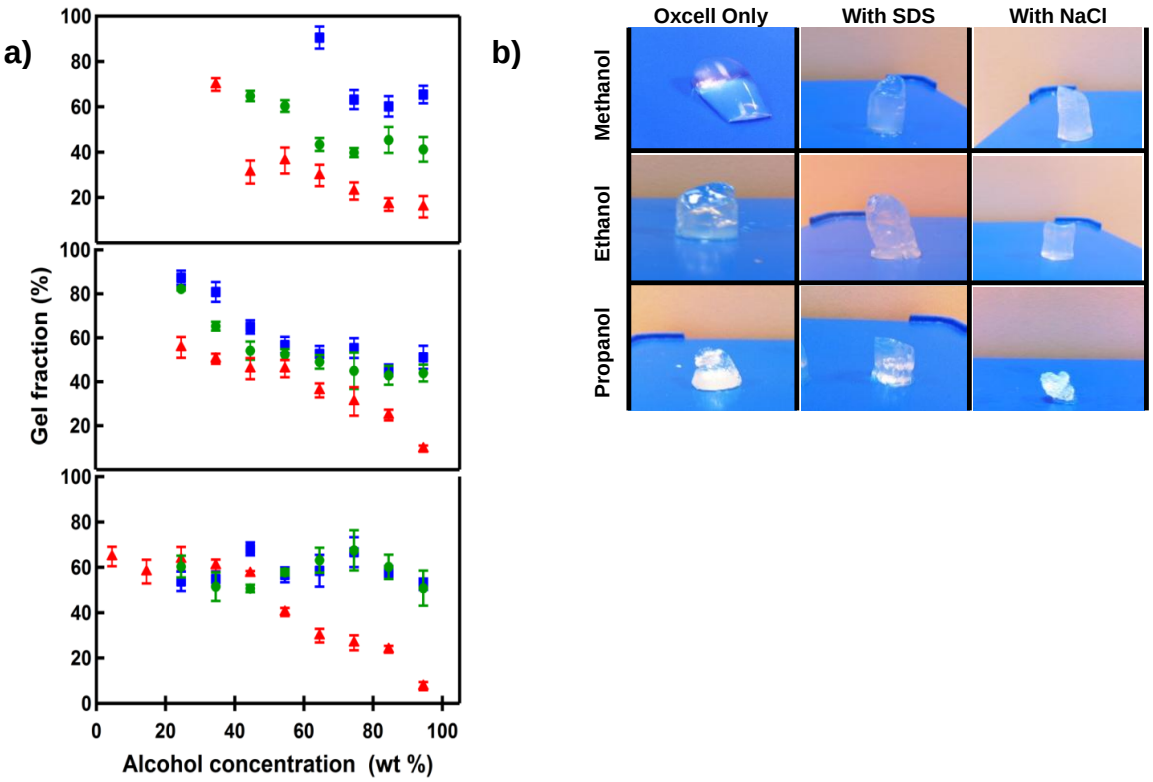

Figure 30: a) Gravimetric analysis of TEMPO-oxidised cellulose-alcohol gels . The graphs shows alcohol gels with no additives (top graph), with SDS (middle graph) and with NaCl (bottom graph); methanol (■), ethanol (●) and propan-1-ol (▲). b) Images of TEMPO-oxidised cellulose-alcohol gels in 100 wt % alcohol: oxidised cellulose only, with SDS and with NaCl.

The TOCN gels in aqueous medium formed shear thinning soft gels. The stiffness of the gels increases with increased anionic surfactant concentration. The gels in the presence of surfactants are stiffer than the gels with NaCl.[1] The top graph in Figure 30a shows the gravimetric measurements made on oxidised cellulose-alcohol gels with no SDS or NaCl where the gelation becomes significant in the presence of > 70 wt % methanol and at > 50 wt % ethanol and propan-1-ol. The trend for the alcohols was similar when SDS was added however, in the presence of propan-1-ol the gel became firmer at lower concentration, finally forming a firm solid, rather than a gel, once the concentration of alcohol increases >70 wt % (Figure 30b). The images in Figure 30b illustrate the difference in appearance of the gels containing propan-1-ol compared to those with the methanol and ethanol. In all cases the quantity of gel recover post centrifugation was lower in the absence of SDS or NaCl (Figure 30a).

The methanol and ethanol gels in the presence of SDS follow a similar trend where the gel mass proportionately decreases as the concentration of alcohol is increased. On contrary propan-1-ol which is a relatively more hydrophobic alcohol, the gel formation displays a steadier and steeper decrease in gel quantity.

The addition of NaCl results in a similar decreased in gel quantity for TOCN gels containing methanol and ethanol but it has a more significant effect on propon-1-ol-TOCN gels where the aggregated gel particles were detected >70 wt % propan-1-ol.

The dielectric constant (ε) of a solvent is indicative of the polarity of the solvent, where a high value of ε indicates higher polarity. This value for water is higher (ε = 78) than the alcohols used where the order of magnitude is listed as methanol (ε = 33)> ethanol (ε= 25)<propanol (ε =20).[219] More polar solvents (with higher dielectric constants) have the ability to effectively screen the attractive, or repulsive, forces between ions, which weakens the charge attraction between ions of the solutes.[219] This may suggest why significant differences in gel quantity (and gel density) and gel stiffness result in formulations with varying LMW alcohol concentrations.

Fukuzumi *et al.*[54] also mentioned aggregation in TOCN gels in aqueous dispersion for NaCl concentrations above *0.1 M* suggesting that the stability of the gels was affected by the concentration of salt present in dispersions. The gels become more dense (smaller quantity recovered) as the fibrils network shrinks, holding less water as the salt content increases. The gravimetric analysis results illustrate the gel mass percentage in a decreasing trend as the concentration of alcohol increases. As the alcohol content increases the gels become denser and are able to hold less solvent and so they shrink.

2.6.2 Rheology studies

According to Crawford *et al.*[1] partially oxidised cellulose nanofibrils (aqueous) form shear thinning (non-Newtonian) gels which are optically clear. The SAXS patterns of the gels were measured under shear and no alignment of the fibrils were detected even at high shear rates. They suggested that the links forming gels are soft and labile. The viscoelastic properties of the gels depended on the concentration and the type of the alcohol but also on the SDS and the NaCl content. The complex viscosity ($|\eta^*|$) was three orders of magnitude higher for the gel containing SDS and 30 % propanol, compared to a TOCN gel with SDS dispersed in water (Figure 31). As expected from the relative quantities of gel recovered (and thus gel density and "concentration" of fibrils), the viscosity of the gels was dependent on the medium in which the TOCNs were dispersed and decreased in the order of propanol > ethanol > methanol> water. Overall, the gels dispersed in propanol were thicker compared to the TOCN gels formed using methanol and ethanol.

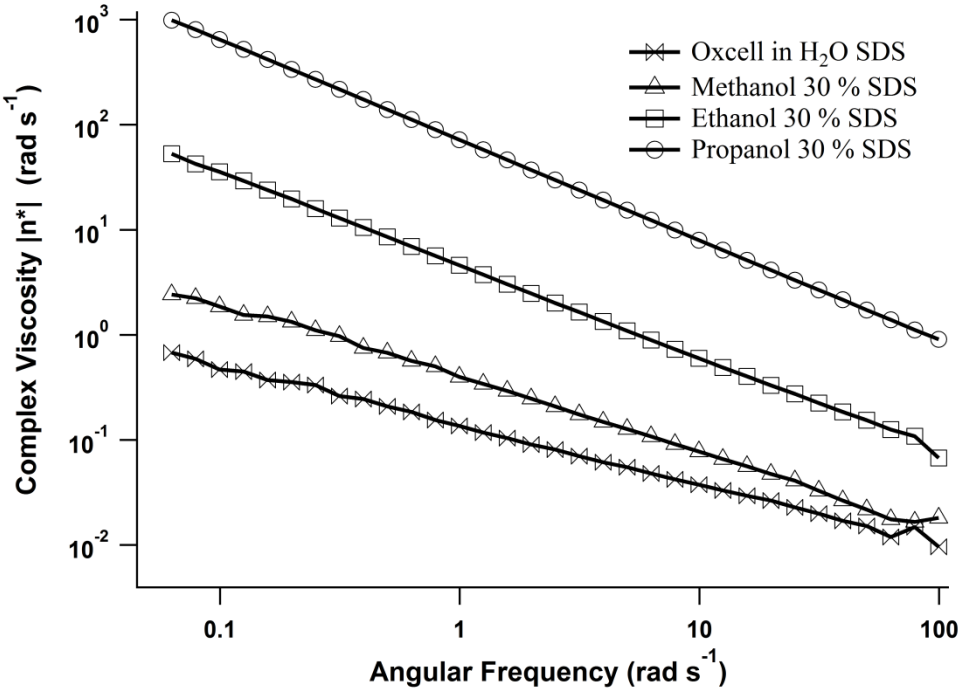

Figure 31: The effect of the solvent on the complex viscosity of TOCN gels (0.8 wt %) with SDS (40 mM)

Lu *et al.*[220] also shows the effect of NaCl on the gelation of nanocrystalline cellulose where the viscosity of the gels increase with the increase in salt concentration. According to a study by Crawford *et al.* [1] the TEMPO-oxidised cellulose nanofibrils, when dispersed in water, forms shear thinning gels in the presence of surfactant and salts. They suggested the clear gels were formed at NaCl concentration of 0.05-0.3M but at higher concentrations, syneresis would take place (without centrifugation as per these experiments). The concentration of salt for this study was kept at *0.2 M*.

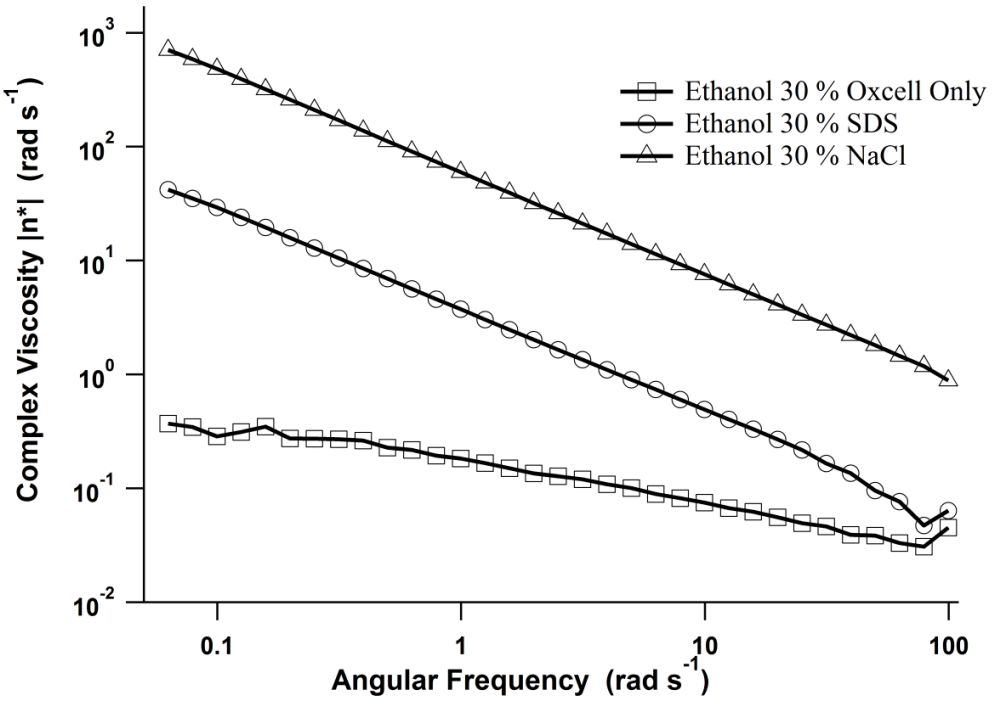

Figure 32: Effect of SDS and NaCl on the viscosity of TOCN gels dispersed in 30 % ethanol

In the earlier study it was suggested that the gels were stiffer in the presence of SDS, compared to NaCl but this was when the TOCNs were dispersed in aqueous medium.[1] This, however, was not the case when the TOCN was dispersed in LMW alcohols, such as ethanol. The complex viscosity of the gel was three magnitudes higher when salt was added to TOCN in 30 % ethanol (Figure 32). This could be due to charge screening by NaCl of negatively charged fibrils, reducing the electrostatic forces between the fibrils, hence allowing these to approach each other more closely forming a denser network, with more cross-links (contact points) between fibrils, leading to thicker gels.

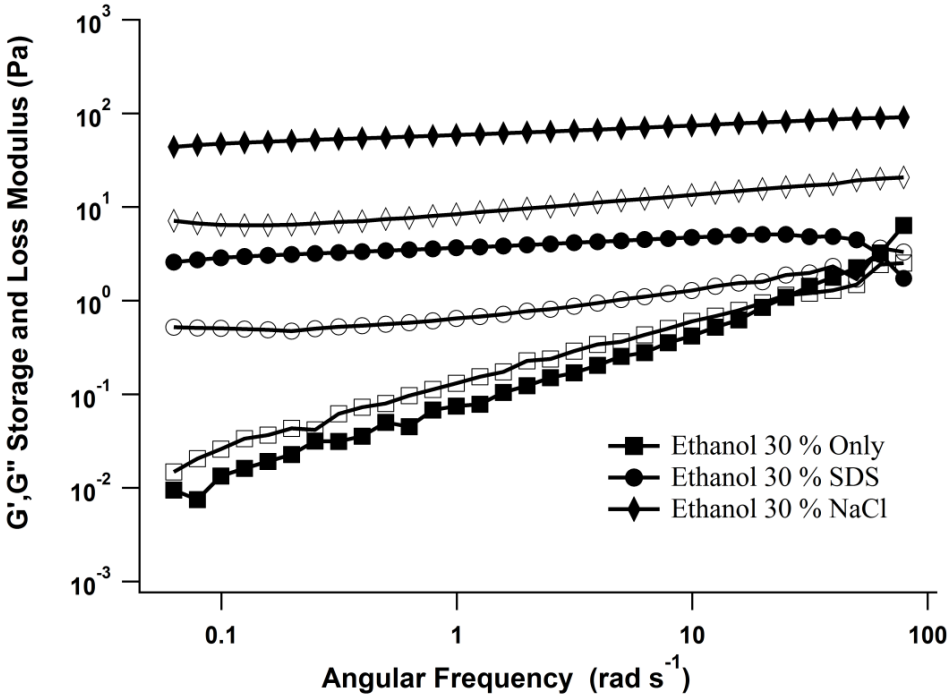

Figure 33: Frequency sweep for TOCN-ethanol gels (30 wt %) with SDS and NaCl. Open points show the storage modulus (G′), closed points indicate loss modulus (G″)

The oxidised cellulose-alcohol gels were characterised by oscillatory measurements of storage modulus (*G′*) and loss modulus (*G″*) where the data values were obtained over the range of 0.1-100 rad s^{-1} frequency (Figure 33). The storage modulus can be used as a measure of the elastic component of the sample and similarly, the loss modulus as a measure of the viscous component of the sample. Oscillation sweeps were carried out by applying sinusoidal strain and therefore the sample is continuously excited below the critical strain in order not to damage the sample. The elastic structure of the sample would be destroyed if the sample was overstrained , therefore prior to the experiments , the linear viscoelastic region (LVR) of the gels were measured and the frequency sweep tests were carried out at this range only. In Figure 33 it is clear that the storage modulus (G′) was about one magnitude higher than loss modulus (G″) for the gels with SDS and NaCl, which is indicative of a true gel. However, this was not the case for the TOCN gels with 30 wt % ethanol (no SDS or NaCl) where there was no plateau at lower frequencies and G″> G′, which is a sign of liquid-like material.[221–223] On the other hand, the loss and storage modulus were independent of the frequency for the gels containing SDS and NaCl which is

indicative of a gel with fibrillar network and shows a characteristic of shear thinning nature.[224,225]

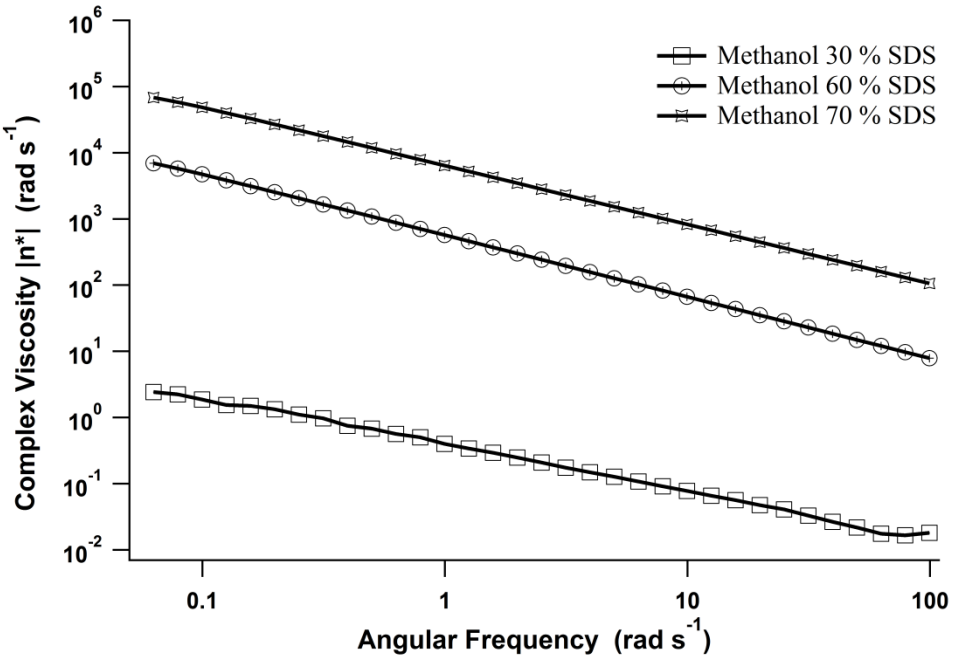

Figure 34: The effect of alcohol concentration on complex viscosity

The concentration of alcohol also plays an important role on the complex viscosity of the TOCN gels with SDS. Figure 34 shows the significant difference between the gels with 30 wt % methanol and 70 wt % methanol. This difference was also seen in the gravimetric analysis where the gel fraction was reduced by almost 20 % across these concentrations. The complex viscosity was 4-5 fold higher for the gels with 60-70 wt % methanol content.

2.6.3 Small angle X-ray scattering (SAXS)

SAXS was used to understand the effect of the alcohols and additives, SDS and NaCl on the aggregation state of the cellulose fibrils where two main fitting models were used; i) elliptical cylinder ii) lamellar structure for the networked/aggregated fibrils. This was combined with a sphere form model for the SDS when necessary to represent the micelles. Table 3 presents the results of fitting the data using the two different models. In most of the alcohol/water suspensions up to 40 wt %

concentration, the structure of the network of fibrils is best represented using an elliptical cylinder (which can assemble into a network at a larger length scale than directly detectable here), but in gels with concentrations above 40 wt % alcohol, a change towards the lamellar structure (for aggregated TOCN) is observed (see Table 3). This trend is true for oxidised cellulose gels with no additives and with SDS, but is not the case with NaCl where there is no clear trend. This might be due to the insolubility of salt in solvent mixtures with higher alcohol concentrations. According to Pinho *et al.*[226], the solubility of salt in water (at room temperature) is around 26.4 wt % whereas it is only 1.3 wt % and 0.05 wt % in dry methanol and ethanol respectively. Thus, it is possible that salt became precipitated and its effect on cellulose fibrils was thus not observed.

The elliptical cylinder model includes parameters such as minor radius of the elliptical cross-section of the fibril and major/minor ratio. The minor radius was kept constant for all the gels. This model calculates the form factor for a cylinder with uniform scattering length density and an elliptical cross section.[195] The lamellar model is used to calculate the layer thickness of sheet-like structures. Inter-lamellar structure is not taken into account with this model.[196]

Table 3: SAXS fitting matrix for cellulose-alcohol gels, the models fitted E (elliptical cylinder),L (lamellar), B (both), N (not measured).

	Alcohol wt %	10%	20%	30%	40%	50%	60%	70%	80%	90%
TOCN Only	Methanol	E	E	E	E	E	E	L	L	L
	Ethanol	E	E	E	E	L	L	L	L	L
	Propan-1-ol	E	E	E	E	L	L	E	N	N
With SDS	Methanol	E	E	L	B	B	L	L	L	L
	Ethanol	E	E	L	L	L	L	L	L	L
	Propan-1-ol	E	E	E	L	L	L	L	N	N
With NaCl	Methanol	E	E	E	L	L	L	L	L	L
	Ethanol	L	L	L	L	B	B	B	L	L
	Propan-1-ol	L	L	L	L	L	L	L	N	N

Table 4: SAXS data fitting results for TOCN in lower alcohol content, with no additives, using elliptical cylinder model, with a fixed minor radius of 18 Å and a fixed cylinder length of 2000 Å

TOCN Only	Methanol		Ethanol		Propanol	
Alcohol concentration (%)	20	40	20	40	20	40
Major/minor radius ratio	2.6±0.3	2.9±0.2	3.8±1.1	2.6±1.3	2.8±0.2	2.6±0.2
Calculated SLD of TOCN (x 10^{-5} $Å^{-2}$)	1.35	1.35	1.35	1.35	1.35	1.35
Calculated SLD of solvent (x 10^{-6} $Å^{-2}$)	9.08	8.72	9.04	8.64	9.06	8.67

Alcohol-TOCN gels were all fitted to elliptical cylinder and lamellar model, based on the chi-square values obtained, χ^2, the model with the lowest χ^2 was chosen for that particular gel. Table 4 shows the parameters obtained when the elliptical cylinder model used was to fit the scattering from the TOCN gels in methanol, ethanol and propanol at 20 and 40 wt % alcohol concentration without any SDS or NaCl. The minor radius was initially fitted and was always close to 18 Å, therefore it was held at that value for all the alcohols. The scattering length density of cellulose for SAXS measurements was calculated and set to 1.35 x 10^{-5} $Å^{-2}$. The scattering length density of each alcohol was calculated based on the alcohol content and was kept constant during the fittings. The length was set to 2000 Å as the q range of the data was not large enough to measure long fibrils; therefore this value was chosen and fixed for all the alcohols. The ratio of the radii of the cross section of the elliptical cylinders modelled reduced for the gels containing only alcohol from 20 and 40 wt % except for methanol gels, where it increased only slightly. The largest decrease was for TOCN gels in ethanol only where the major radius reduced from 68 to 46 Å.

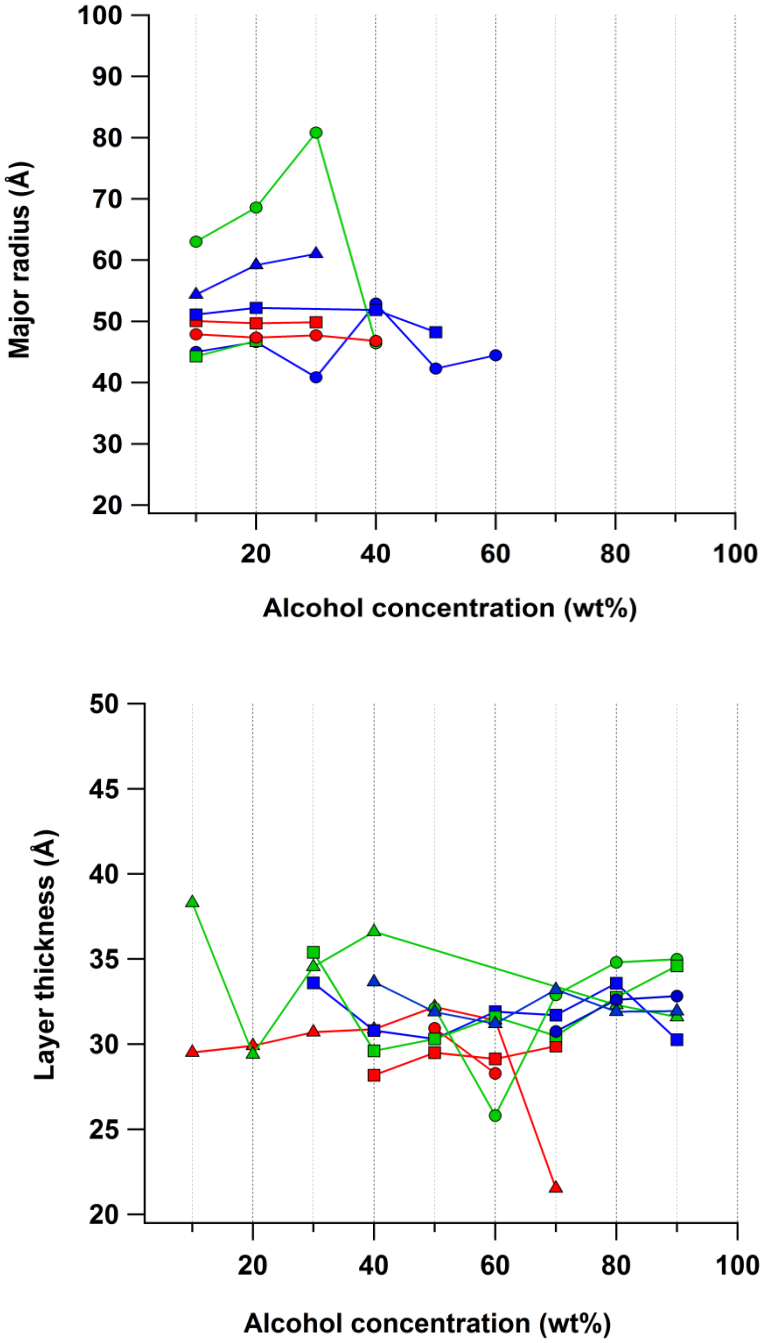

Figure 35: The values for major radius using elliptical cylinder model (top) and thickness using lamellar model (bottom). Alcohols shown are methanol (blue), ethanol (green) and propanol (red). The circle symbols (oxcell only), square symbols (with SDS) and triangle symbols (with NaCl).

The ratio of major/minor radius and the thickness were fitted for all the alcohol concentrations. Figure 35 shows fitted major radius and thickness values with an increase in the alcohol concentration, using two different models. The gels with oxidised cellulose (no SDS or NaCl) and in lower alcohol concentrations (10-40 wt %) were a better fit to the data was provided by the elliptical cylinder model. Amongst all the gels, TOCN gels in ethanol had larger major fibril radii. The major fibril radius was 47 Å and 52 Å for 20 and 40 wt % methanol alcohol gels, respectively. This was increased to 68 Å to 46 Å in the presence of 20 and 40 wt % ethanol, respectively. The major fibril radius however did not change for the propanol where the difference between the radius size for 20 and 40 wt % propanol and the difference was only around 3 Å. There was an increase in the major radius for the TOCN gels in methanol with NaCl. The change in radius size decreased with an increase in the methanol concentration for the gels with SDS. The lamellar model was used for all the concentrations of ethanol gels with NaCl as this was a better model. This was also the case for the propanol gels with NaCl. The major radius size did not significantly changed for gels in propanol with SDS, between 10-30 wt % alcohol. The fitted results for the fibril thickness using lamellar model did not significantly differ between the gels in methanol, ethanol and propanol (Figure 35). There was an exception for the fittings of the ethanol and propanol gels (10-40 wt %) with NaCl where the lamellar model fitted better than the elliptical cylinder model. There was also a sudden decrease in the layer thickness for the TOCN gel in 70 wt % proponal with NaCl where it changed from 31 to 21 Å.

An example of the change in fibril aggregation can be seen in Figure 36. The graph shows the TOCN gels in lower ethanol concentrations (20 and 40 wt %) fitted using elliptical cylinder model (red line). The model was changed to lamellar model (red line) for concentrations 60 and 80 wt % where the fibrils aggregates change to a sheet-like structure. The lamellar thickness at 60 wt % concentration was 26 Å whereas it increased to 35 Å when the concentration was 80 wt % ethanol.

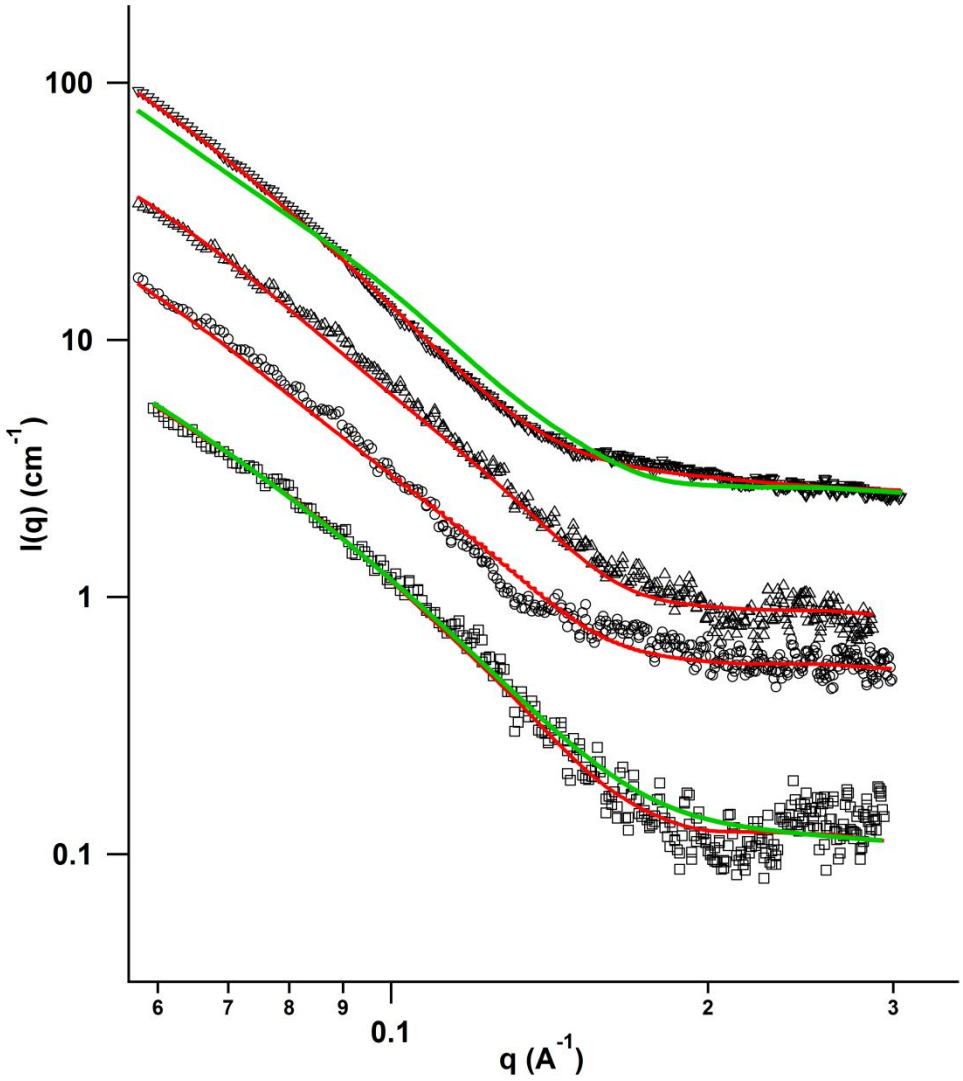

Figure 36: SAXS patterns from oxidised cellulose only, (0.8 wt %) in various ethanol concentrations. 20 wt % (□), 40 wt % (○), 60 wt % (Δ), 80 wt % (∇),where the 20 and 40 wt % fittings are modeled (red line) with elliptical cylinder, and 60 and 80 wt % ethanol gels has a lamellar model as the fit. The green lines show if the fitting of the other models used instead. The data was offset by a factor of three for clarity.

Figure 36 also shows the fittings if lamellar model was used to fit 20 wt % ethanol gels (green line). The fitting is not as well defined as the elliptical model (red line) in the mid q-region. Perhaps the change in the fibrillar aggregation and hence the selection of lamellar model over elliptical model could be better seen at 80 wt % ethanol concentration (green line) where the fitting is clearly much better for the lamellar model.

The SEM images below highlights the difference in the cellulose gels in the presence of different media; water and simple alcohol (Figure 37). In freeze dried cellulose dispersions in water, the cellulose fibrils appear as aggregates that are presumed to reflect a network structure (of largely individualised overlapped fibrils). However, this is not the case for the cellulose gels in 100 wt % methanol and ethanol where the fibrils suggest to form many sheet like (lamellar) structures upon critical point drying.

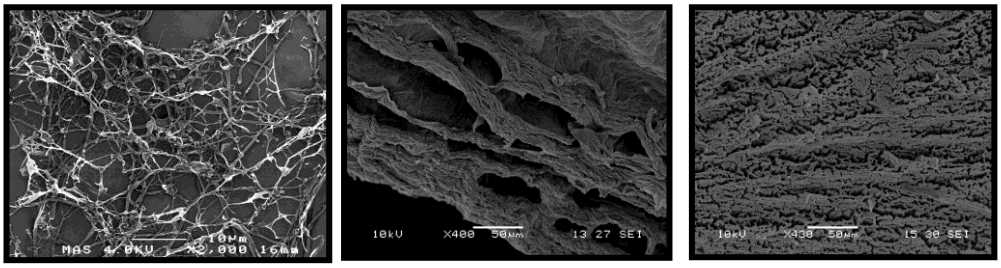

Figure 37: SEM images of different cellulose dispersions a) Freeze dried 0.8 wt% from aqueous dispersion, *scale bar is 10 µm*, b) critical point dried from methanol 100 wt %, *scale bar is 50 µm*, c) critical point dried ethanol 100 wt %, *scale bar is 50 µm*

2.6.4 Small angle neutron scattering (SANS)

The alcohols used for SANS experiments were ethanol and methanol as the gels formed by propanol formed aggregate gels. Deuterated (partially and fully) methanol, ethanol and SDS was also used to highlight the certain parts of the interaction. The scattering data from SANS were similar to that obtained from SAXS where the change in the fibrillar aggregation was also observed with an increase in the alcohol concentration. Furthermore, the effect of alcohol on the micellization of SDS was seen through the SANS experiments as scattering from fibrils and micelles could be separated due to the difference in scattering length densities. The scattering contrast between d-SDS (ρ= 6.73x 10^{-6} Å^{-2}) and D_2O (ρ= 6.38x 10^{-6} Å^{-2}) is less than the difference in scattering length densities of h-SDS (ρ= 0.33x 10^{-6} Å^{-2}) and TOCN (ρ= 1.5 x 10^{-6} Å^{-2}) with respect to D_2O. This means d-SDS molecules are almost contrast matched to D_2O and therefore invisible to neutrons in D_2O solutions. The TOCN was not deuterated but was dispersed in D_2O as described previously.

Therefore the sample either contained TOCN in h-alcohol with d-SDS or in d-alcohol with h-SDS, where the latter would enable the detection of scattering from the micelles isolated from other effects. The CMC of SDS is 8.2 *mM* [227], therefore formation of micelles in aqueous medium would be expected at 40 *mM* and 80 *mM*. However, micelle formation could be affected by the presence of an alcohol.

The effect of alcohol on TOCN has not been studied before. The SANS and SAXS experiments indicate that in general when the alcohol concentration reach a concentration > 50 wt %, a structural change in the aggregation of the fibrils is observed. The lamellar model fits the observed small angle scattering better than the elliptical cylinder model. A possible reason for this could be due to the alcohol replacing the water molecules and disturbing the intermolecular bonding between the fibrils and therefore modifying the apparent structural dimensions of the cellulose fibrils (determined by fitting of data from scattering experiments), hence giving rise to side-by-side aggregation of the fibrils. This effect is not only evident from SAXS/SANS data but also from the changes observed from the gravimetric analysis of the gels where the percentage fraction of gel recovered was reduced with an increase in the alcohol concentration , for all the alcohols, suggesting formation of a more compacted TOCN structure. This was coupled with the SEM images of the TOCN in 100 wt % alcohol where the aggregation of the fibrils was clearly altered in the alcohol compared to the dispersions without the alcohol.

2.6.4.1 The effect of SDS

There have been many studies on the behaviour of SDS molecules in the presence of alcohols which tend to be focused on the LMW alcohols since SDS exhibit low solubility in longer chain alcohols (n=3-6). [181,182,190,193,227–229] Alcohol is often used as a co-solvent in many oil-surfactant systems to create microemulsions, therefore it is important to understand the effect of alcohols upon other additives found in formulations. Alcohols affect the solvent structure around the surfactant headgroup.[181,192] The change in the micellar size depends on the hydrophilic/hydrophobic nature of the alcohol. The LMW alcohols predominantly solubilise in the aqueous medium and have an impact on the micellization process by

modifying the solvent whereas the longer chain alcohols (e.g. pentanol) directly participate in the micellization process by becoming components of the micelle aggregates.[193] The SDS micelle in water has two parts with different polarities: the outer region is hydrophilic and the inner core is hydrophobic. The LMW alcohols thermodynamically and kinetically destabilize the micelles and result in breaking down of the aggregates.[193,230] Førland *et al.*[193] illustrated that the best model for SDS micelles in solution at higher concentration (1.2 mol/kg) of alcohols such as propanol was that of spherical structures, rather than the ellipsoid model used for the micelles at lower concentrations of the same alcohol. They showed that the SANS data fitted with the sphere model yielded a radius of 18 Å for SDS in aqueous solutions and between 13-17 Å in propanol with concentrations higher than 1.2 mol/kg.

The effect of ethanol on the interaction between a non-ionic polymer (poly(vinypyrrolidone)) and SDS was studied by Griffiths *et al.* [192] where they concluded that the micelles affect the polymer conformation and that this effect is weakened in the presence of ethanol. They also showed the effect of ethanol concentration on the micelle peaks measured in SANS experiments. The micelle peaks become less dominant with an increase from 0-20 % ethanol since the ionic nature of the micelle is decreasing. The SANS data also showed a shift in the peak towards higher *q* value indicating closer packing of the micelles. When the data was fitted with core/shell model, the radius of the polymer bound micelle slightly reduced with an increase in the alcohol content.

The data presented in Figure 38 shows the effect of methanol concentrations (20, 40, 60 and 80 wt %) on the micellization of SDS (80 mM) in the presence of TOCN. The methanol was deuterated and the SDS was in hydrogenated form which highlighted the changes in the micelle sphere size as well as the changes in the TOCN particle aggregate. A summed model was used to fit the data for each methanol concentration. For the 20 and 40 wt % alcohol, the sum of an elliptical cylinder with a sphere model was used, which was then changed to the sum of a lamellar with a sphere model with the increased concentration of 60 wt % methanol and finally the highest concentration of methanol of 80 wt % was fitted with the lamellar model only. The SDS micelle scattering is dominant at 20 wt % methanol concentration

however the impact of methanol becomes gradually visible where the peak starts to disappear upon increase of the alcohol content.

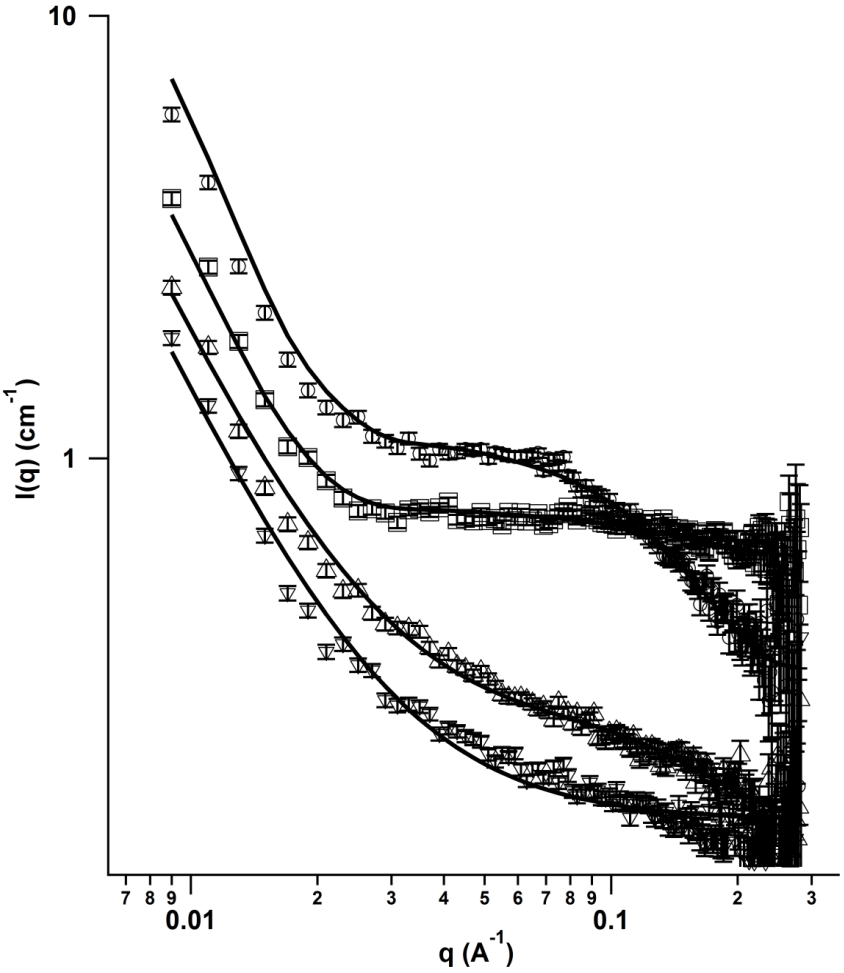

Figure 38: SANS from oxidised cellulose, (0.8 wt %) in d-methanol and h-SDS (80 mM), (○)20 wt %, (□) 40 wt %, (Δ) 60 wt % and (∇) 80 wt %. All the fittings used summed models except at the highest methanol concentration. 20-40 wt % elliptical cylinder+sphere and 60 wt % , lamellar+sphere, 80 wt % lamellar. The data for 60 and 80 wt % methanol was shifted by a factor of 2 for clarity.

The minor and major radius of TOCN increased from 20 to 40 wt% methanol (Table 5). Even though, the ratio was similar to TOCN-alcohol gels in the absence of SDS, the minor radius was five times greater in the presence of SDS (80 mM) from increasing from 18 Å to 102 Å. The model used for the lower alcohol concentrations was the elliptical cylinder model summed with a sphere, as the lamellar model did not fit the data, which may suggest the presence of surfactant bring the fibrils closer to each other but this did not result in formation of sheet like aggregates of TOCN particles. The lamellar model on its own did not fit the 60 wt % methanol data, hence the sphere model was added to this. The increase in the methanol concentration also decreased SDS spherical micelle size ,where a similar change was also reported in the literature.[193] The lamellar sheet structure of the aggregated fibrils become more noticeable with a significant decrease in the fibril aggregate thickness from 50 Å to 15 Å at concentrations 60 and 80 wt % respectively.

Table 5: Fitting results of TOCN-methanol gels in presence of SDS (80mM)

		TOCN			SDS
Alcohol concentration (%)	Model	Minor radius (Å)	Major/minor radius ratio	Thickness (Å)	Sphere size (Å)
20	Elliptical cylinder + Sphere	102 ± 2	2.3±0.1		16± 1
40	Elliptical cylinder + Sphere	109 ± 3	4.5±0.8		15 ± 1
60	Lamellar + Sphere			50 ±3	14 ± 1
80	Lamellar			15 ± 1	

The SLD of deuterated SDS was initially calculated and fixed to 6.7 x 10^{-6} $Å^{-2}$, however this value did not fit the data well when a sphere model was used. The value for the SLD of SDS varied in the literature between 6.3 to 6.7 x 10^{-6} $Å^{-2}$. The value used for the d-SDS was 7.3 x 10^{-6} $Å^{-2}$, higher than previously reported value.

2.6.5 The effect of NaCl

According to Corti *et al.*[231] during the addition of low concentration of NaCl, the electrostatic repulsion effects becomes predominant whereas at higher salt concentration, with the increase in ionic strength, London-van der Waals attraction becomes stronger and may lead to coagulation of the micelles. Sammalkorpi *et al.* shows the presence of salt increasing the aggregation number of the micelle system.[232] Figure 39 shows the effect of salt on the aggregated cellulose fibril size and on the SDS sphere dimensions. The concentration of SDS was 80 *mM* and 0.2 *M* for NaCl for both the ethanol and methanol gels. A study by Førland[193] showed that the minor radius and major/minor ratio of SDS micelles increased at NaCl concentrations above 0.4 mol/kg. Indeed, the presence of NaCl did not hinder the micellization of SDS in low alcohol concentrations neither for methanol nor ethanol. The micelle bump is wider around the high *q* range which suggests the micelles are bigger in size.

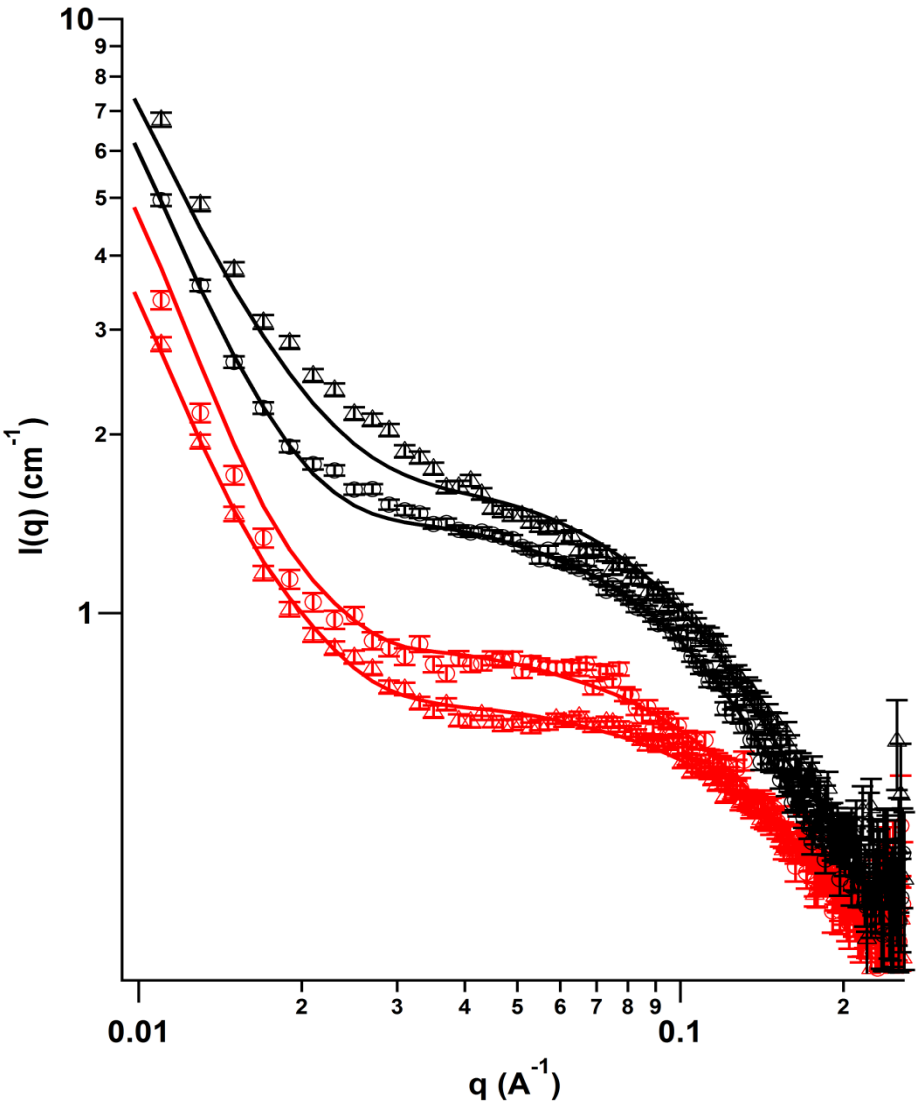

Figure 39: SANS from oxidised cellulose, (0.8 wt %) in 20 wt % alcohol with SDS (80 mM), red points are without NaCl and black points are with added NaCl (0.2M) , where triangles represent ethanol and circles represent methanol gels. All the fittings are to a summed model, of an elliptical cylinder and sphere. The methanol gel data with and without NaCl was shifted vertically by a factor 0.5 for clarity.

The presence of NaCl increased the major/minor ratio, in other words the fibrils appear to become wider, more elliptical, in cross section. Clearly, this is not suggesting a change in dimensions of the individual fibrils, but points to the onset of aggregation, such that on average one cross-sectional dimension appears to increase, becoming more ribbon-like in structure. The size of SDS sphere increased from 14 to 19 Å for ethanol gels (Table 6) upon addition of salt. The sphere size was also increased for the methanol gels but the effect of the NaCl on the micelle was smaller than that of ethanol. On the other hand the major radius of cellulose fibrils increased

by 2 fold for ethanol and 2.5 for methanol which may indicate the clustering of the fibrils.

Table 6: Model fitted data for ethanol (20 wt %) and methanol (20 wt %) containing SDS (80 *mM*), and with and without NaCl (0.2 *M*)

		TOCN		SDS
	Model	Minor radius (Å)	Major/minor radius ratio	Sphere size (Å)
Ethanol	Elliptical cylinder + Sphere	91 ± 2	2.8±0.1	14 ± 2
Ethanol + NaCl	Elliptical cylinder + Sphere	87 ± 2	5.8±1.0	19 ± 2
Methanol	Elliptical cylinder + Sphere	102 ±2	2.3±0.1	16 ± 2
Methanol + NaCl	Elliptical cylinder + Sphere	111 ±2	4.6±0.7	19 ± 2

2.6.6 Discussion

The stability of TOCN gels depends on the charge-derived electrostatic repulsion between the nanofibrils which is initiated from the surface carboxylate groups introduced by the oxidation process. Therefore the medium they are dispersed in and the presence of charged particles may play an important role in the stability of the dispersion.[233] Based on the Debye-Hückel equation, the Debye length $1/\kappa$ decreases when the electrolyte concentration increases; this reflects a shorter-range repulsion and shows that the electrolyte causes changes in the electrostatic interactions between the fibrils. The dispersion of charged oxidised cellulose nanofibrils in water is relatively easy due to the high dielectric constant of water and proves to be more difficult in organic solvents with low dielectric constant such as cyclohexane.[233] In addition, the difference in dispersion will also depend on the choice of alcohol, becoming greater in less polar alcohols. Of the alcohols studied, proponal exhibits the lowest dielectric constant compared to the other two alcohols used in this study. The TOCN gels in propanol were the most viscous of all, but also formed aggregated gels at higher concentrations.

An increase in the ionic strength (addition of NaCl) results in destruction of the double layer on charged particles and yield in contact between the fibres which forms aggregates when salt is added.[1] Fukuzumi *et al*.[54] measured the interaction energies between two fibril cylinders and stated that the maximum potential (V_{max}) must be overcome to allow these to approach each other as Brownian motion is not enough to do so. They showed that at low NaCl concentrations (<50 *mM*), V_{max} was adequate allowing the repulsive forces to be dominant resulting in high nanodispersion. However, this was not the case in higher salt concentrations (>100 *mM*) where the V_{max} value was negative allowing the TOCN fibrils to get approach each other and form aggregates. This is in an agreement with the aggregates formed upon addition of salt. This is supported by the small changes seen in the lamellar fibril aggregate thickness in presence of salt, where the fibrils were already closer to each other and an increase in the alcohol concentration did not affect the thickness of the fibril aggregates.

The mechanism for the gelation of TOCN dispersions upon addition of SDS was described by Crawford *et al.*[1] The repulsion between the negatively charged SDS micelles and cellulose fibrils results in separation of both species into smaller volumes, increasing the volume fraction and yielding gelation. This is coupled with charge shielding effect due to an increase in the ionic strength. The same mechanism was seen in the presence of alcohol where the viscosity of gels containing SDS was higher than gels with no surfactant. The increase in alcohol concentration also increased the viscosity of gels with SDS. According to Zana [181] , the surfactants can develop long-thread like micelles in alcohol solutions where they become gel-like and viscoelastic due to entanglements of the micelles. The SDS micelle formation at high surfactant concentration (80 *mM*) was seen in SANS patterns. This was however only possible at lower alcohol concentrations < 40 wt %. The scattering signal due to the micelles disappeared at alcohol concentration of 60 wt % or above. The micelle size decreased in TOCN-methanol gels containing SDS (80 *mM*) from 16 to 14 Å from 20 wt % to 60 wt % alcohol content which is agreement with other studies. The major radius increased from 20 wt % alcohol to 60 wt% and then the thickness of the fibril decreased to 15 Å where the lamellar

model was used. The significant decrease in fibril size and the use of a lamellar model are both a result of the change in the structure of the gel where the fibrils aggregate into sheet-like structures. The effect of addition of NaCl (0.2 M) to the ethanol (20 wt %) and methanol (20 wt %) containing SDS (80 mM) solutions on TOCN was also investigated. The thickness of the fibrils increased with the addition of salt due to the aggregation of the fibrils but also the micelle size was increased for both ethanol and methanol alcohols. According to Sammalkorpi *et al.*[232] , the NaCl induces an increase in the SDS micelle size and also resulting in densely packed micelles. Moreover, the added ions assist this process by forming stable salt bridges between the charged SDS head groups.

2.6.7 Conclusion:

The effect of simple chain alcohols on the structure of TOCN gels was investigated. In the presence of simple short chain alcohols the arrangements of oxidised cellulose fibrils changed from cylindrical to sheet-like structure as suggested by the SAXS data. This change in the fibrils aggregates was also confirmed by SEM images. The micellization of SDS (80 *mM*) can still be in effect in the presence of alcohols, however in concentrations higher than 50% alcohol, the micelle formation was disturbed by the presence of low molecular weight alcohols such as methanol, ethanol and propanol. The viscosity of the oxidised cellulose gels can be adjusted with changes in alcohol, surfactant and salt concentrations. The addition of SDS and NaCl showed significant changes in the elasticity and viscosity of the gels. Alcohol gels at high alcohol concentrations showed to be affected more from the presence of salt where the gels were aggregated. The charge screening effect of NaCl had a bigger impact on micellization of SDS than the presence of alcohols.

3. TEMPO-Oxidised Cellulose (TOCN) Films

Overview:

The interaction of TOCN films with sodium dodecyl sulfate (SDS) and sodium chloride (NaCl) was studied as part of this study. TOCN thickened formulations are known to form films on the skin surface (one of their benefits in personal care cream products is the pleasant skin feel resulting). In order to probe the structure of this film, and interaction with other formulation components, as well as the capacity for it to act as a drug carrier or drug "encapsulation" material, X-ray and neutron reflectivity of the TOCN films were investigated. In the first instance, changes in TOCN film in the presence of salt and surfactant solutions were probed as these components are known to alter the gel structure of TOCN dispersions. This technique is particularly useful for probing the surface properties of these films, in the presence of these components, at the solid-liquid interface. The films were deposited onto silicon blocks by dip-coating and the surfactant/salt solutions were washed over the surface of the films and the changes in the reflectivity patterns were measured by X-ray and neutron reflectivity. Pre-characterisation of the films was done by atomic force microscopy (AFM). The results showed that it was difficult to deposit a uniform layer of TOCN on the substrates as variations between the coverage on different samples were observed. The results from the individual substrates however showed a difference in reflectivity patterns. SDS at a concentration lower than CMC (6 mM) only weakly interacted with the cellulose fibrils while the addition of NaCl (0.2 M) increased the thickness and the roughness of the films. An increase in the SDS concentration (10 mM) further increased the film thickness and the SLD scattering of the layer.

3.1 Introduction

The understanding of surfactant and salt adsorption on solid surfaces is vital to many industrial applications including detergency, lubrication, dyeing and oil recovery.[82] The interaction with the surfactant/salt system can give rise to changes in the properties of pure material, therefore it is important to understand these changes which could also affect the formulation of cosmetics and pharmaceuticals.[234] The cellulose model surfaces are mainly chosen for their ability to mimic properties of hair and skin as well as fabrics such as cotton.[78,82,235,236] Model films are often prepared by Langmuir-Blodgett (LB) deposition or coating from cellulose onto a solid substrate. [82,96] Different type of cellulose generate films with different thickness and roughness, moreover the deposition of the film on the surface also has an impact. According to Tucker *et al.*[82] the model films prepared from trimethylsilyl-cellulose (TMSC) by spin coating from chloroform onto silicon substrates are ~1000 Å in thickness and relatively rough. On the other hand, the same cellulose deposited on the surface by LB deposition form films with thickness of ~100 Å which are smoother. The model cellulose surfaces have been studied to understand the swelling of cellulose in various conditions, adsorption of surfactants, polymers and surface forces between the cellulose surface and the material.[96] Products containing cellulose are exposed to humid conditions and often present in aqueous formulations. Therefore it is vital to understanding the swelling mechanism of cellulose where often water molecules penetrate between the hydrogen bonded fibrils, resulting in fiber wall expansion. [237] The swelling of the gel can be described as the swelling of a polyelectrolyte gel where it is regulated by the charge density of cellulose, ionic strength of the medium it is in, type of counterion and degree of crosslinking.[96] The characterisation methods used for model cellulose surfaces include diffraction, reflectivity, contact angle measurements, atomic force microscopy and quartz crystal microbalance with dissipation monitoring (QCM-D).[68,80,97]As well as the swelling properties, the interaction between cellulose fibers is also of importance, especially in the paper industry where the strength of the final paper is determined by this relationship. According to Ahola *et al.*[96], any charged groups on the fiber surface or

within the fiber wall can generate repulsive forces due to overlapping of electrical double layer. This is affected by the electrolyte concentration of the medium cellulose in. However to far to our knowledge, there have been no detailed studies of the properties of TOCN films at interfaces, with most work, as described above using polymeric derivatives of cellulose (rather than cellulose nanoparticles) to form model surface.

3.2 Materials and Methods

3.2.1 Chemicals

3-Aminopropyltrimethoxysilane (APTS) and hydrochloric acid (ACS reagent, 37 %) was purchased from Sigma Aldrich. For the substrate cleaning procedure, DECON 90 (Fisher Scientific UK), ethanol and acetone (Sigma Aldrich) were used. Sodium dodecyl sulfate (ACS reagent, ≥99.0%), sodium chloride (BioXtra, ≥99.5%), sodium dodecyl sulfate (D25, 98 %), deuterium oxide (D, 99.8 % at.) were all purchased from Sigma Aldrich. All materials were used without further purification.

3.2.2 Preparation of oxidised cellulose films

The same batch of TOCN was used for the film coating experiments as described in Chapter 2. The oxidation level and the dispersion of TOCN were also same as the aqueous dispersions prepared for the aqueous TOCN gels. The cellulose films were produced by dip-coating silicon substrates. Prior to dip coating the substrates went through a meticulous cleaning procedure for both X-ray and neutron reflectivity experiments in order to keep the substrates clean and dust-free before and after the film coating. Both the glass and silicon substrates used for the reflectivity and AFM measurements were prepared in same way.

Substrate Cleaning Procedure

It was particularly important to keep the substrate surfaces free from any organic material for the reflectivity measurements not only because this technique is very

sensitive to residuals on the substrate surface but also any oil on the substrates may prevent the adhesion of 3-aminopropyltrimethoxysilane (APTS) to the surface which in turn could affect the cellulose coverage on the substrate surface.

The cleaning procedure involved sonicating the substrates in different cleaning solvents in an ultrasound bath in the following order: Decon 90 (5 vol %), ultrapure water, acetone and finally ethanol for 15 minutes each at ambient temperatures. Once dried, the any organic residue left on the surface was removed by dipping the substrates in Piranha solution (3:1; H_2SO_4/H_2O_2) for 15 minutes. This mixture is a strong oxidiser and will also hydroxylate most surfaces (adding OH groups), making them extremely hydrophilic. They were then rinsed off using ultrapure water, placed in a covered container and left to dry in the oven at 50 °C.

TOCN Film Casting

The ability of cellulose to adhere to the substrate surface was optimised by aminosilanisation via vapour phase deposition as reported by Wang et *al.*[238]which method forms an anchoring platform for the cellulose fibers to adhere to. Once cleaned and dried in the oven, the substrates were laid inside a sealed desiccator with 1 mL of 3-aminopropyltrimethoxysilane (APTS) and kept under APTS vapour over night in a fume cupboard. The treated glass substrates were then placed in the oven at 60 ℃ prior to dip-coating as annealing the substrate was suggested to create smoother films.[238] The aqueous TOCN dispersions were diluted (1 g L^{-1}) and centrifuged for 15 minutes at 11 000 rpm before proceeding to dip-coating. This was done to remove of any big particles present in the dispersions. The supernatant of these dispersions was used for the coating. The final step before dip-coating the substrates was to dip them in HCl acid (0.1 M) in order to further enhance the adherence of the cellulose to the glass surface. Substrates were dipped into the cellulose dispersions using an automated dip-coater (KSV NIMA single vessel dip-coater, move down 300 mm/min, wait in the dispersion 30 sec, move up 500 mm/min and placed in the oven for 15 minutes at 50 ℃ prior to analysis.

3.2.3 AFM

Previously cleaned glass substrates (2 cm x 2 cm) were used to cast TOCN films and study their surface morphology. AFM images were obtained on a Nanosurf Easyscan 2 Atomic Force Microscope. Aluminium-coated silicon cantilevers (Tap190-Al, BudgetSensors) having a tip radius <10 nm, a force constant of 48 Nm^{-1} and a resonance frequency of 190 kHz in tapping-mode were used for the measurements. The images were taken with 256 x 256 points and for an area of 5 µm. The programme Gwyddion 2.26 was used to analyse the images.

3.2.4 X-ray Reflectivity (XRR)

Silicon substrates (2 cm x 2 cm) were used as the solid support for the cellulose films (Figure 40). All the substrates were amino functionalised and dip-coated with cellulose films using the previously described procedure for the glass substrates.

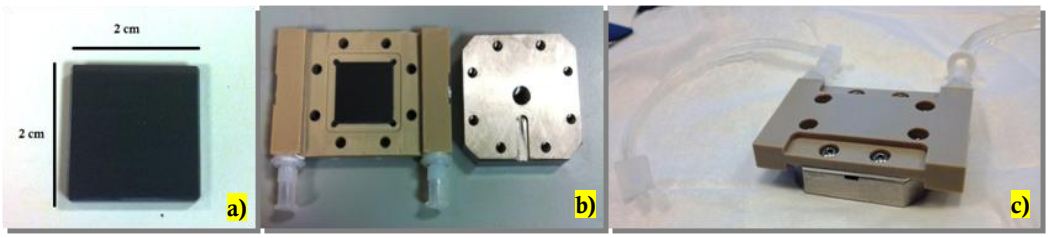

Figure 40: Solid-liquid cell used for XRR experiments. a) Silicon substrate (2x 2 cm), b) Silicon substrate fitted inside the cell, c) Substrate ready for the measurement where the liquid can be injected through the cell.

The XRR measurements were carried out on beamline I07 at the Diamond Light Source (Didcot, UK), using the solid- liquid cell and an X-ray energy of 18.0 keV (= 0.4992 Å). I07 has a "double crystal deflector (DCD)" which allows the measurement of different incident angles without the need to tilt the sample. The DCD uses sequential Bragg reflection from two silicon crystals, Si(111) and Si(220) to generate an overall deflection. This geometry means the sample is no longer required to track the deflected beam since, as the crystals are rotated, the beam

rotates at a fixed sample position.[239] The incident beam size defined by slits was 210 μm (vertical) x 210 μm (horizontal) having an incident flux of 10^6 photons s^{-1}. The specular X-ray reflections were measured at variable incidence angles (θ) using a Pilatus 1K detector.

The third generation synchrotron X-ray source at Diamond provided the required intensity for this experiment. The beam path length was reduced to measure a reasonable X-ray reflectivity for the substrate area due to beam attenuation by the liquid layer or the solid Si support. A complete reflectivity profiles requires three q scans with varying attenuation to cover the entire q range. The reflectivity of the substrates was therefore measured over three dynamic ranges of intensity from q= 0.032 to 1.32 $Å^{-1}$. The intensity was measured in three smaller q ranges and later added together to form one single reflectivity profile. These measurements take place in the low q region and therefore a higher attenuation (consisting of aluminium and molybdenum foils to absorb X-rays) must be used to avoid damaging the detector. At higher incidence angles the attenuation must be reduced to improve the signal to noise ratio. The intensity of the incident beam captured by the sample was not the same over the entire q_z (momentum transfer perpendicular to the surface) range. Therefore the overlapping regions of data in the first of the three intensity measurements were normalised to one above the critical edge and the other two patterns adjusted in order to put the reflectivity on a consistent scale.

XRR can provide structural information between interfacial layers on films , as well as film thickness, roughness and crystallinity.[240] The wavelength or the incidence angle is measured during the experiment and a theoretical model layer is used to fit the results. It is therefore possible to obtain information from the model about the surface roughness, thickness of the layer and the electron density of each layer.The reflectivity data was fitted with the aid of Motofit plug-in for IGOR Pro 6.22A using the Levenberg-Marquardt least-squares method. The reflectivity panel of Motofit fits the data based on variables such as the layer thickness, scattering length density (SLD), solvent penetration used and the roughness which makes a large impact on the fitting. The SLD for the backing (silicon substrate) was fixed at 20.1 x 10^{-5} $Å^{-2}$ and for the 1st layer (SiO_2) it was 18.9 x 10^{-5} $Å^{-2}$ for each fitting.

3.2.5 Neutron Reflectivity (NR)

The core of a neutron reflection experiment is to measure the specular reflection as a function of the wave vector transfer, q, which is perpendicular to the reflecting surface.[92] This is often related to the scattering length density, obtaining information about the structural composition and density gradients at surfaces and interfaces. The NR experiments were carried out at D17 and OFFSPEC reflectometers.[241,242] The advantages of neutron reflectivity include the ability for deep penetration and isotope labelling which allows us to study the structures buried underneath a layer. The neutrons also have low thermal energies therefore they are benign compared to X-rays. This is of convenience if one tries to study changes in the sample as a function of time. One disadvantage of NR is the low flux incident and sensitivity to hydrogenated components which has a very high background incoherent scattering. This limits the reflectivity measurement to 10^{-6} after which the background gets bigger than the reflectivity. Therefore, very thin films (i.e. those less than 10 Å) are not easy to measure with neutron reflectivity.

The neutron reflectivity experiments were carried out at two reflectometers D17 (ILL, Grenoble, France) and Offspec (ISIS, Didcot,UK).. All the substrates were coated with TOCN as described above.

3.2.5.1 D17 instrument

The neutron scattering facilities around the world generate neutrons by two methods; with nuclear reactors or with high flux particle accelerators. D17 is an instrument based in Institut Laue–Langevin (ILL) which is an example of the nuclear reactor. The instrument functions in two modes where one is to carry out time of flight (TOF) and the other one is for monochromatic experiments. The latter is used to perform polarised-neutron experiments.[241] TOF mode was used for this study which provides entire range of q to be measured in less than a minute. The neutrons at ILL are generated by the fission of atoms in the reactor fuel (uranium) unlike the neutrons produced at ISIS which are generated by spallation source. In a high flux neutron reactor, the fission splits the heavy nucleus of uranium into lighter ones and also produces neutrons as well as gamma rays which are also used by other instruments

on site. However, the neutrons generated have very high energies and need to be cooled down before they could be used for a scattering experiment.[209] This is often achieved by a moderating material with a large scattering cross section such as heavy water or liquid hydrogen. The moderator is placed near the neutron source and once the neutrons enter the moderator, they collide with the moderator material.

One set of NR measurements were performed at the Institut Laue Langevin (ILL, Grenoble, France) using the D17 reflectometer. The specular reflection was measured as a function of the wave vector transfer perpendicular to the surface, $q= (4\pi/\lambda)\sin\theta$), where θ is the angle and λ is the wavelength of the incident beam. The silicon blocks with one polished side (diameter of 80 x 50 mm, thickness of 15 ± 0.3 mm, roughness < 3 Å) were obtained from SIL'TRONIX Silicon Technologies in France (Figure 41).Silicon substrates were held between two aluminium plates vertically and the temperature was set at 25 °C. The reflected beam was corrected by measuring the direct beam and calibrated to an absolute reflectivity.[241] The contrast variation method was used by changing the medium between H_2O and D_2O to different components in the film in different measurements. Deuterated sodium dodecyl sulfate (SDS) was also used. The minimum thickness, *d*, of adsorbed layer, or thin film, accessible is determined by the maximum q value (where $d\sim2\pi/q$) [81]. The wavelength of the incident neutrons was between 2 Å and 20 Å. Time-of-flight settings were used for this experiment and the data was recorded at three fixed incidence angles in order to cover the necessary q range. The q range was between 0.01-0.2 A˚. The super-mirror coated guide enabled a white beam flux of 9.6×10^9 n/s/cm^2. An ILL tube detector filled with ^{3}He gas was used and the maximum counting rate was 0.75 MHz. The resolution was 5 % and the experiments were performed at 25 ℃ .

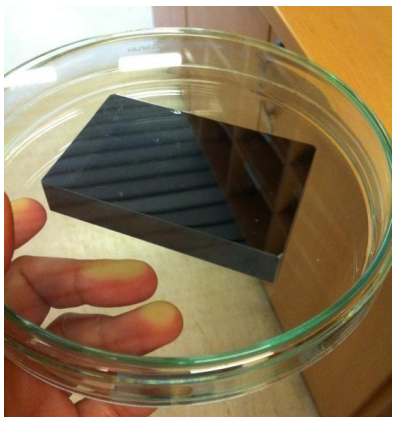

Figure 41: Silicon substrate used for neutron reflectivity experiments

3.2.5.2 Offspec instrument

The Offspec instrument is based at the neutron spallation sources ISIS at Rurtherford Appleton Laboratory, UK. It is a low background reflectometer which measures off-specular reflection and it has the ability to investigate in-plane length scales similar to atomic force microscopy at buried interfaces. The measurement of the reflectivity is achieved by separating the background intensity arising from the bulk material from the intensity due to the interface. This is done by defining the path of the neutrons in the vertical plane (the sample is horizontal) and only allowing the neutrons on the same path passing along both arms of the instrument (specular beam). This allows a measurement on a pixel by pixel and wavelength basis which yields the proportion of total scattering in specular and offspecular.[242]

The same procedure was followed for the TOCN films as the D17 experiment. The substrates were placed horizontally unlike the D17 experiment set up but similar silicon blocks and holders were used. The contrast variation method was also used during this experiment and the substrates with oxidised cellulose films were washed with various solutions of deuterated sodium dodecyl sulfate ($d\text{-}_{25}$) with and without sodium chloride. Offspec has a wavelength band between 1.5 – 14.5 Å with a primary flight path of 23.7 m from the solid methane moderator and the sample is 3.6 m from the linear detector and 3.2 m away from the ^{3}He gas detector. The q range measured was 0.006–0.3 A˚.[242] The resolution was 3 % and the instrument is equipped with rotating disc chopper at a rate of 10 Hz. The experiments were performed at 25 ℃ . Mantid was used for the data correction.[243] The data set was stitched using the data obtained from three incidence angles in order to achieve data collection in the desired q range and a single reduced data set was obtained.

3.2.6 Theory of reflectivity

The X-ray and neutron reflectivity have been used to study interfacial behaviour of materials. Small angle scattering experiments offer information on the aggregate properties in solution while reflectivity gives information on different layers adsorbed at an interface.[88] X-ray reflectivity was used to study the surface roughness of materials and neutron reflectivity was used, initially, to establish the scattering length density of materials by the location of the critical angle.[244] The critical angle is the angle of incidence below which the total reflection takes place. The contrast between the material and the solvent it is in is a necessary factor to have in reflectivity as well as in scattering experiments. The contrast is the variation of refractive index in this case.

The refractive index, *n*, is given by:

$$n = 1 - \delta + i\beta \tag{31}$$

where δ is the real part of the refractive index and the β is the imaginary part which is responsible for the absorption. For X-rays:

$$\delta_X = \lambda^2 \rho_{el} r_0 / 2\pi \tag{32}$$

$$\beta_X = \mu\lambda / 4\pi \tag{33}$$

where λ is the X-ray wavelength, $\rho_{el}$is the electron density, r_0 is the electron radius (2.82 x 10^{-13} cm) and μ is the linear absorption coefficient.

In the case of neutrons: $\beta = 0$ and

$$\delta_N = \frac{N_A \rho \lambda^2}{2\pi} \frac{b}{M} \tag{34}$$

where ρ is the mass density and *M* is the molecular weight of component with a scattering length of *b*. A strongly scattering sample (for X-rays) or a sample with a large incoherent scattering cross-section (for neutrons) will attenuate the radiation as well. [244]

Figure 42 illustrates the basic reflectivity principle where a beam hits the surface, a substrate in this case, and is reflected away. The detector records the angle of the reflection. If the incidence angle, θ_i , is equal to reflected angle, θ_f, then the reflectivity is said to be *specular*. When this is not the case, then the beam is refracted and this is called *diffuse* or *off-specular* reflectivity.

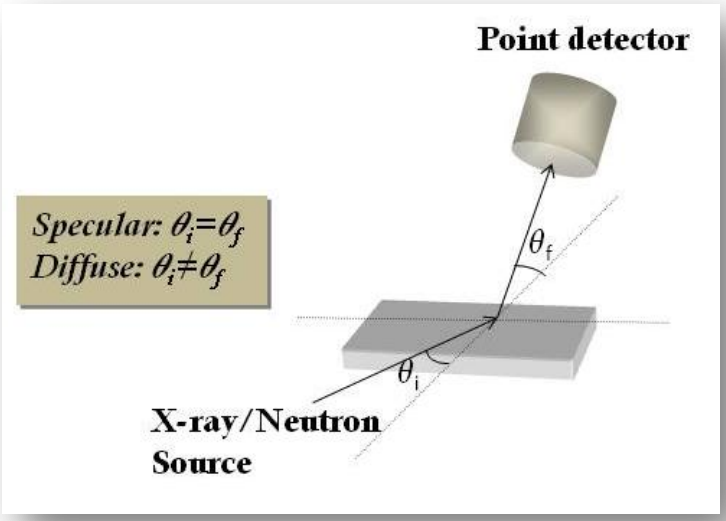

Figure 42: A schematic diagram for the x-ray reflectivity of sample from the surface, adapted from 304

If the incidence angle is less than critical angle, then this will cause the X-rays or neutron to experience total external reflection. The *off-specular* reflectivity is very similar to *specular* reflectivity, with the exception of the θ being offset by a small angle relative to θ_i. It measures the incoherent scattering from the sample. In general, both *specular* and *off-specular* reflectivity is measured in order to obtain the full reflectivity data profile. The off-specular reflectivity is used as a background and substracted from the specular reflectivity signal during data reduction. The momentum transfer Q_z for specular reflection is described as:

$$Q_z = \left(\frac{4\pi}{\lambda}\right)\sin\theta = 4(\pi\rho\Sigma b^{\frac{1}{2}}) \tag{35}$$

where Q_z is momentum transfer expressed along z-direction , θ is the critical angle and $\rho\Sigma b$ is the total scattering length. With X-rays, the contrast is achieved by the variations in atomic number of elements where the number of electrons per unit volume can be large. With neutrons, on the other hand, the scattering length does not vary between atomic numbers but instead the main difference is in scattering lengths between two isotopes, the proton and the deuteron, as in the small angle scattering experiments. Neutrons are more penetrating than X-rays, thus one can easily examine interfaces that are hidden well within a sample, or the absorption of a component from solution onto a substrate by neutron reflectivity. The fact that neutrons can travel through centimetres of a material without a significant loss in flux and don't

interact strongly with other matter is of great value in the design of sample cells where in situ measurements are preferred.[244]

It is the change in the refractive index from one medium to another that results in reflectivity. For both X-rays and neutrons, the differences in the refractive index, can occur from differences in the mass density. This change can be due to the interface between two different materials or from a continuous change in the scattering length density. In any case, a gradient in the scattering length density is necessary to reflect the incoming radiation.

Parratt[245] derived the reflection coefficient $r_{0,1}$ for the film surface with a thickness of d , given that it has a uniform SLD. Reflectivity, R, is defined as:

$$R = rr^* \tag{36}$$

where r* is the complex conjugate of r.[244] A reflection on a substrate with a thin film layer on top is illustrated, Figure 43.

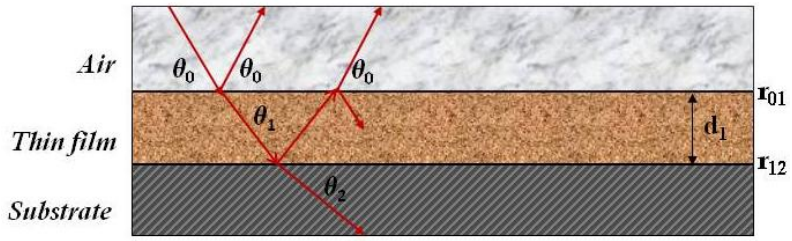

Figure 43: A schematic drawing of single thin film layer on a substrate, with a thickness of d_1, image redrawn from referece 305

The X-rays or neutrons will reflect from the surface, but some of the incident beam will be transmitted and then interact with the second interface where again some radiation will be reflected or transmitted. The reflected beam will interfere with the reflected beam from the first interface before they hit the detector and the transmitted beam will continue the interaction with the second interface. As a result, the data will be collected due to reflection at each interface and the interference between the beams until a value for total reflectivity is obtained.[246]

The wave vector, k , under vacuum , is given by :

$$k_{z,0} = \frac{2\pi}{\lambda} sin\theta \tag{37}$$

where the θ is the incidence angle. The z indicates the direction of the wave perpendicular to the surface of the film and the 0 is used for vacuum conditions. If the reflected X-rays or neutrons are measured at an angle which is same as the incidence angle, then the diffraction vector is aligned normal to the surface, i.e. in the z direction.

The reflection coefficients at the substrate/sample interface, r_{12}, and at the sample/air interface, r_{01}, and wave vector, k, normal to the surface, shown in Figure 43, can be expressed as:

$$r = \frac{r_{01} + r_{12}\exp(2ikd_1)}{1 + r_{01}r_{12}\exp(2ikd_1)} \tag{38}$$

Therefore, the reflectivity can be written as:

$$R = \frac{r^2{}_{01} + r^2{}_{12} + 2r_{01}r_{12}\cos(2kd_1)}{1 + r^2{}_{01}r^2{}_{12} + 2r_{01}r_{12}\cos(2kd_1)} \tag{39}$$

3.2.7 The Footprint Calculations

The corrected data can be obtained by subtracting the *off-specular* scan data from the *specular scan* to remove any background scattering which is not due to the layers within the sample. However, sometimes it is also necessary to carry out footprint corrections for the rocking scans too. A rocking scan is performed in order to make sure the alignment set up is done correctly. This scan is achieved by scanning across the sample, keeping the detector angle at a fixed position and recording the angle at which the reflection takes place.[247]

The footprint of the incident beam on the sample is bigger at low angles compared to that at high angles. This results in low angles being reflected more than high angles, giving rise to an asymmetrical rocking scan.

The geometrical corrections for the area of total external reflection can be done by correcting the effective beam height to below the *spill-over angle*, $2\theta_{so}$.[248] It is the angle for which the full beam height illuminates the sample in the scattering plane.

This is important to note that the below $2\theta_{so}$, not all the incident beam intensity is utilised, while beyond $2\theta_{so}$ the beam footprint on the sample is smaller than the surface itself. Hence, further corrections are necessary. The beam width can be defined by an entrance slit (Figure 44).

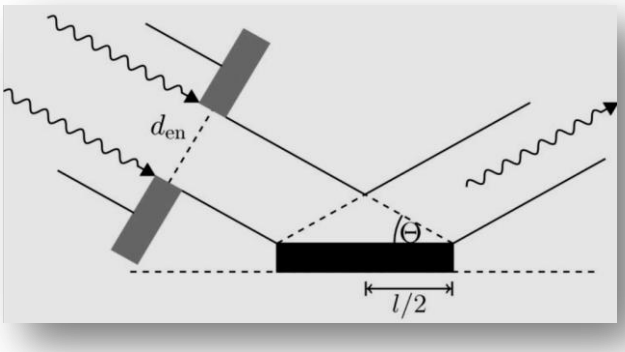

Figure 44: Schematic diagram of an entrance slit for reflectivity from reference 248

Given that d_{en} is the entrance slit height, the *spill-over angle* in this setup can be shown as:

$$2\theta_{so} = 2\arcsin\left(d_{en}/l\right) \tag{40}$$

The relevant correction should be made below the spill-over angle and if the reflectivity happens to be larger than 1.0, it should be reset to 1.0. Gibaud *et al.*[249] suggested that for the corrections to be applied to calculated reflectivity, a non-linear approximation should also be used, which especially considers the divergence of the beam.

$$I_{exp,corr}(2\theta) = I_{exp}(2\theta)\theta_{so}/\theta \tag{41}$$

Therefore it is important to apply the approximation to the experimental curve.

3.2.8 Reflectivity Data Fitting

In order to find a mathematical model for the data, a curve must be fitted to the data points. Igor Pro 6.2 with installed MOTOfit package[250] was used for the reflectivity results. MOTOfit uses a model consisting of a series of *n* layers, each with a defined thickness, roughness and scattering length density. Because the incident beam is refracted by each of the layers, the value of wavefactor, *k*, in layer *n* is defined as: [250]

$$k_n = [k_0^2 - 4\pi(\rho_n - \rho_0)]^{1/2} \quad (42)$$

where $k_0 = q/2$.

A phase factor, β, is included, which accounts for the thickness (d_n) of each layer: [250]

$$\beta_n = k_n d_n \quad (43)$$

A matrix, c_n, is then calculated for each layer within the sample. The matrix is composed of the reflectivity coefficients and the phase factor, β:

$$c_n = \begin{bmatrix} exp\beta_n & r_n \exp(\beta_n) \\ r_n \exp(-\beta_n) & \exp(-\beta_n) \end{bmatrix} \quad (44)$$

The matrix within the model for each layer is then defined as:

$$M = \prod_{n=0}^{n} c_n \quad (45)$$

From which the reflectivity is calculated as:

$$R = \left|\frac{M_{11}}{M_{21}}\right|^2 \quad (46)$$

The fit finds the precise coefficients of each layer that would make the function calculated from the model to get as close to the real data points as possible. The best values of coefficients are the ones generating the minimum chi-square value which is defined as:

$$X^2 = \sum_i \left(\frac{y - y_i}{\sigma_i}\right)^2 \quad (47)$$

where y is the fitted value for a given point , y_i is the measured data point ,σ_i is an estimated standard deviation of y_i.

Iterative fitting is used for the fitting which involves non-linear least-squares data fitting. The fitting programme attempts many coefficient values to find the best fit with minimum chi-square value. The programme uses the Levenberg-Marquardt algorithm to find this minimum value searching through multidimensional error space until finding the minimum coefficient values of fitting function.[251]

3.2.9 Imaging techniques

3.2.9.1 Atomic Force Microscopy (AFM)

The basic set-up of an AFM apparatus includes a probe mounted on a piezocrystal which helps the probe to move with respect to the surface. Deviation of the cantilever is screened by the change in the direction of the beam of laser light deflected from the end of the cantilever by a photodetector. The piezocrystal helps to detect the deflection as the tip is approached closer to the surface of the sample. This deflection is then used to calculate the interaction forces between the probe and the sample where the probe is in contact with the surface, relative height information of features on the surface of the sample can be obtained. When the probe gets closer to the surface, van der Waals interactions start to pull the probe towards the surface. As contact is made, the overall net interaction becomes repulsive as electron shells in atoms in the opposing surfaces repel each other.[252]

There are many modes for analysing sample surfaces depending on the texture and the nature of the sample. *Contact mode* is preferred for flat and hard surfaces. However, this mode has some disadvantages including the possibility of the damaging probes or the sample. The deformation of the sample may result in inaccurate measurements of the height of surface features.[252]

Another mode was developed in order to avoid the limitations of contact mode, called *intermittent (tapping) mode*. The advantages of this mode are an increase in resolution and decrease in the damage to soft samples.[253] In tapping mode, the cantilever oscillates close to the sample surface and the probe taps the surface and then withdraws. When the surface is scanned, the oscillatory amplitude of the cantilever changes and the surface topography is recorded.[252]

Non-contact mode is where the probe does not touch the surface but instead oscillates over a fluid layer on the surface e.g. water. However, the water layer might be thicker than the range of the van der Waals forces being probed and the probe will be stuck in the water layer. [252] In this project, all the images of TOCN films were obtained by the widely used mode for films which is the tapping mode.

3.3 Results and discussion

3.3.1 Characterisation of TOCN Based Films

AFM and Substrate Surface Modification

Thin, smooth, uniform TOCN films, supported on silica substrates, were prepared by a dip-coating method. Prior to dip-coating, the substrates were modified by aminosilanisation with APTS overnight and followed by dipping in aqueous HCl (0.1 M) to enhance the anchoring of the negatively charged TOCN on the substrates.

As well as dip-coating, spin-coating and spraying of TOCN on the substrates were also examined. However, it was not possible to obtain a uniform film by these methods. Aminosilanisation of the substrate surface to create a layer of anchoring substance on the surfaces is a widely known procedure.[238,254–258] Factors such as solvent choice, conditions for deposition and the concentrations of APTS and/or solvents all affect the surface roughness and the ability of TOCN to attach to APTS.

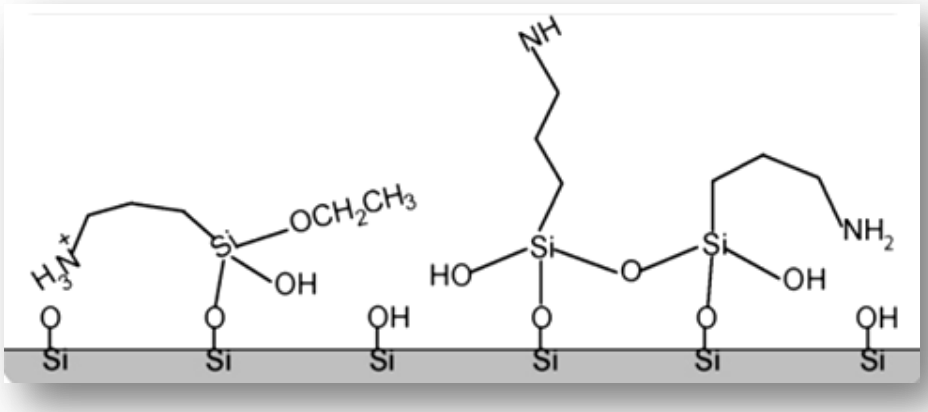

Figure 45: Adsorbed APTES on a silicon wafer in an anhydrous toluene solution, adapted from reference 259

There are a number of methods for functionalising the surface using either solution or vapour phases, including concentrated vapour-phase deposition, dilute vapour-phase deposition, anhydrous organic-phase deposition and aqueous-phase deposition. [238] In this study, only the first three methods were considered initially, simply because the aqueous-phase deposition method was reported as less preferred in previous published studies (using different film forming materials). It was suggested that in water, APTS layers were weakly bonded to and hence formed thinner layers on the substrate surface, producing films of poor stability. [238,259]

Chemically adsorbed silane on the substrate surface creates a platform for further chemical reactions through another species with a charge opposite to the silane. Therefore, macromolecules can be fixed onto the platform by linking to the silane functional group.[238] Figure 45 shows 3-aminopropyltriethoxysilane (APTES), slightly different than APTS, adsorption on silicon wafer where the ethoxy groups of adsorbed APTES are hydrolyzed and form siloxane bonds with surface silanols.

TOCN has an overall negative charge, however in order to enhance the interaction of TOCN with the APTS-treated substrate, it was decided that increasing the charge on both species should contribute this interaction. TOCN bears negatively charged COO- groups on the surface, balanced by Na^+ counterions at the pH at which it is dispersed (pH 7). Films formed from such dispersions did not adhere well to APTS modified surface, however, washing the substrate surface with dilute aqueous HCl and lowering the pH of the TOCN dispersions to pH 5, resulted in improved

adhesion of TOCN to the modified substrate and more even film coverage. The substrates were dried in an oven at 50 ℃ prior to dip coating.

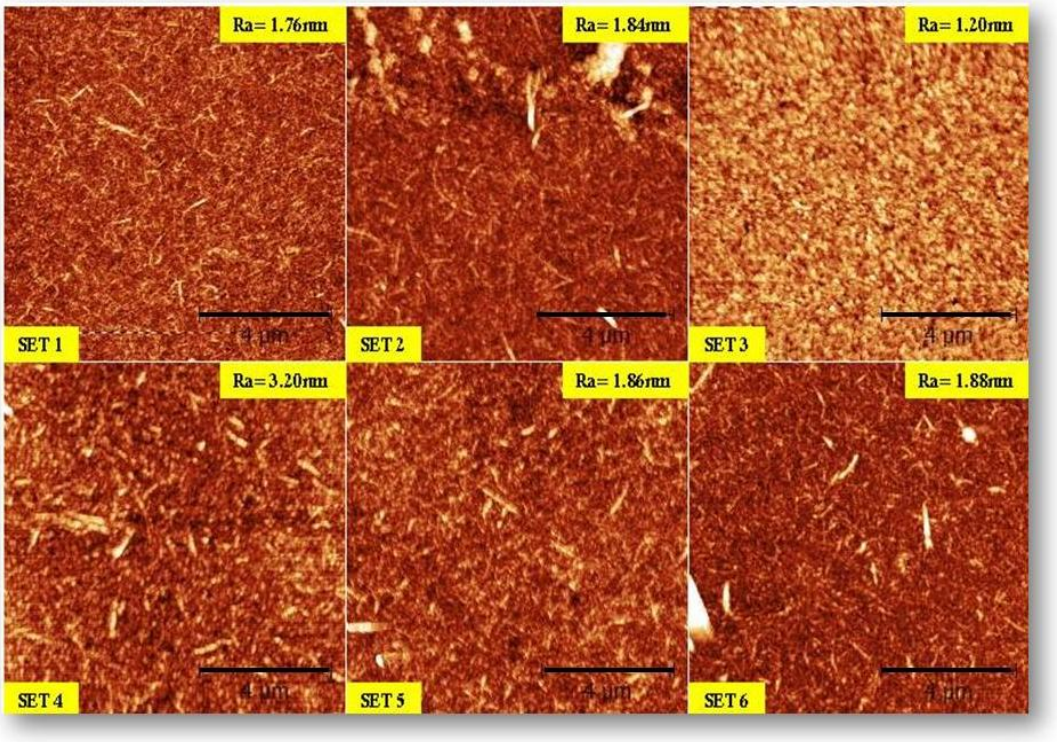

Figure 46: Set 1: Organic-phase deposition of APTS (substrate treated with HCl & TOCN at pH 5) , Set 2: Vapour-phase deposition (substrate treated with HCl & TOCN at pH 5), Set 3: Organic-phase deposition (substrate NOT treated with HCl & TOCN at pH 7), Set 4: Vapour-phase deposition (substrate NOT treated with HCl & TOCN at pH 7), Set 5: Organic-phase deposition (ONLY substrate treated with HCl & TOCN at pH 7), Set 6: Vapour-phase deposition (ONLY substrate treated with HCl & TOCN at pH 7). *Ra= Average surface roughness. The scale bar is 4 µm for all the images.*

The differences in films formed under various coating regimes are illustrated in (Figure 46). Six sets of APTS deposition conditions were studied. Sets 1, 3 and 5 were completed by organic-phase deposition where the substrates were kept in a bottle with dry toluene (20 mL) and APTS (3 %) for 2 hours and washed with toluene/chloroform and left to dry.

The sets 2, 4 and 6 were prepared using vapour-phase deposition where APTS (1 mL in volume, placed in a small vial) was left to vaporise over the substrates over

night. For the sets 1, 2, 5 and 6, the substrate was dipped into HCl (0.1 M), whereas, in case of sets 3 and 4, neither the substrates nor the TOCN was treated. The only pair of sets for which the pH of TOCN lowered to pH 5 were sets 1 and 2. It is important to note that when the substrates were only dipped into low pH TOCN, it was not possible to form smooth films; therefore, further treatment was necessary. This was achieved by treating the glass substrates with HCl prior to dipping as demonstrated for the 1 and 2.

Set 1 and 2 were prepared by lowering the pH of the TOCN to more acidic dispersion. Set 1 gave relatively smooth surface compared to the Set 2; however, it was not the best option as the original dispersion pH was modified. Therefore, Sets 1 and 2 were eliminated.

The TOCN fibrils were clearly observed in the AFM images of Set 1. The results showed that when neither the substrate nor the TOCN was treated, as shown in Figure 46, it was not possible to see the fibrils on the surface. Unexpectedly, the fibrils seemed to be adhering to the surface when the same conditions applied for vapour deposition method for Set 4. However, the surface roughness of the film was high; hence Sets 3 and 4 were also eliminated. (The surface roughness was measured by selecting the entire area and Ra value was given by the programme for AFM image analysis, Gywddion.)

Since the roughness was not significantly different between Sets 5 and 6, and given that the fibrils were well-distributed over the surface of the substrates, it was decided to use the Set 6 as the standard method.

In conclusion, the film coatings on the substrates were carried out on APTS vapour-deposition treated surfaces where only the substrates were treated with aqueous HCl (0.1 M) prior to dip-coating into the TOCN dispersion (1 g L^{-1}) which had been previously centrifuged at 11 000 rpm for 15 minutes to remove a small number of larger particles. The surface roughness was considerably reduced from 1.88 nm to 1.30 nm after including the centrifugation step. The AFM images from the substrate with a smooth TOCN film are shown below (Figure 47).

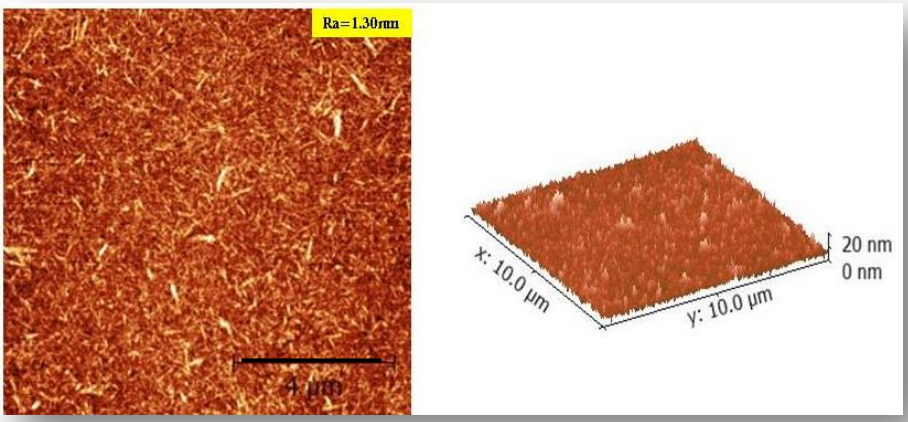

Figure 47: AFM images of smooth TOCN film obtained after the dispersion spun at 11000 rpm for 15 minutes, *scale bar is 4 µm.*

Unfortunately, it was not possible to measure the film thickness in the AFM experiment, despite various attempts (including creating an incision in the film with a blade and imaging across the film edge). The X-ray reflectivity method is a much more accurate technique to measure the film thickness and the details of the TOCN film XRR analysis will be discussed in the following section.

3.3.2 X-ray Reflectivity (XRR) of TOCN Films

With means of creating thin, uniform, smooth films in hand, samples were prepared for the subsequent X-ray reflectivity experiments at Diamond Light Source, Didcot, UK. Selected substrates with TOCN films were analysed by AFM and used for the XRR experiments. The surface modification method for the silicon substrates for XRR was the same as used for glass substrates used for AFM. The TOCN dispersions were prepared at 1 g L^{-1} and centrifuged at 11000 rpm for 15 minutes to remove a small number of large particles, as described above.

Before the start of the XRR experiments, it was important to expose the films supported on silicon substrates to similar conditions to those to be used during the XRR experiments. Therefore, the TOCN coated silicon substrates were stored in either deionised water or $NaCl_{(aq)}$ (0.2 M) solution overnight and reanalysed by AFM, to detect any gross changes to the films under these conditions. The films were dried in the oven prior to measurements.

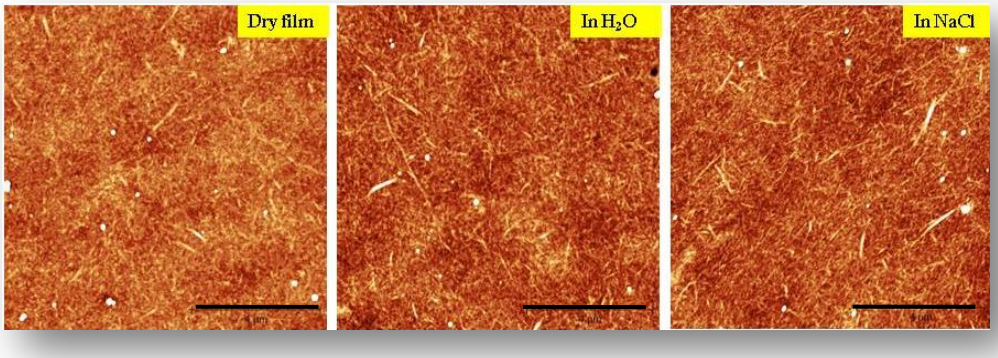

Figure 48: TOCN films after kept in deionised water and NaCl overnight, *scale bar is 4 µm.*

As seen in Figure 48 the films were stable when left exposed to deionised water or NaCl solution overnight. This was taken as evidence that it would prove possible to flow solutions over the films without detaching TOCN films, as intended during the XRR experiments.

The same protocol was followed for each substrate: at first, reflectivity measurements were carried out on a dry TOCN films supported on the substrate (no liquid injection); then deionised water was flowed through the cell, in order to detect any effect on the reflectivity of the film (e.g. for instance due to swelling of the TOCN fibrils). When the liquid is injected through the cell, it forms a thin layer on top of the substrate which is then used as one of the parameters for the reflectivity data fitting. After the injection of water through the cell, a salt solution was injected. The concentrations of these solutions were all kept at 0.2 M. This was followed by injections of surfactant and the salt together and in some cases a higher concentration of surfactant and the salt together .

In order to investigate the interaction between the TOCN and surfactant molecules, SDS (anionic surfactant) was selected. The critical micelle concentration (CMC) for SDS is 8.2 mM[260] and so selected concentration of SDS was 6 mM. After the reflectivity experiments, the substrates were analysed once again by AFM to make sure that the TOCN fibrils were still present after the experiment. This revealed an area which had sustained damage from the X-ray beam. Unfortunately, it appeared that the X-ray beam had effectively "*burned off*" the TOCN film over time, so that

eventually there was no film present where the reflectivity was measured on the substrate. The AFM images, clearly displaying damage of the substrate surface are shown below (Figure 49). It is important to note that the fibrils were present on the surface where the beam did not impinge on the substrate, but there was no evidence of any cellulose along the beam line.

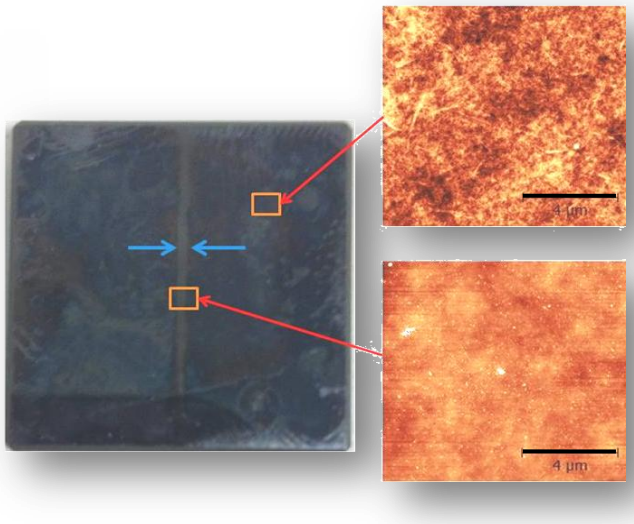

Figure 49: A substrate after XRR experiments. Blue arrows indicate the damage caused by the beam on the substrate and at right AFM images of burnt and unaffected areas. *The scale bar on the AFM images are 4 µm.*

The following reflectivity profiles were selected to show the successful coating of thin and relatively smooth TOCN films on silicon substrates. The same experiment will be repeated using neutron reflectivity to avoid the sample burn. Neutron reflectivity also revealed more about the interaction of surfactants and salts with TOCN by the use of support of contrast difference between the molecules and fibres which is another advantage of neutron reflectivity. Some XRR data however was able to be analysed despite the destruction of the films.

The SLD calculator which was built into the MOTOFit programme was utilised to calculate the values for each layer as shown in Table 7. These values were held during fitting.

Table 7: Calculated SLD values for each layer

	Layers	SLD (x 10^{-6})
Fronting	Water	9.45
Layer 3	TOCN film	13.2
Layer 2	APTS	8.9
Layer 1	Silicon Oxide	18.9
Backing	Silicon Substrate	20.1

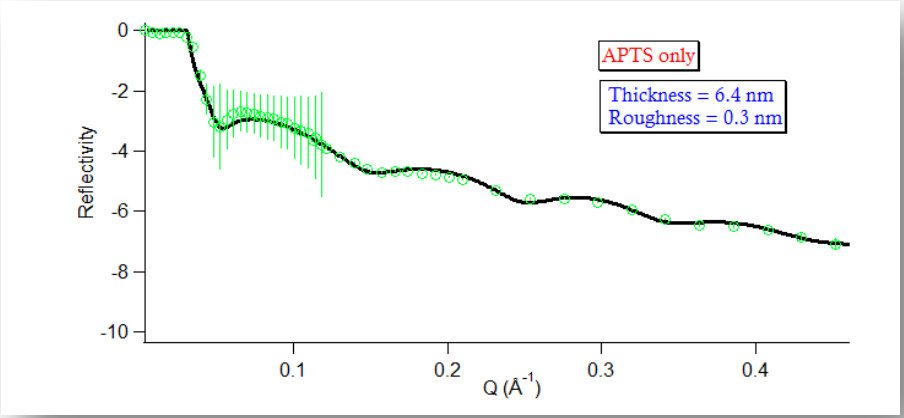

Figure 50: Reflectivity profile of silicon substrate with APTS layer only, without the cellulose film.

Figure 50 shows the reflectivity fitting for the bare silicon substrates without any TOCN film cast on it. The only layer present on the substrate was the vapour-deposited APTS layer. Although, the surface is very smooth as expected (roughness~0.3 nm), the data obtained from the fitting model and the fringes show that the layer is thicker than anticipated. A monolayer of APTS should be 1-1.5 nm thick, but in this case, it was around 6 nm which may suggest overlay of many layers (Table 13:). It was reported by Vandenberg *et al.*[261] that when APTES is vaporised over a substrate for 24 hours, the thickness of the film increases considerably, up to 30 nm. This might be due to formation of islands of APTS which is not possible to distinguish from a monolayer of APTS film.

Table 8: Layer thickness and roughness found for APTS only on substrate

	Layers	Thickness (nm)	Roughness (nm)
Layer 2	APTS	6.4 (±0.1)	0.3 (±0.04)
Layer 1	Silicon Oxide	2.0 (±0.7)	0.5 (±0.06)
Backing	Silicon Substrate	-	0.8

The SLD profile in Figure 51 shows a sharp increase in the SLD profile suggesting a smooth film.

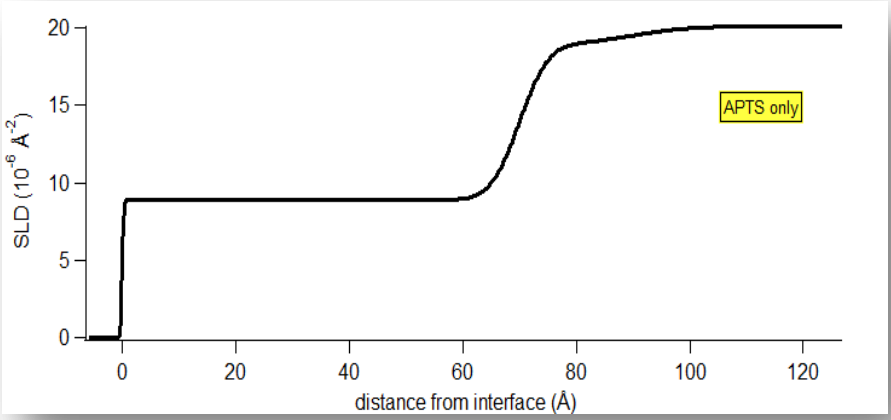

Figure 51: SLD profile for APTS layer on the bare silicon substrate

It is important to highlight that there are two other layers in this SLD profile: the silicon oxide coating of the silicon substrate surface and APTS layered on top this. Therefore, the fitting was calculated based on the following order of layers; the backing (silicon substrate), silicon oxide and APTS layer on top.

The next fitting was carried out for a reflectivity pattern from a substrate treated with APTS and coated with a TOCN film. It was evident that the thickness of the layer increased substantially compared to a substrate bearing no film, unsurprisingly (Figure 52). The thickness was measured to be 23.6 nm. The surface roughness was also ~ 3 nm. This roughness value was higher than the measured by the AFM which was ~ 1.8 nm. The fringes disappeared due to presence of a thick and relatively

rough film layer on the substrate. However, since different substrates were used for each XRR experiment, the thickness of the various layers might therefore be expected to be different.

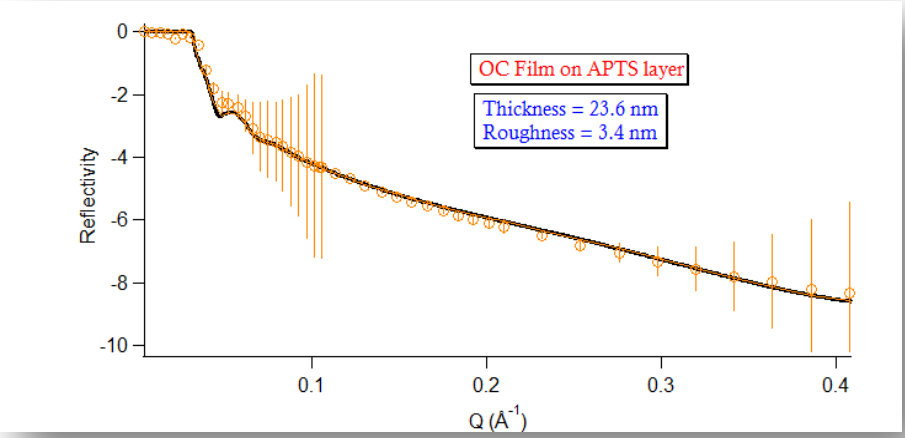

Figure 52: XRR profile of TOCN film on APTS layer.

The SLD profile of the TOCN film is shown in Figure 53 where the distance between the substrate and the film can be seen from the graph. The SLD is gradually increasing as the distance from the interface increases as opposed to a sharp increase in the previous SLD profile for APTS layer, showing the effect of roughness. It is also important to note that treated substrates bearing TOCN films, show thinner and much rougher APTS layers, possibly indicating that part of the multi-layered APTS film is washed off during casting (Figure 53).

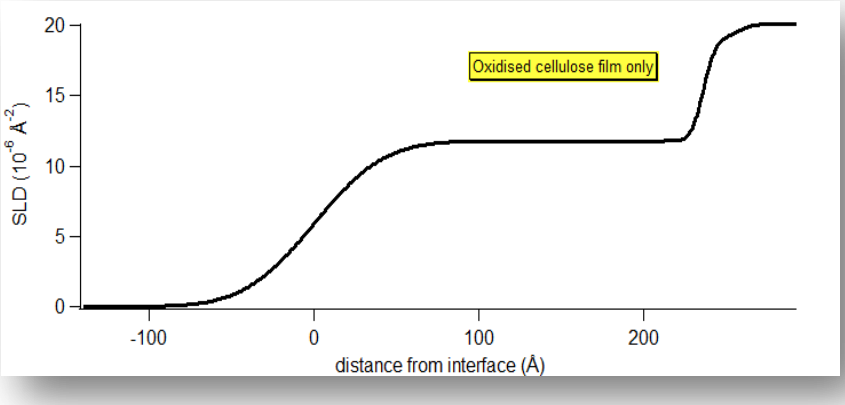

Figure 53: SLD profile for dry TOCN film on a substrate.

Table 9: Layer thickness and roughness found for dry TOCN film on substrate

	Layers	Thickness (nm)	Roughness (nm)
Layer 3	TOCN film	23.6 (±3.8)	3.4 (±1.6)
Layer 2	APTS	2.0 (±0.1)	3.0 (±0.8)
Layer 1	Silicon Oxide	2.0 (±0.2)	0.5 (±0.02)
Backing	Silicon Substrate	-	0.8

The next reflectivity measurement was taken immediately after injecting deionised water through the cell. The surface roughness is nearly doubled which suggests that the fibrils had absorbed water and swelled.

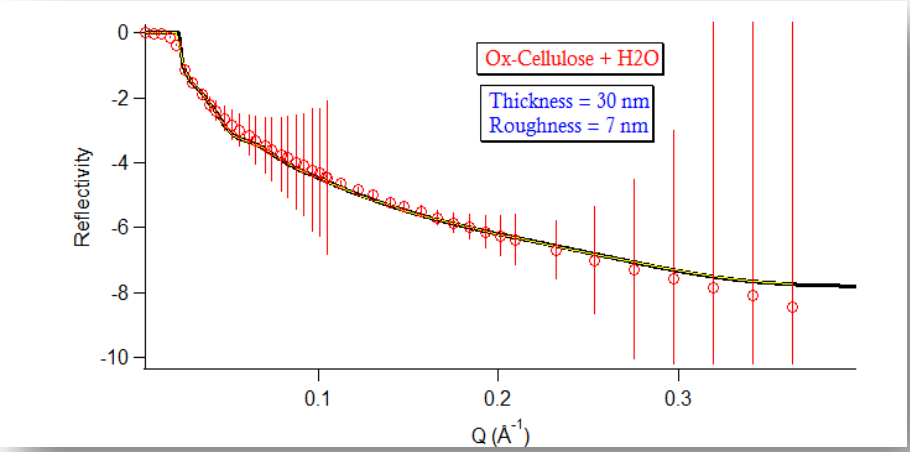

Figure 54: XRR profile of TOCN film after filling the cell with deionised water.

The thickness of the film was measured to be 30 nm and the roughness was ~ 7 nm. The critical edge falls off more quickly compared to that illustrated in Figure 52 as the surface roughness increases.

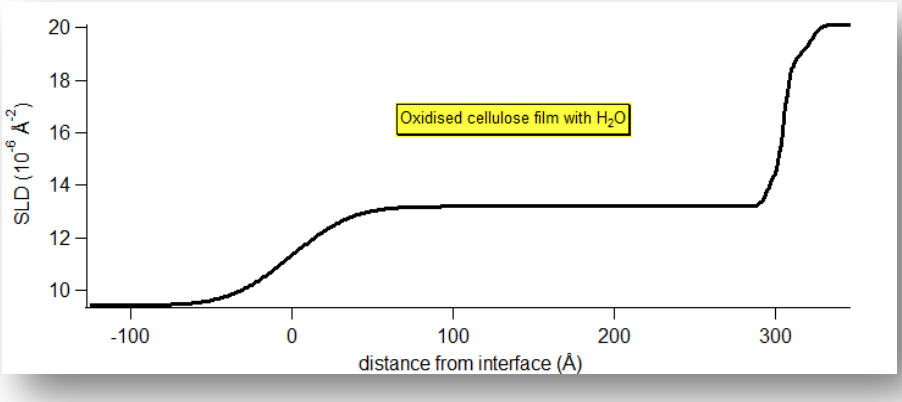

Figure 55: SLD profile of TOCN with a layer of water on top.

Table 10: shows the increase in the roughness and the thickness of the film. The APTS layer is much thinner than reflectivity results found for APTS only layer as above mentioned and also slightly rougher than in the case of dry film only (Figure 55).

Table 10: Layer thickness and roughness found for TOCN film with water on top

	Layers	**Thickness (nm)**	**Roughness (nm)**
Layer 3	TOCN film	30.0 (±1.3)	7.0 (±2.6)
Layer 2	APTS	0.2 (± 0.04)	0.5(±0.1)
Layer 1	Silicon Oxide	0.2(± 0.1)	0.5(±0.02)
Backing	Silicon Substrate	-	0.8

3.3.3 Neutron Reflectivity (NR)

The initial NR experiments were done on silicon substrates with dry TOCN films only. All the fittings include the layers of silicon block, silicon dioxide and APTS. In the case of patterns collected after washing the cellulose film surface with D_2O/H_2O another layer was added for the fittings. When the surface was washed with SDS with or without NaCl, one more layer was added, therefore the cellulose layer was characterised as two layers, one inner layer and one outer layer. Each layer was characterised by the thickness, roughness and a scattering length density. According to Tucker *et al*[82]*.,* the total thickness of a molecular hydrophilic cellulose (trimethylsilyl-cellulose) layer deposited by Langmuir-Blodgett method was 9.5 nm in thickness. The same cellulose deposited on the substrate surface by spin coating measured by Kontturi *et al.*[237] was however, 23 nm. This shows the impact and variation in different deposition methods on the film thickness and the roughness. The films prepared for this study were deposited on the silicon substrates by dip coating and pre-treating the substrate surface with APTS to ensure a uniform coverage of the film. However, this proved to be a challenge for the NR reflectivity experiments. These experiments were carried out at different instruments and 4 or 5 substrates were prepared for each experiment. The reflectivity patterns however showed that the film thickness and roughness varied between the substrates. The thickness of the dry films prior to any wash, for example, varied between 10-20 nm. The roughness was also much higher for the films produced for NR experiments compared to the films used in the X-ray experiments due to the difficulty of carrying out the same preparation on larger silicon blocks.

An NR profile of a dry TOCN film with underlying layers as listed in can be seen in Figure 56. The APTS layer formed for this particular substrates was thinner (4 nm) compared to the one seen for the X-ray reflectivity (6.4 nm). The dry film thickness measured by NR was also around 15 nm.

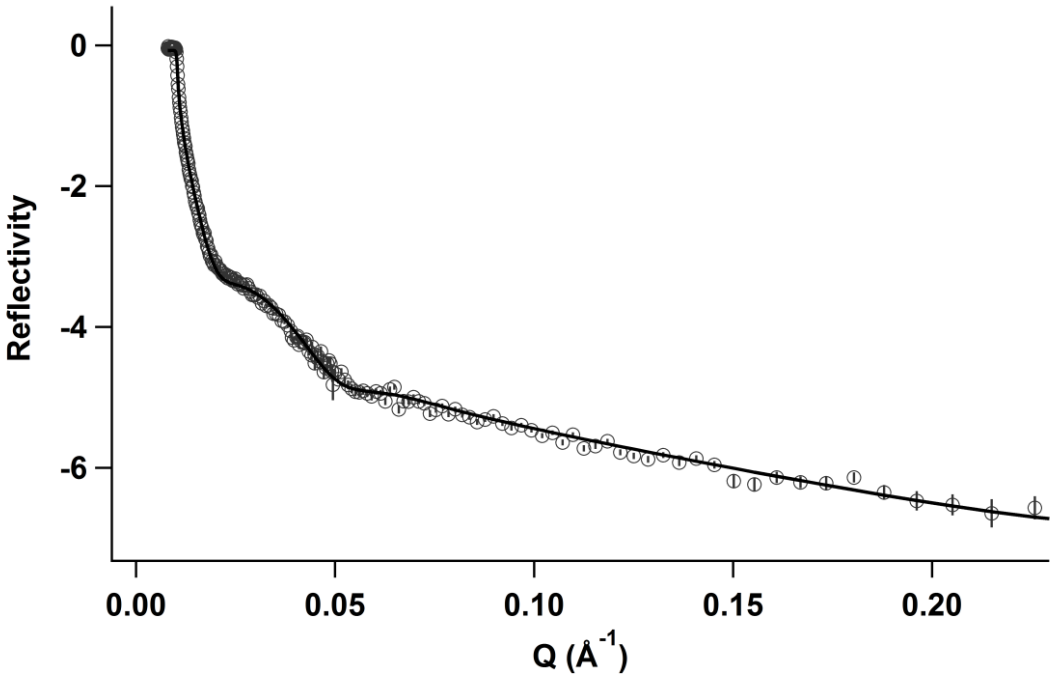

Figure 56: Neutron reflectivity profile of dry TOCN film with APTS layer

Table 11: Model parameters used for TOCN dry film fitting, showing different layers

Sample	Roughness (nm)	Thickness (nm)	SLD (x 10^{-6})
Si	0.2 (±0.1)	INF	2.07
SiO_2	0.4(±0.1)	0.8(±0.1)	3.47
APTS	0.7(±0.2)	4.0(±0.4)	0.23
TOCN	4.2(±0.2)	14.3(±1.3)	1.5

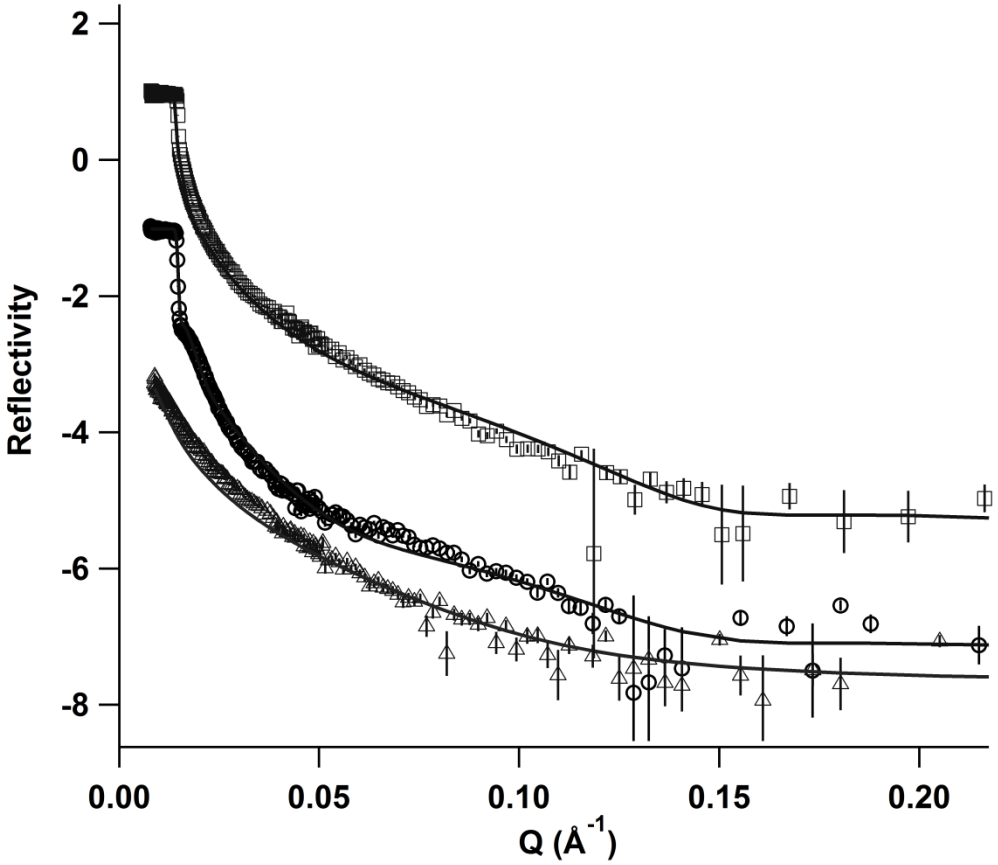

Figure 57: Neutron reflectivity profile for TOCN cellulose in D_2O (circle), H_2O(triangle) and 6 mM d-SDS/D2O(square). The solid lines are model fits using the parameters listed in Table 12:. The data is shifted vertically by a factor of 1 for clarity.

Unlike the X-ray reflectivity experiments, it was possible to complete the reflectivity measurements in the presence of SDS and NaCl. Figure 57 shows the NR profile of TOCN films washed with a variety of solutions in the order: D_2O-H_2O-6 mM d-SDS in D_2O. The thickness of cellulose film was the same after the D_2O and H_2O washes but it became thicker and rougher when washed with the deuterated surfactant in D_2O. The deuterated surfactant in deuterated water can be used to highlight the change in the fibrils which have a greater contrast compared to these since the fibrils are not deuterated. The increase in the SLD for films of the cellulose alone and the cellulose after exposure to the surfactant is also indicative of the interaction between the fibrils and the SDS head group.

Table 12: Model parameters for TOCN films, NR data shown in Figure 57. The SLD value was fitted for the 6 mM surfactant wash.

Sample	Roughness (nm)	Thickness (nm)	SLD (x 10^{-6} Å^{-2})
D_2O	12.5 (±1)	40.2(±2.3)	1.5
H_2O	12.5(±1)	40.2 (±2.4)	1.5
6 mM d-SDS/D_2O	17.6(±1.4)	59.7 (±2.2)	2.3

However, in the presence of hydrogenated SDS in D_2O, the changes in the reflectivity profiles were more dominant. A new substrate was used for this profile. The swelling of the fibrils (indicated by the increase in the thickness) in the presence of deuterated water was less on this substrate. Figure 58 shows the effect of SDS on the TOCN where two layers of cellulose were used to fit the surfactant profile. Penfold *et al.*[262] described the reflectivity based with additional layers as the adsorbed layer of surfactant is expected to form a "fragmented bilayer" or "flatted micelles". The layer thickness then comprises of the surfactant head group and associated hydration. There is also a change in the thickness and the roughness of the TOCN film. This could indicate the adsorption of the surfactant on the fibrils however this is not a strong absorption. Table 13: shows that the layer thickness is almost identical after washing the surface of the film with deuterated water again, indicating total removal of the surfactant. The structure of cellulose film was restored. This suggests that the surfactant was not strongly adsorbed on the surface. According Tucker *et al.*[82] the SDS adsorption is controlled by the hydrophobic interaction and not electrostatic interaction. The suggested reasons for this was explained by the cellulose being weakly anionic or the hydrophobic patches on the surface of the cellulose film (Figure 59).

Table 13: Model parameters for TOCN for the fits shown in Figure 58.

	TOCN Layer 1			TOCN Layer 2		
Sample	Roughness (nm)	Thickness (nm)	SLD (x 10^{-6} Å^{-2})	Roughness (nm)	Thickness (nm)	SLD (x10^{-6} Å^{-2})
D_2O	7.0(±0.5)	20.4(±2)	1.5			
6 mM h-SDS/D_2O	8.0(±0.8)	23.0(±2.4)	2.3	0.4(±0.2)	2.2(±0.2)	1.5
D_2O wash	7.7(±1.3)	20.1(±2)	1.5			

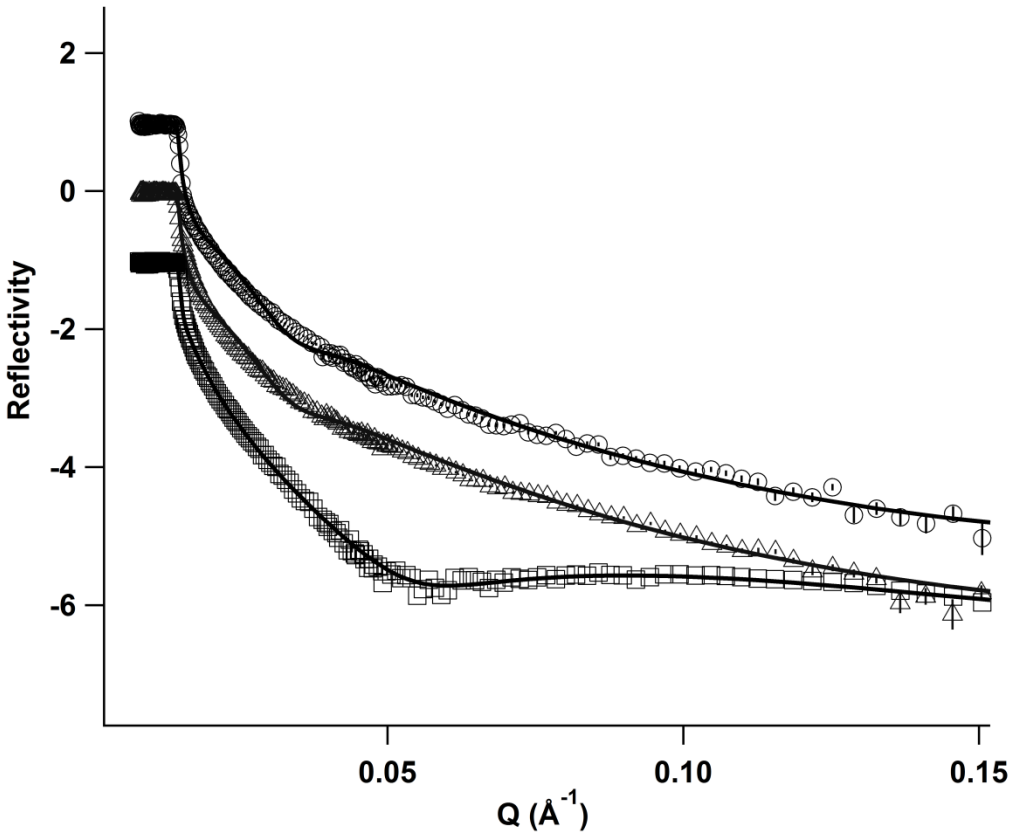

Figure 58: Neutron reflectivity of TOCN film, washed with D_2O (circles), then with h-SDS(6mM)/D_2O (squares), post-washed with D_2O(triangles). The data was shifted vertically for clarity by a factor of 2.

The adsorption of SDS on cellulose film in the presence of salt seems to be greater since the thickness of the film increased by almost 10 nm in the presence of NaCl whereas it only increased by 3 nm when there was no electrolyte. Table 14 also shows the results of the fittings where again a two layer cellulose film was used to model the data. The roughness was also increased although not as much as the thickness. After washing the surface with salt water this time, the film structure was once again restored. This pattern is in an agreement with the literature.[82] The NR profile of these fits are shown in Figure 59.

Table 14: Model parameters for TOCN for the fits shown in Figure 59.

	TOCN Layer 1			TOCN Layer 2		
Sample	Roughness (nm)	Thickness (nm)	SLD (x 10^{-6})	Roughness (nm)	Thickness (nm)	SLD (x10^{-6})
0.2M NaCl	6.7(±0.7)	19.0(±0.5)	1.5			
6 mM h-SDS/0.2M NaCl/D_2O	8.2(±0.6)	28.0(±0.9)	2.3	0.7(±0.1)	2.4(±0.4)	1.5
0.2M NaCl/D_2O wash	6.4(±0.6)	19.2(±0.7)	1.5			

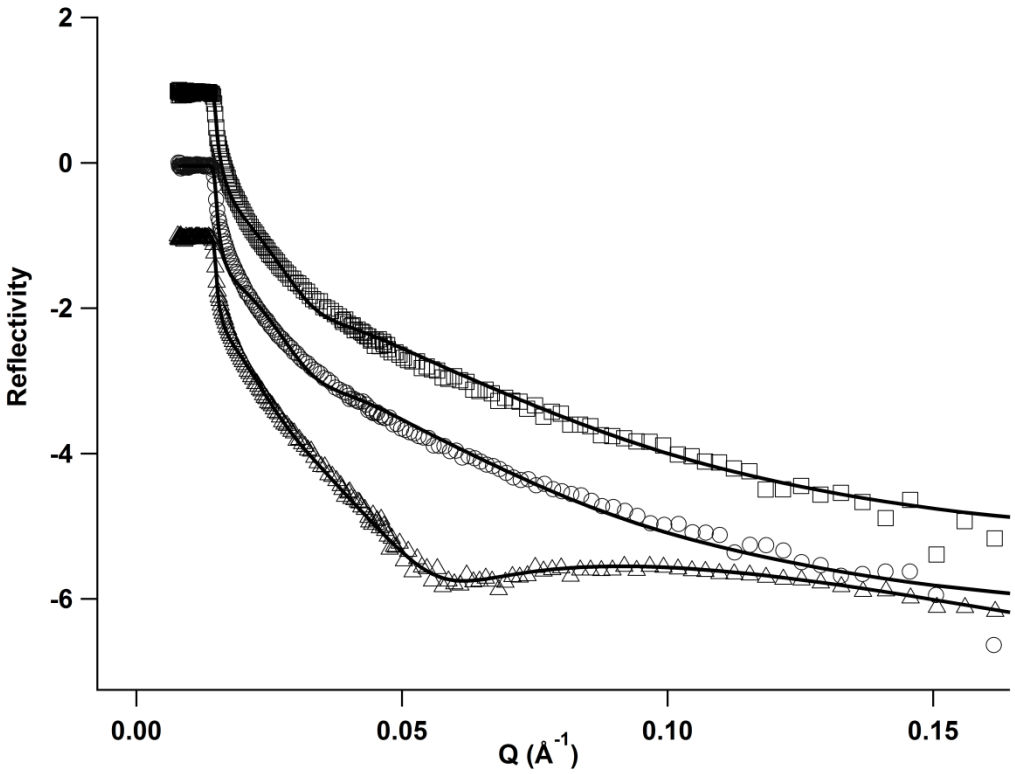

Figure 59: Neutron reflectivity of TOCN films in 0.2M NaCl only (squares), 0.2 M NaCl and 6 mM h-SDS (triangles) and post wash with 0.2 M NaCl (circles), data points shifted vertically for clarity.

The critical micelle concentration (CMC) of SDS is 8.2 mM therefore at 6 mM, the surfactant would be present as monomers interacting with the film surface. At a concentration slightly higher than the CMC, micelles are expected to interact with the cellulose film as well as the few monomers still present in the solution. The thickness of the dry cellulose film for this substrate was 11 nm and the roughness was 2 nm. Figure 59 shows the change on the thickness and the roughness of the

cellulose films. The film thickness and the scattering length density of the cellulose layer increased significantly. The adsorption of the surfactant at 10 mM was greater compared to the surfactant at 6 mM concentration. The presence of salt affected the film thickness to a greater extent at the higher surfactant concentration. Figure 60 shows the fittings and the changes in the NR profile of the cellulose surface washed with high concentration SDS in the presence and absence of salt.

Table 15: Model parameters for TOCN for the fits shown in Figure 60.

	TOCN Layer 1			TOCN Layer 2		
Sample	Roughness (nm)	Thickness (nm)	SLD (x 10^{-6} $Å^{-2}$)	Roughness (nm)	Thickness (nm)	SLD (x10^{-6} $Å^{-2}$)
10 mM h-SDS/D_2O	8.3(±0.4)	24.0(±1)	3.0	0.4(±0.1)	2.2(±0.3)	1.5
10 mM h-SDS/ 0.2 M NaCl/D_2O	9.0(±0.9)	30(±1.3)	3.0			

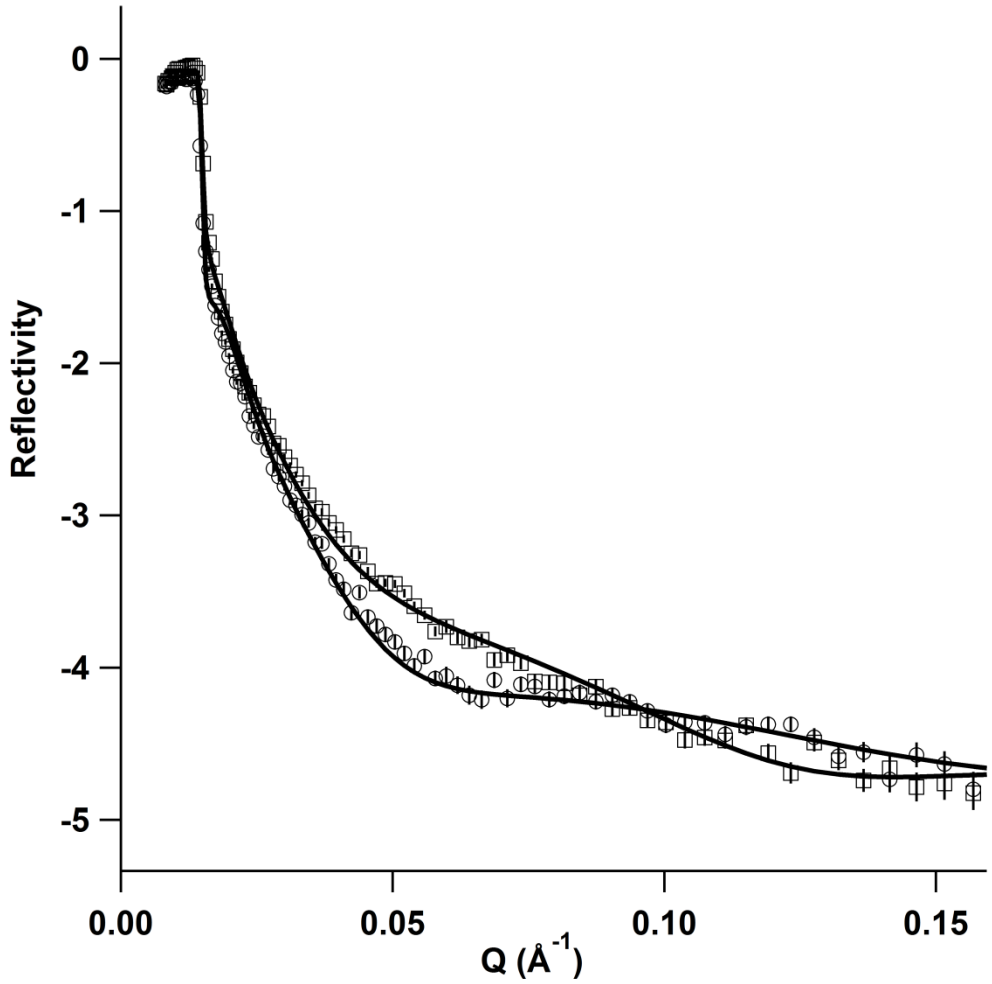

Figure 60: Neutron reflectivity of TOCN films washed with 10 mM h-SDS only (squares) and 10 mM h-SDS with 0.2 M NaCl (circles).

3.3.4 Discussion

The TOCN films were deposited on silicon substrates and analysed by X-ray reflectivity. The X-ray reflectivity experiments were not completed despite the prior surface modification studies. The cellulose films were damaged by the X-rays and therefore after a couple of measurements, the film was burned. Another difference between the X-ray and the neutron reflectivity experiments was the size of the substrates. The size was much smaller for the X-ray experiments and the deposition of the film was less challenging. The biggest challenge of the neutron reflectivity experiments was to create an uniform cellulose film which could be identical across the experiments and between different reflectometers. However, unfortunately this was not the case. The dry film thickness varied across the substrates. There are couple of factors which could yield such outcome. One reason could be the deposition of the APTS vapour. Some of the substrates showed less coverage compared to the others and repeating the vapour deposition process may have resulted in uneven surface coverage. Since the APTS plays a key role as the anchoring material for the TOCN film deposition on the substrate, the variation in the film thickness is perhaps not surprising. Another reason could be the surface area of the substrates since it was difficult to handle the dip coating of these substrates. In general, the films were rough and it was not possible to get smoother films by the dip-coating method for the neutron reflectivity experiments.

The adsorption of the anionic surfactant on the hydrophilic TOCN surface was shown in this study. This could be regarded that unusual behaviour due to the charge repulsion but Penfold *et al.*[262] showed that SDS adsorbs on the hydrophilic silica surface in the presence of non-ionic surfactant. The adsorption of SDS and penetration into a molecular cellulose film in NaCl but also in the absence of electrolyte was also demonstrated by Tucker *et al.*[82] Charge reversal by polyelectrolytes was previously introduced in the literature and was suggested to modify the adsorption behaviour of ionic surfactants.[94,263] Nevertheless, the adsorption of SDS even in the absence of the electrolyte suggest that charge reversal was not a factor in this case.[82] This was supported by another study from the same group on the hydrophobic cellulose.[80] They observed that surface electrolyte either improves or prevents SDS adsorption on the cellulose surface. Therefore, the SDS adsorption is suggested to be due to hydrophobic interaction rather than electrostatic

interaction. However, the studies carried out by other groups on the nature of surfactant penetration onto cellulose model surfaces do not often agree with each other. Torn *et al.*[264]reported an increase in the adsorption of non-ionic surfactant on the cellulose surface with an increase in the surfactant concentration. On the contrary, Singh *et al.*[265] did not observe any penetration of non-ionic surfactant into the cellulose surface. Paria et al.[266] showed the adsorption of anionic surfactant increases in the presence of salt. They suggest salt ions partially neutralises the cellulose surface and as a result anionic surfactant adsorption gets enhanced. In addition, the negative charge of the surfactant molecules is shielded by positively charged salt ions and the compressed double layer at the cellulose surface shields the surface charge. Therefore, the adsorption of anionic surfactant molecules such as SDS, is not inhibited due to electrical repulsion.

3.4 Conclusion

The TOCN films swelled in the presence of water. This was observed both in X-ray and neutron reflectivity experiments. The anionic SDS at concentration 6 mM forms aggregates and weakly adsorbs on the TOCN film surface. At higher surfactant concentration (10 *mM*), the cellulose film becomes thicker. In the presence of NaCl (0.2 *M*), the film structure slightly changed. In addition, the adsorption of SDS was enhanced in the presence of salt. The structure of the film is restored after washing the surface with water or NaCl in water.

The anionic surfactant, SDS, adsorbs onto the hydrophilic TOCN surface and this is shown both in the absence and presence of electrolyte. The thickness of the films can be controlled by the surfactant or the salt. The concentration of the surfactant and the salt present plays an important role in changing the film structure.

4. Ibuprofen delivery into and through the skin: A comparative study of TEMPO-Oxidised Cellulose (TOCN) gels with commercial topical formulations

Overview

The delivery of ibuprofen from formulations containing TOCN (0.6, 1.2 and 1.8 wt %) was compared to that from the commercial gels, Ibuleve and Sainsbury's in order to evaluate the ability of different formulations to deliver the drug. The gels were topically administered *in-vitro* (silicon membrane, pig skin) for eight hours and *in-vivo* (human volunteers) for one hour. Tape-stripping method combined with transepidermal water loss (TEWL) measurements was employed to determine the thickness of stratum corneum (SC). The tapes were gravimetrically quantified and extracted for drug analysis. The SC drug concentration-depth profiles were then fitted mathematically to obtain partition/diffusion coefficient values. The results showed that ibuprofen delivery from TOCN gels with only 1 % w/w of the drug was comparable to that from the commercial gels that contain 5 % w/w of the active drug. The formulations prepared with higher amounts of TOCN were more viscous and the ibuprofen delivery from these formulations was significantly reduced. The formulation with 1.2 wt % of TOCN had the highest steady-state flux which led to highest amount of drug penetration through pig skin whereas and this was lowest for the formulation with TOCN concentration of 1.8 wt %. The findings suggest that the new ibuprofen formulations containing TOCN could be of potential use for topical drug delivery but further optimisation of the formulations is necessary for clinical application.

4.1 Introduction

Ibuprofen is a non-steroidal anti-inflammatory (NSAID) drug that is available as a topical gel for application to the skin to treat local pain and inflammation associated with, for example, for rheumatic disease or other musculoskeletal discomfort.[125] It is a lipophilic compound and has a low water solubility; therefore the delivery of ibuprofen via topical application proves to be a challenge due to its inherently poor skin permeability.[125,130,143,152,267–272] This however, could be overcome by including penetration enhancers in topical formulations to promote the passive drug delivery across the skin. The enhancers such as ethanol interact with stratum corneum and increase the solubility of the drug in the skin as they modify the barrier function of skin.[273] The solubility of ibuprofen in different alcohols has been reported by various research groups.[274–276] In the interest of this study, ethanol was selected as the co-solvent, mainly because it has been commonly used in similar formulations and it is less irritant to the skin compared to other alcohols. There have been many studies on formulation of ibuprofen gels in the literature.[151,271,277,278] The ibuprofen transport to the skin both *in vivo* and *in vitro* was reported by Herkenne *et al.*[124] A study by Hadgraft *et al.* compared the skin penetration of topical formulations of ibuprofen 5 % where the results revealed that the Ibugel (similar to Ibuleve used in this study) performed more efficiently compared to other commercial gels in the market such as Deep Relief Gel™.[150] They also highlighted that the composition of the vehicle plays a key role in the drug penetration qualities of the formulations. The commercially available gel formulations of ibuprofen often comprise alcohols (ethanol, isopropanol, or a mix of alcohols) up to 40 wt %, polymeric thickeners (Carbomer®, chitosan, hydroxyethylcellulose, hydroxypropyl cellulose), permeation enhancers (propylene glycol (PG), polyethylene glycol (PEG)) and other chemicals for pH adjustment (triethanolamine, sodium acetate).[271]

In this study, the rheology modifier was replaced by TOCN which is derived from renewable resources unlike the polymeric thickeners commonly used in products found in the market. TOCN is a non-irritant, colourless, odorless material which can be used as a thickener in pharmaceutical, personal care and cosmetic products.[1] Oxidised cellulose in general found many uses in the pharmaceutical industry (see Chapter 1). Perhaps most relevant to this study however is that TOCN is known to form shear thinning gels. It also has good suspending power and can tolerate alcohols

and hydrophobic species which makes it a promising material for use in aqueous formulations.[1,15,27,279] Crawford *et al.*[1] suggested the combination of low molecular weight alcohols such as ethanol and propanol with TOCN could yield gels even in the presence of surfactants. However, the use of TOCN in hydroalcoholic formulations for topical drug delivery has never been published before. The aim of this chapter was to examine the ability of new vehicles prepared with TOCN to deliver a model drug (ibuprofen) across membrane/skin as well as the commercial formulations.

4.2 Materials and Methods

4.2.1 Chemicals

Ibuprofen (≥98 % GC), sodium dodecyl sulfate (ACS reagent, ≥99.0%), acetonitrile (HPLC grade, ≥99.9%), hydrochloric acid (ACS reagent, 37 %), triethylamine (≥99%), phosphoric acid (≥99%), were all purchased from Sigma Aldrich (Gillingham, UK). The commercial gels Sainsbury and Ibuleve were purchased from Sainsbury's Pharmacy (Bath, UK) and Diomed Developments Limited (Hertfordshire, UK) respectively. Sodium chloride (99.7+%), potassium chloride (99.5+%), sodium phosphate (99+%) and potassium phosphate (99+%) were all purchased from Fisher Scientific (Leicestershire, UK) and used for the buffer preparation.

4.2.2 Preparation of aqueous TOCN dispersions

TOCN dispersed in deionised water was kindly provided by Unilever (Port Sunlight, UK). It was freeze-dried and maintained at 4 ℃ for further use. Oxidised cellulose nanofibers were prepared from purified α-cellulose fibers by 2,2,6,6-tetramethyl-piperidin-1-yl)oxyl (TEMPO) mediated NaOCl/NaBr oxidation process in water, followed by mechanical dispersion as described previously.[15,31] If the process is taken to completion, it would generate poly(glucuronic acid) which dissolves in water, but here the oxidation is limited to 20-25 % by controlling the quantity of oxidant used.[1] The TOCN dispersion was first dialysed using dialysis membrane (MWCO 12000, diameter 16 mm, Sigma Aldrich, Gillingham, UK) in deionised water for a week (changing the water three times a day). The dialysed cellulose was then freeze-dried and dispersed in deionised water at desired concentrations. 2 g of oxidised cellulose was weighed out and dispersed in 100 g of water and was stirred overnight at room temperature. This was used as the stock solution (pH 6.5). Milli-Q

water (18.2 MΩ cm^{-1}) was used for the preparation of the dispersions. The dispersion (20 g) was then sonicated for 30 minutes and was set to 1 second on and 1 second off mode and at a power of 2 W cm^{-2}. The dispersions were sonicated using Vibra Cell Sonicator and the tip used was ultra-high intensity (tip diameter 3 mm) purchased from Sigma Aldrich (Gillingham, UK).

4.2.3 Optimisation of TOCN gels

Hydroalcoholic TOCN gels were prepared using previously dispersed aqueous stock dispersion. The ibuprofen was first dissolved in the alcohol and then the cellulose dispersion was added to this mixture. The constituents of TOCN formulations are listed in Table 16.

Table 16: Formulations prepared with TOCN and ibuprofen.

Formulation Code	*TOCN Conc.*	*TOCN in water* (wt %)	*Ethanol* (wt %)	*Ibuprofen* (% w/w)	*SDS* (wt %)	*PG* (wt %)
A	1.8 wt %	60.0	37.0	1.0	-	2.0
B	1.8 wt %	60.0	39.0	1.0	-	-
C	1.2 wt %	60.0	39.0	1.0	-	-
D	0.6 wt %	60.0	39.0	1.0	-	-
E	1.8 wt %	60.0	39.0	1.0	0.07	-

The concentrations of the TOCN-alcohol-ibuprofen drugs varied (between 0.6-1.8 wt %) in order to compare the differences in drug delivery (Figure 61).Throughout this chapter I will refer the prepared gels with their formulation codes listed above.

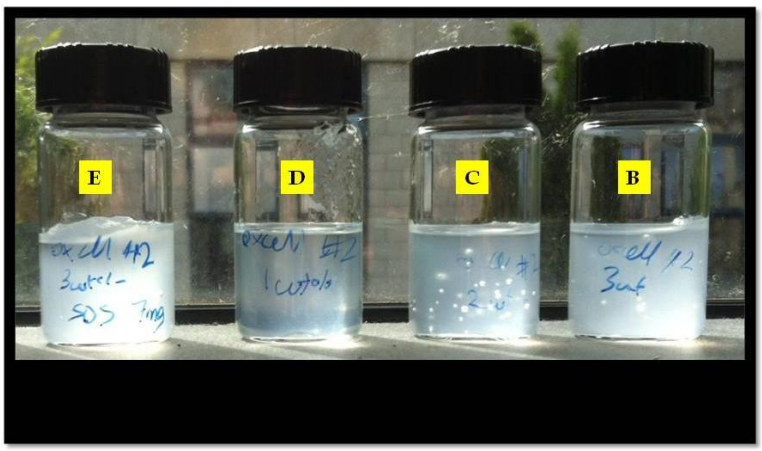

Figure 61: Formulated TOCN-alcohol-ibuprofen gels used for *in vitro* pig skin experiments.

Formulations A and B were used in the initial silicone membrane experiments and compared to two commercial gels, Ibuleve and Sainsbury. Four TOCN formulations with ibuprofen (B, C, D and E) were selected for the pig skin *in vitro* studies. Only formulation B was used for the *in-vivo* experiments. The components of the commercial and formulated TOCN gels are shown in Table 17. It is important to point it out the concentration of ibuprofen drug was 1 % w/w in the TOCN gels whereas it was 5 % w/w in both of the commercial gels. This concentration was the maximum amount of drug that can be dissolved in these formulations.

Table 17: Components of the gels used in this study.

Type of gels	***Components***
Sainsbury's Gel	Ibuprofen (5 % w/w) , hydroxyethylcellulose, sodium hydroxide, benzyl alcohol, isopropyl alcohol and purified water
Ibuleve®	Ibuprofen (5 % w/w), IMS, carbomer, propylene glycol, diethylamine, purified water.
Oxidised Cellulose Gels	Ibuprofen (1 % w/w), oxidised cellulose, ethanol, purified water.

4.2.4 Stratum Corneum (SC) Sampling Protocol:

The non-invasive method to determine the rate and extent of the active drug to reach its site of action was performed by sampling of ibuprofen from the SC. This method was used for both abdominal pig skin and human skin subjects. The amount of drug present in SC was measured by sequential removal of the skin by adhesive tape-stripping (Scotch Book Tape, 3M, St Paul, MN). The template (tape with a hole cut in the middle) was centred over the drug application site prior to tape-stripping. The size of the opening in the circular template (diameter 2 cm) was smaller than the size of the tape-strips (2.5 cm x 2.5 cm). The amount of SC removed by each tape strip was determined by the weight difference (SE2-F, Sartorius AG Microbalance, Gottingen, Germany) before and after the tape-stripping. By knowing the area of the tape, the mass of SC and the density of SC is ~1 g cm^{-3} [139,280–282] it was then possible to determine the SC thickness removed on each strip and thus the depth within the skin barrier.

The apparent SC thickness was calculated from the measurements of transepidermal water loss (TEWL) (Aquaflux, Biox Systems Ltd, London, UK) by tape-stripping the control site (no drug) adjacent to the drug application sites (Figure 62). This was done by the reasons of: a) volatile solvents from the formulation can give inaccurate TEWL readings, and b) each TEWL measurement requires around two minutes during which the ibuprofen continues penetrating into the SC and therefore changes the concentration profiles.[124] These measurements then enable us to present ibuprofen concentration profiles across SC as a function of relative depth and by doing so normalising the results from subjects with different SC thickness and thus compare the drug delivery. [283,284] TEWL measurements were performed by successively placing the pre-weighed adhesive tapes over the template-delimited area, applying gentle pressure with a stainless steel roller in an attempt to remove uniform layer of SC.[267,285] Typically 20-30 tapes were used until the value for TEWL had reached 4 times the baseline measured initially or >70 g/m^2/h, which indicate the removal of at least 75 % of the total SC thickness.[285]

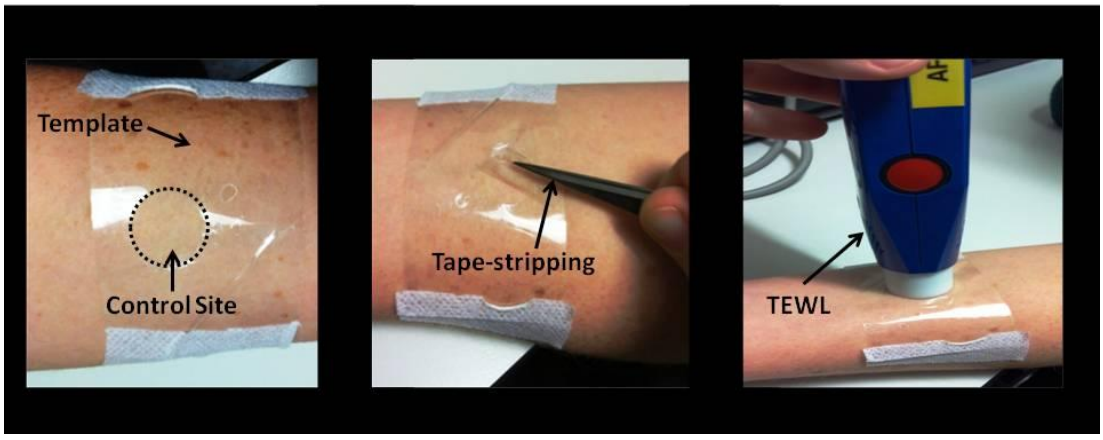

Figure 62: Tape-stripping and TEWL measurements on a volunteer.

4.2.5 In-vitro penetration studies

4.2.5.1 Silicone membrane

Artificial silicone membrane (serial number 7-4107, thickness 75 μm) was donated by Dow Corning Ltd. (Cardiff, UK). The permeation studies were carried out in vertical Franz diffusion cells (PermeGear Inc., Bethlehem, PA) (Figure 63) with a receptor volume of 9-9.5 ml (accurately measured for each sample). The receptor solution was phosphate buffered saline (0.1 M, pH 7.4) and the experiments were

performed at 37 °C. The experiments taken place at 37 °C. The area of exposed membrane surface was ~3 cm^2. The amount of gel deposited in the donor compartment of the diffusion cell was approximately 1 g. Five replicates of each experiment were carried out. The cells were occluded with Parafilm (Bemis, Oshkosh, WI) immediately after placing the gel in the donor compartment. At various times up to 8 hours post-initiation of the experiment, 1 ml of receptor medium was removed and replaced with 1 ml of fresh receptor solution. The cumulative amount of drug penetrated from each formulation was measured by high-performance liquid chromatography (HPLC).

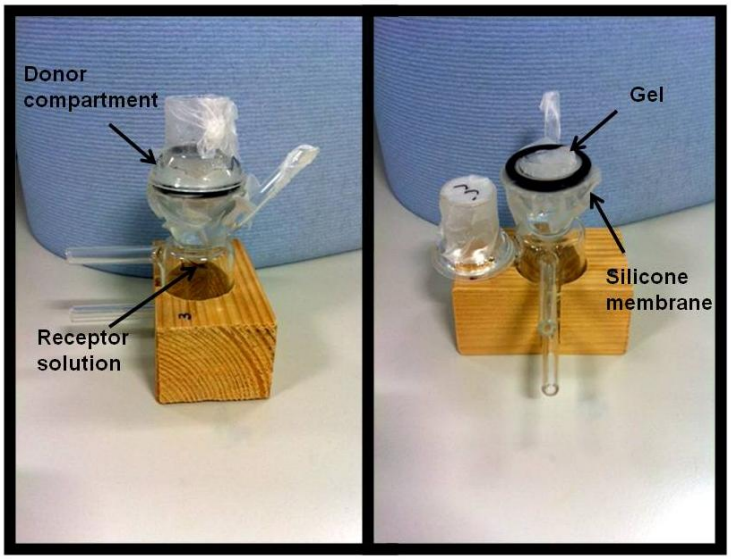

Figure 63: Franz-type diffusion cell used for the experiments. The cells were occluded with Parafilm and silicone membrane can be seen between the donor and receptor compartment.

4.2.5.2 Skin tissue

Abdominal porcine skin (B&J Pigs Ltd, Somerset, UK) was used for this study. After cleaning and trimming off coarse hairs, the tissue was dermatomed (Zimmer® Electric Dermatome, Warsaw, IN) to a nominal thickness of ~750 μm. The skin was then stored at -20℃ and was used within three months. Before the permeation experiment, the skin was thawed and any remaining hairs were carefully trimmed using scissors. Approximately 0.64 g of gel was deposited in the donor compartment of the Franz diffusion cell, which was then occluded with Parafilm™ (Bemis, Oshkosh, WI). Four to six replicates of each experiment were carried out. The

exposed skin surface area was ~ 2 cm^2 and the receptor volume was 7-7.5 ml (accurately measured for each sample).At various times up to 8 hours post-initiation of the experiment, 1 ml of receptor medium was removed and placed with 1 ml of fresh receptor solution.

At the end of eight hours of diffusion experiment, the pig skin was removed from the diffusion cells and pinned to a sheet of foam; any excess formulation on the surface was removed using tissue (Kimberly Clark, Fisher UK).Tape-stripping of the stratum corneum (described below) then commenced immediately.

4.2.6 In-vivo penetration studies

Human Volunteers

Four healthy volunteers (aged 22-30 years, two male and two female) with no history of dermatological disease participated in this study which was approved by the Research Ethics Approval Committee for Health (REACH; EP 14/15 2) of the University of Bath (Forms in Appendix 1). Informed consent was obtained from all subjects. The ibuprofen formulations were applied to less hairy sites on the ventral forearm inside a foam ring and were occluded with plastic Hill Top chamber (33 mm, Sarasota, FL) (Figure 64). Mefix self-adhesive tapes (Mölnlycke Health Care, Sweden) were used to cover the individual treated sites to secure the chambers. The formulations were placed on three different sites on the forearm and one site was used as a control site where no drug was applied which was the site used to determine the SC thickness of individual subject.

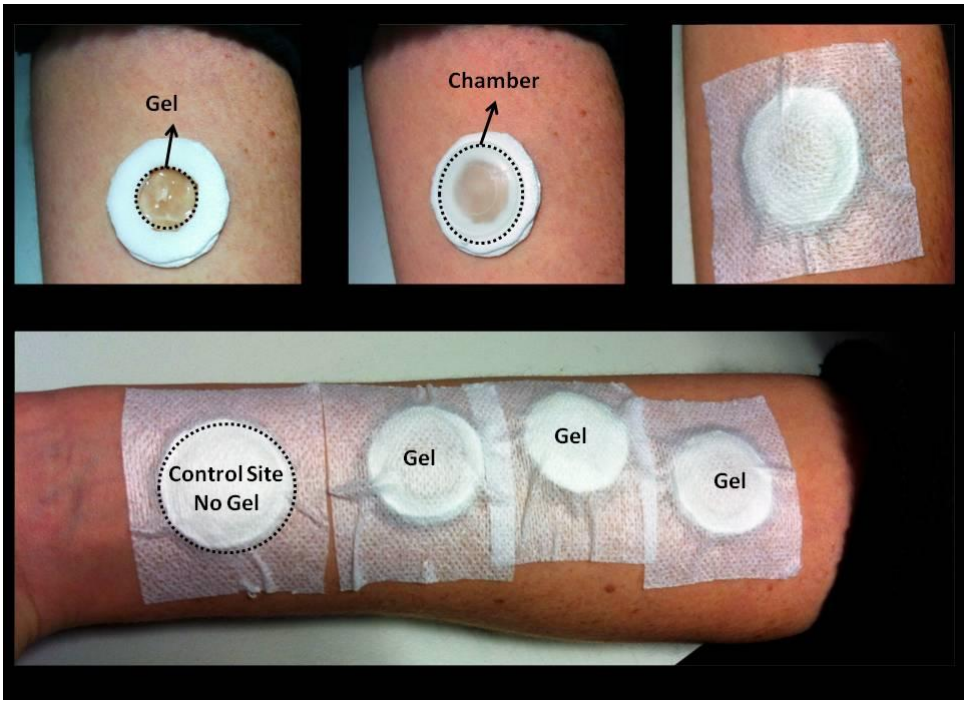

Figure 64: Drug application on the forearm of a volunteer for the i*n-vivo* experiments

4.2.7 Extraction and analysis of ibuprofen in the tape strips

After tape-stripping, each tape was re-weighed individually and was rolled inside a 1.5 ml HPLC vial. Ibuprofen present on the tape was quantitatively extracted by immersing the tape in 1 ml of 90:10 mixture of acetonitrile and 1 M hydrochloric acid, shaking overnight. The extracted solution was then filtered (0.45µm nylon filter, SMI-LabHut Ltd, Gloucestershire, UK) to remove any large residues prior to analysis. Ibuprofen was quantified by HPLC (Jasco, Great Dunmow, UK) using Dionex Acclaim 120 (C18, 5 µm, 4.6 x 150 mm, Thermo Scientific, US) column, UV-vis detector (Waters, Milford, MA) at 227 nm, and a mobile phase of 60:40 v/v mixture of acetonitrile and triethylamine (TEA) (0.2 % v/v aqueous) adjusted to pH 2.84 by phosphoric acid. The flow rate was 1.1 ml/min and the retention time for the drug was around 6 minutes. A previously determined standard curve (over an ibuprofen concentration range of 0.05 (limit of quantification) to 100 µg/ml enabled the amount of drug present in each sample to be found.

4.2.8 Data Analysis

The diffusion through SC is an example of diffusion through passive membrane. Fick's second law of diffusion has been generally recognised for explanation of transport of drug molecules through the skin [106133]:

$$\frac{dC}{dt} = D\frac{d^2C}{dx^2} \tag{48}$$

Where *C* is the concentration of diffusing substance, *D* is the diffusion coefficient, *x* is the thickness of the barrier and *t* is time. The SC concentration (C_x) can be then plotted against normalised SC depth (x/L) profile of ibuprofen and fitted using Fick's second law of diffusion for *in-vivo* experiments[124,272]:

$$C_x = KC_v\left\{\left(1-\frac{x}{L}\right)-\frac{2}{\pi}\cdot\sum_{n=1}^{\infty}\frac{1}{n}sin\left(\frac{n\pi x}{L}\right)exp\left(\frac{-Dn^2\pi^2t}{L^2}\right)\right\} \tag{49}$$

This equation allows measurement of the drug's SC/vehicle partition coefficient (*K*) which indicates the attraction of the drug for the SC over the vehicle and a kinetic parameter (D/L^2) which is related to the rate of diffusion of ibuprofen across the SC. The conditions required for this to be valid are as follows [124] :

- The applied drug concentration (C_v) is constant during the time *t*
- The viable epidermis acts as a perfect sink for the drug
- SC contains no drug in the beginning *t=0*

The cumulative amount of drug penetrated from each formulation was fitted as a function of time *Q(t)* by integrating in to Eq (49) (where number of observations, n=10) :

$$\mathrm{Q(t)} = \mathrm{(KL)C_v}\left\{\left(\frac{\mathrm{D}}{\mathrm{L^2}}\mathrm{t}-\frac{1}{6}\right)-\frac{2}{\pi^2}\cdot\sum_{\mathrm{n=1}}^{\infty}\frac{(-1)^{\mathrm{n}}}{\mathrm{n^2}}\exp\left(\frac{-\mathrm{Dn^2\pi^2t}}{\mathrm{L^2}}\right)\right\} \tag{50}$$

Where *Q* is the cumulative amount of drug permeated per unit area, *t* is the time, C_v is the applied concentration which is constant throughout the experiment, *L* is the

thickness of the skin barrier, K is the partitioning coefficient and D/L^2 is the diffusion coefficient of the drug.

Data analysis was performed using GraphPad Prism version 5.00 (Graph Pad Software, San Diego, California, USA) and the statistical tests to determine the significance of the results were carried out by means of one-way ANOVA with Tukey's multiple comparison test and the level of significance was described at 0.05.

4.2.9 Rheology measurements

The viscosity studies were performed using a Bohlin C-VOR viscometer (Malvern Instruments, MA, US) equipped with CP 4/40 cone and plate (4° cone angle and 40-mm cone diameter). The experiments were completed at 25 °C and approximately 5 g of formulation was placed on the plate for each measurement. Shear rate range was between 0.01 to 100 s^{-1}. Each measurement was repeated three times and the results were averaged. The data was collected using software Bohlin CVO-120.

4.2.10 pH measurements

The pH of each formulation was measured using a pH meter (Orion 420Aplus, Thermo Scientific, US). The pH meter was calibrated prior to measurement with buffer solutions at pH 4, 7 and 10. The measurements were repeated three times.

4.3 Theory of the instruments

4.3.1 High performance liquid chromatography (HPLC)

HPLC is an advanced technique used to separate and measure sample with very little volume and at great accuracy. The sample preparation usually only involves filtration prior to analytical system however it is important to separate the compounds effectively and therefore it's important to select the correct column, mobile phase and understand the chemistry of the compound being analysed. The separation of compounds in a sample is accomplished by injecting the sample (pre-dissolved in solvent) into a stream of solvent being pumped into a column which has a solid separating material. As a result, solid-liquid separation takes place. When a mixture of compounds in injected into the HPLC, some of these compounds will have affinity

for the solvent and some for the packing material in the column. The separation can be a challenge since there will be compounds which has affinity for both, though on a reverse-phase column, the separation can take place because each compound has different partition rates between the solvent and the packing material. [286,287] The solvent is constantly pumped through the column enabling components with highest affinity for the packing material stay the longest and leave the last. This is the essence of HPLC separation. The separated compounds move towards the detector flow cell and start to appear as peaks identified by the detector. These peaks can be then used to quantify the compound present in that sample.

A HPLC system consists of high-pressure pump, an injector, a column, an UV-vis detector and a data recorder. The HPLC column works on the basis of polar molecule attracting polar and vice versa for the non-polar molecules. The non-polar part is the moist, fine, solid packing material inside the column whereas the polar solvent travelling through the column is called *mobile phase* which is the immiscible phase. If the compound is dissolved in the mobile phase and pumped through the column, then the components will diverse between these opposite phases. The polar components in the sample will favour the mobile phase and move faster down the column and hence be separated. Solvent gradients are used to achieve the ideal separation of the components in order to quantify them accurately. This is done by changing the polarity of the column or the mobile phase. If the difference in the polarities of the phases is small then the compounds will elute quickly but if the difference is larger, than the compounds will come off later. HPLC is a common method used in quantification of pharmaceuticals and therefore it was used to detect the cumulative amount of ibuprofen in the diffusion cell experiments for the drug delivery part of this study. The column used for this study was packed with alkylated (C18) silica particles which makes the surface of the column highly non-polar. The mobile phase used was a mixture of aqueous/organic solvent. The affinity of ibuprofen molecules for the non-polar silica surface was slightly decreased by this mixture of solvents where ibuprofen drug molecules would elute earlier compared to aqueous solvent only mobile phase.

4.3.2 Transepidermal water loss (TEWL)

TEWL is used to measure the flux of water evaporation in the adjacent air. The measurement chamber consists of a hollow cylinder (Figure 65) and the lower end of the cylinder contacts the skin surface. The upper end is closed with condenser which is kept at below freezing temperature (-7.65 ℃) by a Peltier cooler. The condenser constantly removes water vapour arising from the skin, storing it as ice.[288] This maintains a low humidity at the condenser and the humidity at the skin surface increases with increasing water evaporation rate.The difference in the humidity results in water vapour to move from bottom of the chamber to the top by passive diffusion yielding a linear distribution of humidity which enables us to measure water vapour flux based on calculations from this gradient and Fick's first law of diffusion.[288]

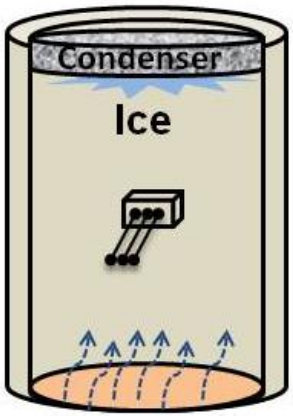

Figure 65: TEWL instrument placed on the skin with a closed chamber and vapour detector inside, image redrawn from 288.

In part of this project, the drug penetration profiles of individuals were compared to each other. However, since the thickness of the stratum corneum (SC) is different for each individual, it was necessary to normalise the drug-penetration profiles in order to make the results comparable to each other. It is possible to measure the rate and the extent of the drug penetration into the skin and since SC is the outer most layer of the skin, the kinetic data through this pathway can be correlated to bioavailability of the target tissue.[284,289,290]

It is important to note that it's not possible to determine the exact SC thickness (*H*) in a non-invasive way , however, it has been accepted that a Fick's first law can be related to values obtained from TEWL measurements to allow us to obtain relative information on the SC thickness :

$$TEWL_0 = \frac{D \cdot K \cdot \Delta C}{H} \tag{51}$$

Where $TEWL_0$the baseline of TEWL, *D* is is the diffusion coefficient of water in SC, *K* is the SC tissue partition coefficient of water; ΔC is the water concentration gradient and *H* is the thickness of SC. This equation acknowledges that the SC is the

main barrier to water loss, and assumes that it offers a uniform barrier for water diffusion.[284,291] Consequently, when a certain fraction of the SC (corresponding to a thickness, *x*), has been removed by tape-stripping, the TEWL value will increase accordingly:

$$TEWL_x = \frac{D \cdot K \cdot \Delta C}{H - x} \tag{52}$$

where *x* is calculated from area of tape-stripped section, mass of SC on tape (the difference before and after tape-stripping) and the density of the SC (~1g/cm^3) [281]. A reciprocal transformation of above equation yields a linear expression which relates $1/TEWL_x$ to *x*. When $1/TEWL_x = 0$, then $x=H$, hence enabling us to find the *H*. [284]

4.4 Results and Discussion

4.4.1 Effect of viscosity on permeation

The release of a drug molecule from a vehicle across a membrane takes place by diffusion and the apparent viscosity of the formulation could affect the diffusion of particles.[153–155] A study by Tas *et.al.*[153] show that the active substance released from the formulations decreases as the polymer concentration increases which also means higher viscosity. The viscosity profiles of all the formulations used for in this study is shown in Figure 66.The formulations with the highest viscosity are the two commercial gels whereas the least viscous formulation was the formulation D.

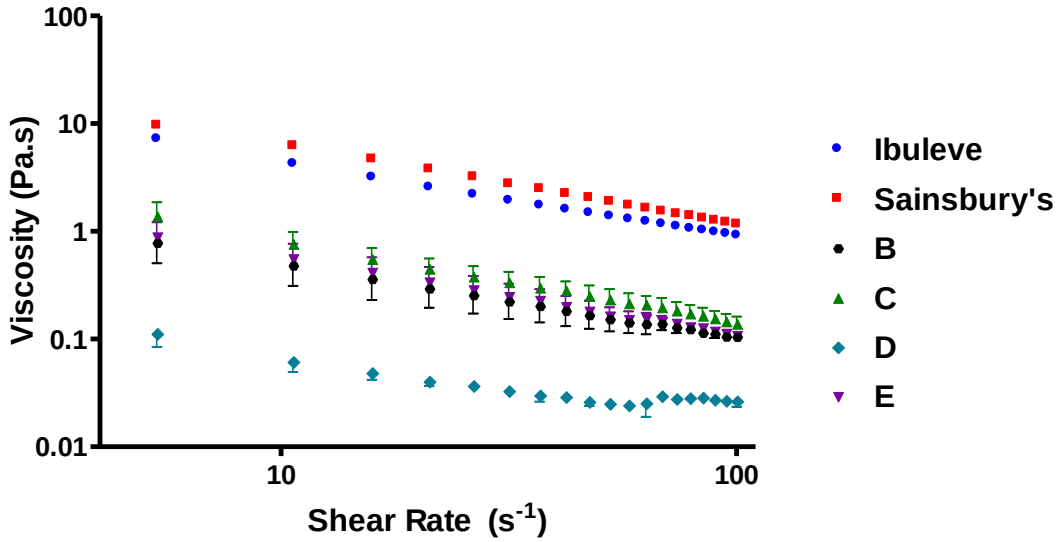

Figure 66: Viscosity plotted against shear rate for all the gels used in in vitro pig skin experiments. mean±SD, n=3

The concentration of TOCN in formulations B and E was 1.8 wt %, whereas it was 1.2 and 0.6 wt % for formulations C and D respectively. The difference in viscosity was less apparent between formulations B, C and E. The low amount of SDS (0.07 wt %) did not have an impact on the viscosity between formulations B and E where both had the same concentration of TOCN. However, there was a significant difference between the formulation D and the rest of the formulations. The diffusivity parameters for pig skin *in-vitro* were similar for all the gels including the commercial ones. However, the *in-vitro* measured flux values of two commercial gels and formulation B were closer to each other whereas the values were much higher for the less viscous formulations C and D (Figure 66).

4.4.2 SC thickness determination

Figure 67 shows an example of a tape-stripping experiment (pig skin) where the cumulative amount of SC removed (µm) by each tape was plotted against 1/TEWL. The measurements indicated that SC on the pig abdominal skin was thicker than that on human skin. The average SC thickness was 26.4 ± 2.7 for pig skin, whereas it was 10.8 ± 3.5 for human skin (mean ± SD, n=3). The determination of SC thickness enables us to convey all the concentrations on a common scale of normalised depth.

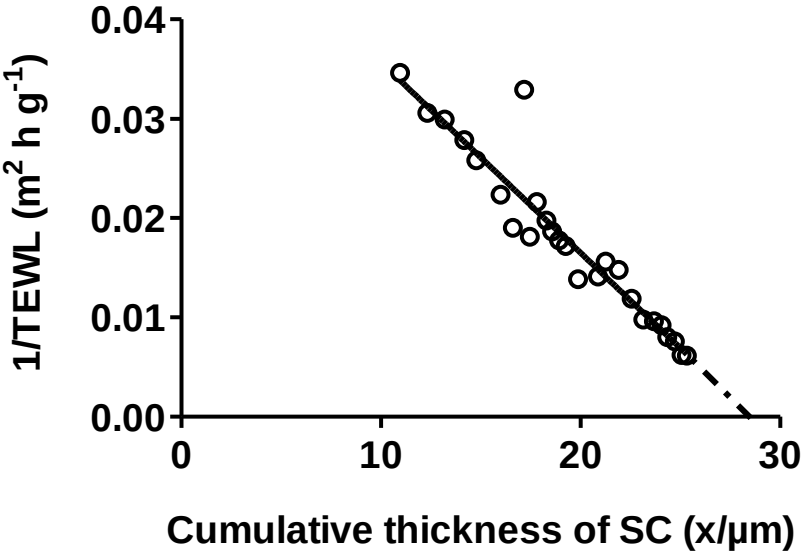

Figure 67: Illustrative experimental data for the determination of normalised SC thickness by TEWL measurements

4.4.3 In-vitro experiments

4.4.3.1 Silicone membrane

The most commonly used *in vitro* model to evaluate the drug delivery across the SC involves Franz diffusion cells.[149,152,278,292–296] It is a cheap and simple method where the experimental conditions can be modified based on the requirements.[297] These cells are often used with human or animal skin. However, the skin may not be always readily available and this is when the artificial membranes are used as an alternative.[297,298] Their function includes skin simulation but mostly quality control.[297–299]

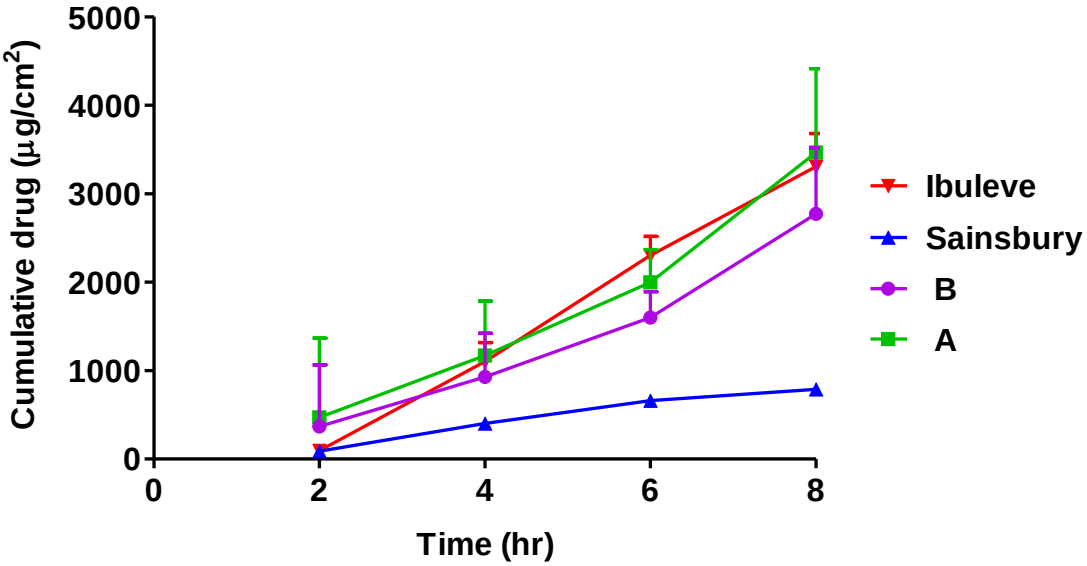

Figure 68: Drug permeation profiles from different formulations across silicone membrane, mean ±SD, n=5.

The amount of ibuprofen that permeated across the silicone membrane was measured for the two commercial and two TOCN formulations (A and B) over a period of eight hours. The results are shown in Figure 68. Formulation A had propylene glycol (PG) and was closer to liquid composition. One-way analysis of variance ($P<0.05$, followed by Tukey's Test) showed that there is no significant difference between the release profiles of the Ibuleve and the TOCN formulations but there was a significant difference between Sainsbury and the rest of the formulations. The results also showed that the ibuprofen is as efficiently released from the TOCN formulations as from Ibuleve, and that release from the Sainsbury's gel is significantly lower.

4.4.3.2 Pig skin

After the initial permeation experiments using silicone membrane, the commercial gels and formulation B were taken forward for the pig skin studies. The amount of drug permeated across pig skin from Ibuleve, Sainsbury and formulation B is shown in Figure 69.

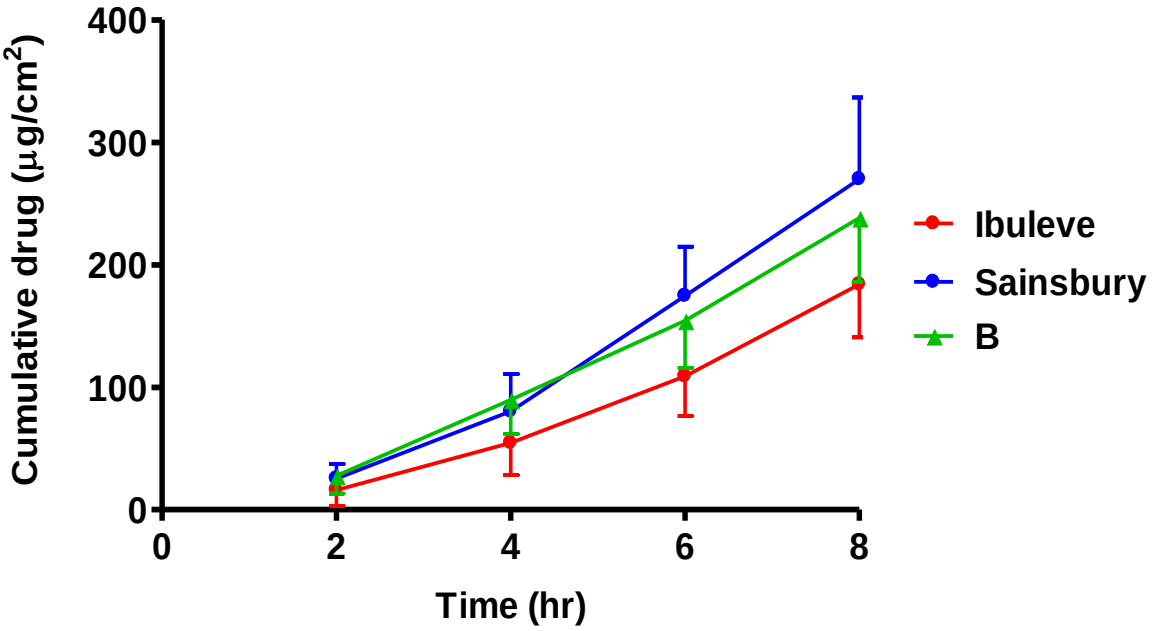

Figure 69: Drug permeation profiles of commercial gels and TOCN formulated gel across abdominal pig skin, mean ±SD, n=4-6

This result shows the amount of cumulative drug collected was significantly lower for the pig skin compared to that of silicone membrane (Figure 68). The nearly 10 fold difference in permeation could be attributed to the interaction of the excipients with the SC and changing the skin barrier which is not possible with the silicone membrane. [124,273] The difference in the delivery of the drug between the Sainsbury and formulation B was also similar unlike the cumulative delivery profile observed in silicone membrane.

The drug permeation profiles were fitted to the Fick's second law of for Eq (50) to yield the partition (KL) and diffusion (D/L^2) parameters as shown in Table 18. The KL value for formulation B was significantly higher than those of the commercial gels; whereas the diffusion parameters were not considerably different. The drug's solubility increases with an increase in the pH of the vehicle.[126] Formulation B has a lower pH in comparison to the commercial formulations; therefore the ibuprofen solubility is also lower which inversely affected the partition coefficient value (KL). In addition, the permeability coefficient (K_p) of the drug was higher from formulation B. Although the increase in pH increases the ibuprofen's solubility, this on the other hand has a negative effect on the permeability coefficient.[126]

The measured values for the steady-state fluxes (J_{ss}) were obtained from the linear part of the cumulative drug versus time profiles. The J_{ss} values were statistically different from all gels, but the overall all the formulations behaved in similarly.

Table 18: The diffusion parameters calculated for pig skin, mean±SD, n=4-6.

Formulations[1]	KL x 10^3 $(cm)^{2,3}$	D/L^2 $(h^{-1})^{3,4}$	K_p x 10^3 $(cm/h)^{5,6}$	J_{ss} $(\mu g\ cm^{-2}\ h^{-1})^{7,8}$	pH[9]
Ibuleve	4.73 ± 0.44	0.22 ± 0.05	1.07 ± 0.03	32.3 ± 2.9	7.0
Sainsbury	6.90 ± 1.65	0.23 ± 0.03	1.60 ± 0.05	47.4 ± 0.2	8.2
B	28.43 ± 11.90	0.28 ± 0.11	8.0 ± 1.30	41.2 ± 3.5	5.3

[1] The concentration of ibuprofen in Ibuleve and Sainsbury gels was 5 % w/w and 1 % w/w for formulation B.
[2] One way ANOVA with Tukey's test reveals formulation B is statistically different ($P<0.05$) to Ibuleve and Sainsbury gel.
[3] Values were obtained by fitting cumulative amount of drug permeated versus time profiles using Eq (50).
[4] One way ANOVA with Tukey's test reveals the values were all similar.
[5] The permeability coefficient K_p= KL (D/L^2) L; where the KL and D/L^2 were obtained from best-fits of Eq (50)
[6] One way ANOVA with Tukey's test reveals B is statistically different ($P<0.05$) to Ibuleve and Sainsbury gel
[7] Values were determined experimentally from the linear part of the cumulative amount of drug permeated versus time profiles, where the slope=J_{ss}.
[8] One way ANOVA with Tukey's test reveals the values were all statistically different ($P<0.05$).
[9] All pH measurements were repeated three times.

4.4.4 Comparison of TOCN formulations

The cumulative transport of ibuprofen across the pig skin from four TOCN formulations is shown in Figure 70. The values were fitted to Eq (50) and yielded the parameters listed in Table 19. The steady-state fluxes (J_{ss}) were calculated from the linear parts of the slope for each formulation.

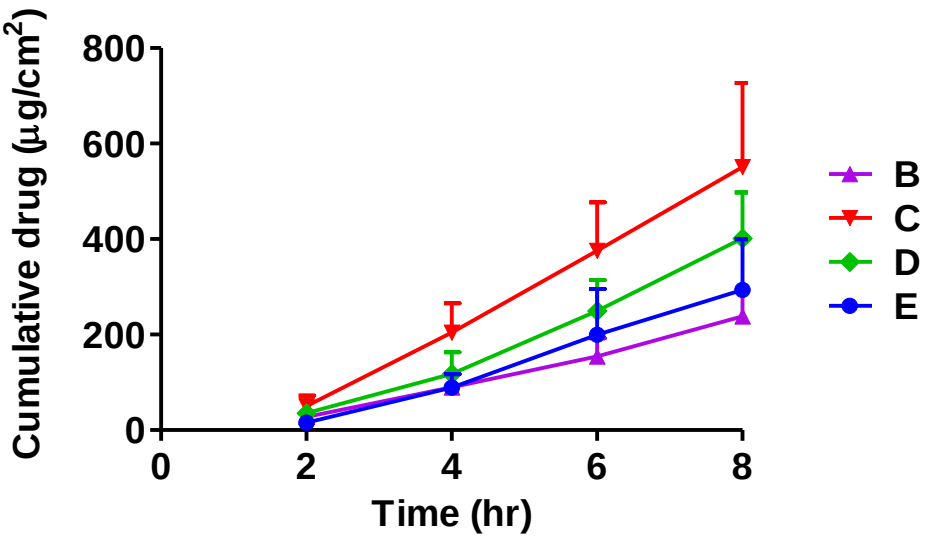

Figure 70: Ibuprofen delivery across pig skin for all the TOCN formulations

The partition parameter (KL) and diffusion parameter (D/L^2) did not change by the type of formulation or the concentration of TOCN in the gel. The permeability coefficient (K_p) was similar between formulations B and E and this value was higher for formulations C and D. The experimentally determined steady-state flux values were statistically different between all TOCN gels. The flux was the highest for formulation C and lowest for B. This difference however, was only about a factor of two across all the formulations.

Table 19: Diffusion parameters of TOCN gels across pig skin

Formulations[1]	KL x 10^3 (cm)[2,3]	D/L^2 (h^{-1})[3,4]	K_p x 10^3 (cm/h)[5,6]	J_{ss} (μg cm^{-2} h^{-1})[7,8]
B (1.8 wt %)	28.4 ± 11.9	0.28 ± 0.11	8.0 ± 1.3	41.2 ± 3.5
C (1.2 wt %)	64.8 ± 25.9	0.26 ± 0.04	16.9 ± 1.0	86.7 ± 0.6
D (0.6 wt %)	50.9 ± 23.6	0.27 ± 0.12	13.8 ± 2.9	70.9 ± 3.0
E (1.8 wt %)	43.0 ± 15.7	0.21 ± 0.01	9.0 ± 0.1	51.2 ± 2.3

[1] The concentration of ibuprofen in all formulations was 1 % w/w ,TOCN concentrations in brackets.
[2] One way ANOVA with Tukey's test reveals the values were all similar.
[3] Values were obtained by fitting cumulative amount of drug permeated versus time profiles using Eq 50.
[4] One way ANOVA with Tukey's test reveals the values were all similar.
[5] The permeability coefficient K_p= KL (D/L^2) ; where the KL and D/L^2 were obtained from best-fits of Eq 50.
[6] One way ANOVA with Tukey's test reveals the values between formulations B-E were similar but the rest of the pairs were statistically different ($P<0.05$)
[7] Values were determined experimentally by linear regression of the cumulative amount of drug permeated versus time profiles, where the slope=J_{ss}.
[8] One way ANOVA with Tukey's test reveals the values were all statistically different ($P<0.05$).

The total amount (%) of ibuprofen released from the pig skin via each TOCN formulation at the end of eight hours is depicted in Table 20. This was highest for formulation C due its high flux, whereas almost half of this amount was released from formulation B. The total amount of drug extracted from the tapes for each TOCN formulation was also statistically different between formulation B and the rest of the formulations. The values were similar between the other formulations.

Table 20: Amount of drug released (%) to the receptor solution at the end of 8 hrs and total amount of drug extracted from all the tapes.

TOCN formulations	TOCN concentration (wt %)	Total amount of drug released (%)[1]	Total amount of drug recovered (µg)[2,3]
B	1.8	3.9	188.2 ± 46.0
C	1.2	8.6	529.4 ± 118.9
D	0.6	6.3	466.4 ± 87.4
E	1.8	7.4	358.6 ± 52.2

[1] The percentage of ibuprofen released at the end of 8 hr in-vitro experiments with pig skin
[2] The total amount of ibuprofen extracted in SC after tape-stripping experiments
[3] One way ANOVA with Tukey's test reveals the formulation pairs of C-D and D-E are not significantly different and the rest of the values are statistically different ($P<0.05$)

4.4.5 In-vivo studies

The total amounts of ibuprofen taken up into the SC *in vivo* from the different formulations are shown in (Figure 71). The amounts found in the SC of the human volunteers were approximately one half of those in pig skin *in vitro*. This is not surprising given the difference in application time of the formulations where the pig skin *in vitro* experiments were for eight hours whereas the human *in vivo* experiments were for one hour.

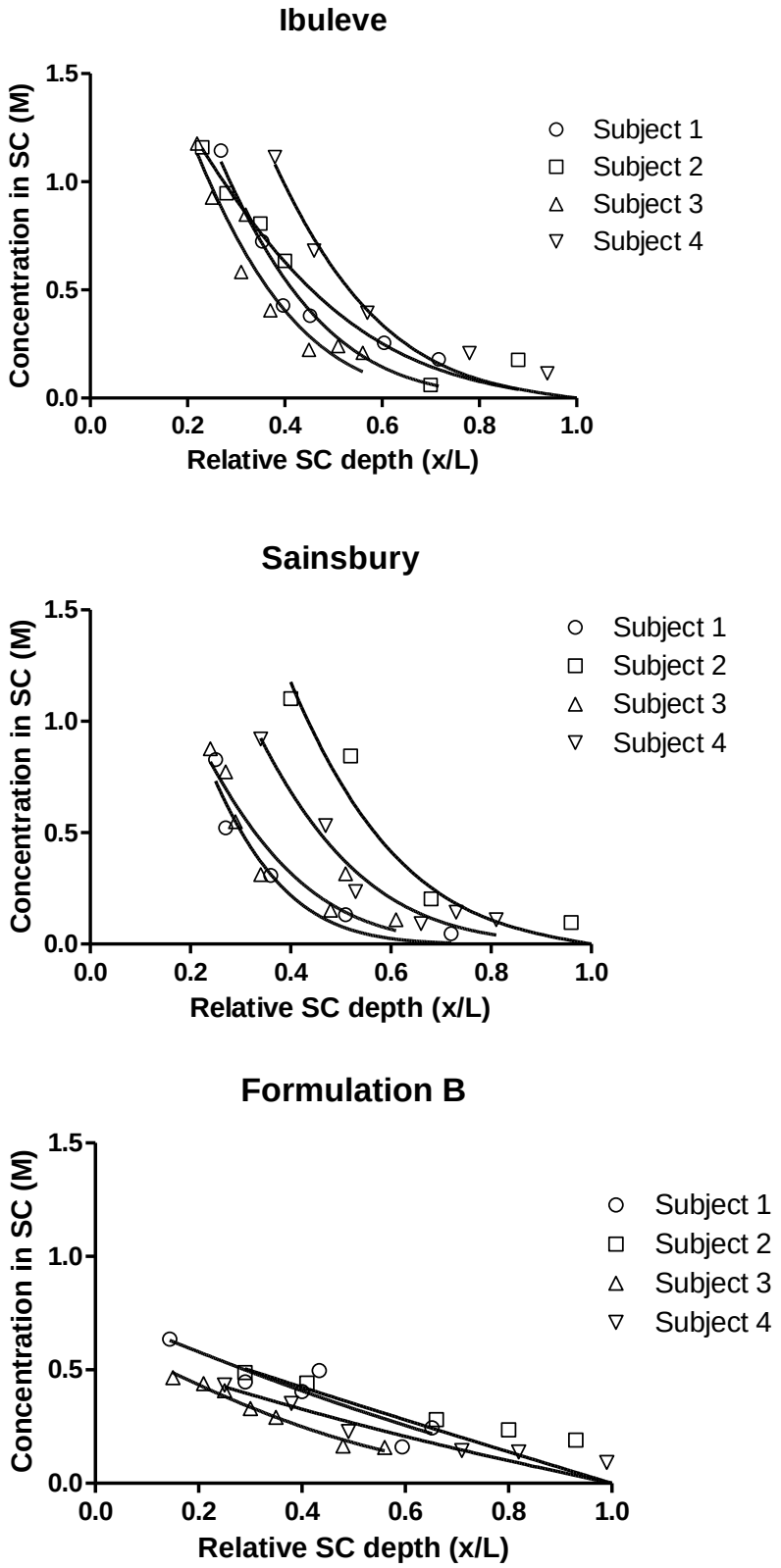

Figure 71: In-vivo concentration versus relative depth profiles of Ibuleve, Sainsbury's and formulation B. The results were obtained after 1 hour application of the formulations, (n=4).

Figure 71 compares the concentration profiles of ibuprofen across the SC in four volunteers after one hour of application. The weight of SC removed and the area stripped (combined with the concomitant TEWL measurements as explained above) enables the drug concentration to be expressed as a function of normalised SC depth. The lines drawn show the best fits of Eq (49) to the results and yield values for the SC-vehicle partition coefficient (*K*) of ibuprofen and its diffusivity parameter D/L^2 (Table 21).The values for *K* are similar for the commercial gels and relatively lower for formulation B.

Table 21: Parameters of ibuprofen across SC after application of the gels in-vivo, mean±SD, n=4.

Formulation[1]	**K**[2,3]	**D/L^2 (h^{-1})** [2,4]	**K_p (cm/h)**[5,6] **x 10^3**	**J_{ss} (µg cm^{-2} h^1)**[7]
Ibuleve	2.85 ± 0.74	0.06 ± 0.02	0.18 ± 0.01	8.77 ± 0.64
Sainsbury	3.07 ± 1.02	0.05 ± 0.02	0.15 ± 0.02	7.73 ± 0.91
B	0.69 ± 0.07	0.24 ± 0.12	0.18 ± 0.01	1.81 ± 0.09

[1] The ibuprofen concentration of Ibuleve and Sainsbury were 5 % w/w and 1 % w/w in formulation B.
[2] The values for K and D/L^2 were determined by best fits of Eq 49.
[3] The one-way ANOVA with Tukey's test shows no significant difference ($P<0.05$) between Ibuleve and Sainsbury gels.
[4] The one-way ANOVA with Tukey's test shows no significant difference ($P<0.05$) between Ibuleve and Sainsbury gels.
[5] The permeability coefficient $K_p = K (D/L^2) L$; where the K and D/L^2 were obtained from best-fits of Eq 49 and thickness used for the skin was L=11 µm.a
[6] The one-way ANOVA with Tukey's test indicates that the values were different between Sainsbury and formulation B.
[7] Predicted flux $J_{ss}=K_p \times C_v$
[8] The one-way ANOVA with Tukey's test shows no significant difference ($P<0.05$) between Ibuleve and Sainsbury gels.

The fitted D/L^2 values for formulation B were significantly higher than that for the two commercial gels. The difference in the kinetic parameter must be due to the difference in diffusivity rather than skin thickness as all formulations were applied to the same set of four volunteers. A lag time calculation ($L^2/6D$) reveals the time needed for the commercial gels to reach steady state is over 3 hours whereas it is only 45 minutes for the formulation B. On the other hand the permeability coefficient (K_p) values were not affected by this difference. Figure 71 shows tape stripping removed more SC when commercial formulations were applied than formulation B.

4.4.6 Comparison of *in-vivo* and *in-vitro* experiments

The concentration of TOCN gels had an impact on the percentage of drug permeated through pig skin. The commercial gels Ibuleve and Sainsbury's had the highest viscosities. This was followed by the TOCN formulations B, C and E. The lowest viscosity belong to formulation D due to low concentration of TOCN (0.6 wt %). Given that all the cellulose formulations had the same concentration of ibuprofen (1 % w/w) and same excipients, the amount of drug permeated through the skin was considerably lower for formulation B which had the highest concentration of TOCN (1.8 wt %). The total amount of ibuprofen removed from tape-stripping was also the lowest for formulation B (Table 20), suggesting that less drug was absorbed across the skin compared to the rest of the TOCN formulations. Although formulation E had the same amount of TOCN, more ibuprofen was removed from the SC which may suggest the presence of SDS alter the skin barrier hence allowing further drug penetration. However, more work needs to be carried out to confirm this. The measured steady-state flux (J_{ss}) was also lower for formulation B and E (Table 19). On the other hand, the highest flux was only 2-fold higher than the lowest value. The diffusivity of the drug in SC was similar for all the TOCN gels (Figure 72-D). The partition coefficient (KL) values were not significantly different between the TOCN formulations. Overall, the formulations that performed better *in vitro* (pig skin) were formulation C and D which had lower TOCN concentrations.

Initial permeatition experiments across silicon membrane showed that steady state fluxes were much higher than those seen across pig skin which overestimated the values to be predicted for a mammalian skin.

In-vitro studies showed that the commercial gels (Ibuleve and Sainsbury) and formulation B (1.8 wt % TOCN) had a similar pattern for the cumulative amount of drug diffused through the membrane/pig skin. However, the amount of drug permeated was much higher in silicone membrane. Therefore, the silicone membrane remains as preliminary testing procedure to try out new formulations with potential for drug delivery. [124,273] In order to compare the *in-vivo* and *in-vitro* SC-vehicle partition coefficients, the *in-vitro* partitioning parameter (KL) was divided by the pig skin thickness (L) which was L=11µm as determined by the tape-stripping experiments. The values were in an agreement for Ibuprofen and Sainsbury gels;

however this was not the case for the formulation B where there was a significant difference between the partitioning of the drug in *in-vivo* (estimated) and *in-vitro* (measured) (Figure 72-A). The measured drug permeatition (D/L^2) values through pig skin (Figure 72-C) were similar to those found by Herkenne *et al.*[124]who also studied four commercial gels both *in vivo* and *in vitro*. The lower partitioning of the drug and higher permeation into the skin could be attributed to low pH of the vehicle in formulation B. [126,300] It has also been suggested that a hydroalcoholic gel of pH 3.5 to 6.0 is far more effective than a cream, non-alcoholic or hydroalcoholic gel of above pH 7.0 for delivery of ibuprofen through the skin.[271] This suggestion however, requires further investigation on the effect of pH on ibuprofen delivery from TOCN formulations. Table 22 shows the total amount of ibuprofen recovered from the skin by tape-stripping. The values showed that the amount of drug present in SC was almost twice for pig skin in comparison to human skin.

Table 22: Total amount of ibuprofen removed (μg) by tape-stripping

	Ibuleve	**Sainsbury**	**B**
Human skin[1]	229 ± 29	166 ± 32	106 ± 17
Pig skin [2]	403 ± 80	344 ± 74	188 ± 45

[1] The one-way ANOVA with Tukey's test shows all the values are statistically different ($P< 0.05$)

[2] The one-way ANOVA with Tukey's test reveals similarity between Ibuleve and Sainsbury gels whereas formulation B is significantly different to the other formulations.

The steady-state flux values (J_{ss}) across pig skin (Table 18) were similar between the commercial gels and the formulation B. These values were also in a an agreement with the values given by Herkenne *et al.*[124]. The estimated fluxes for the human skin *in vivo* experiments on the other hand were considerably lower (Figure 72-B).

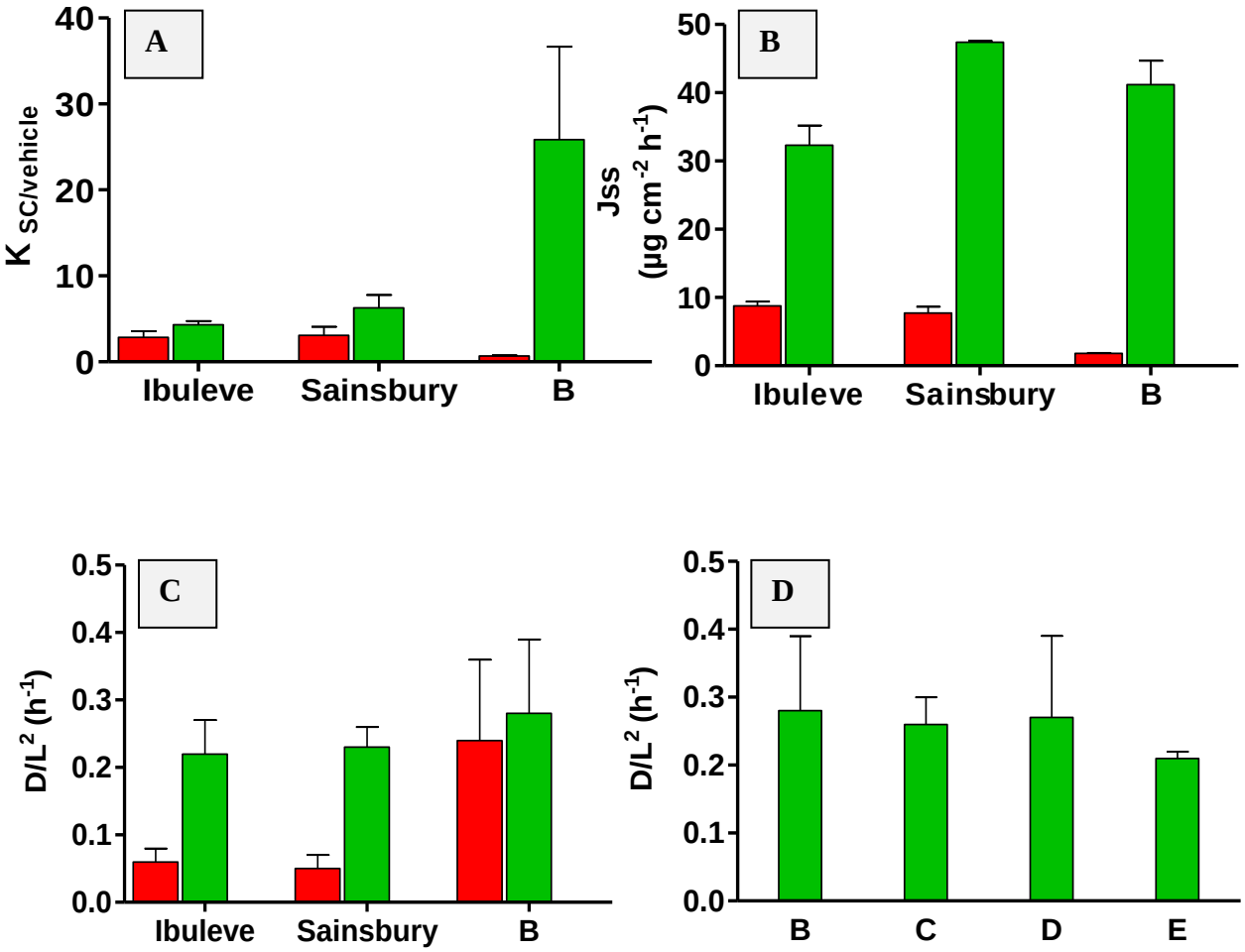

Figure 72: Ibuprofen transport parameters for pig skin *in vitro* (green bars) and human skin *in vivo* (red bars), for Ibuleve, Sainsbury and Formulation B : A) Ibuprofen partition coefficient across pig and human skin, B) Steady-state flux across pig and human skin ,C) Ibuprofen diffusivity parameters through pig and human skin; D) Ibuprofen diffusivity parameters through pig skin only for all TOCN formulations, all data mean±SD, n=4-6.

4.5 Conclusion

The results showed the absorption of ibuprofen across the skin is possible through topical application for formulations containing TEMPO-oxidised cellulose nanofibrils (TOCN). Moreover, in comparison to two commercial gels used in this study, Ibuleve and Sainsbury, this could be achieved even with less drug incorporated in the formulation. The amount of ibuprofen permeated through silicone membrane from formulations Ibuleve, Sainsbury and formulation B was considerably higher than those measured across the pig skin. Overall, based on the drug delivery parameters measured *in vitro* (pig skin) as well as the viscosity results compared, formulation C could be a candidate for *in vivo* studies. Some differences in behaviour of the drug were found between pig skin and human skin; however the values for drug diffusion through pig skin were generally in an agreement to those found on the literature. Future work should include further optimisation of the TOCN formulations. The application should also be based on "*finite"* doses rather than "infinite" doses used for this study and perhaps a more realistic prediction could be achieved by this. The effect of pH on the drug delivery should also be investigated further where a different range of TOCN could be prepared. Integration of other additives which affect the viscosity such as salt and surfactants could also be studied.

5. Conclusions and Future Work

TOCN is a potential new thickener for personal care product formulations. It forms optically clear gels which are non-irritant to the skin, have the ability to modify the rheology of the formulations and moreover obtained from plant-based source.[1] Given all these characteristics of the gels, it was in our interest to study this material further. The overall aim of the work presented in this thesis was to develop an understanding of the interaction of TEMPO-oxidised cellulose nanofibrils with sodium dodecyl sulfate and sodium chloride. These additives are commonly found in cosmetic and pharmaceutical products. Small angle X-ray and neutron scattering techniques enabled us to study this interaction in LMW alcohol medium. Since TOCN forms thin films on the skin and the same interaction was also examined by X-ray and neutron reflectivity where the changes in the TOCN film thickness and roughness upon exposure to surfactant and salt solutions were further explored. Since TOCN still forms gels in alcohol medium, in order to probe the potential of such alcohol gels, ibuprofen drug was introduced to TOCN-ethanol gels. The ability of alcohol gels to deliver ibuprofen in formulations with different TOCN concentrations were studied as part of this chapter.

5.1 TOCN-Alcohol Gels

Overall, the TOCN-alcohol gels were more viscous in the presence of SDS or NaCl, in comparison to those with no additives. The quantity of the gel recovered post centrifugation was also lower in the absence of these additives. This was lowest for the gels dispersed in propan-1-ol which has the lowest dielectric constant amongst all the alcohols used in this study. The gels formed aggregates > 70 wt% propan-1-ol in the presence of NaCl where the gel holds less water due to the salt content and it shrinks. This was in agreement with the change in the aggregated layer thickness of this gel from 31 to 21 Å measured by SAXS. Upon addition of charged particles to the TOCN-alcohol gel systems, the fibrils move closer to each other (forming denser network) forming more viscous gels. The scattering data from SANS and SAXS experiments agreed on the changes in the fibrillar aggregation at higher alcohol concentrations. SANS data showed the effect of alcohol concentration on SDS (80

mM) micellization where at alcohol concentrations > 40 wt %, the peak for the micelles was no longer seen as the presence of alcohols is known to affect the micellization process. The micelle sphere size also reduced from 16 Å to 14 Å when the methanol concentration was increased from 20 wt % to 60 wt %. Therefore the models used to fit the data were different for alcohols at <40 wt % (elliptical cylinder) and < 40 wt% (lamellar sheet). The minor radius of the gels in the presence of high surfactant concentrations (80 mM) resulted in significant change in the minor radius from 18 Å to 102 Å which could be due to the fibrils aligning closer to each other due to the negatively charged surfactant micelles. Upon addition of NaCl at this high concentration of SDS, the major/minor radii were increased which is an early indication of the aggregation of the fibrils, suggesting a change to ribbon-like structure. The TOCN-alcohol gels were also shear thinning similar to those gels dispersed in aqueous medium as previously reported by Crawford *et al.*[1]. The frequency sweep tests showed that the storage modulus (G′) was greater than loss modulus (G″) for the ethanol gels (30 wt %) with SDS and NaCl which indicates a gel network. However, when no additives was present, the gel behaved similar to a liquid-like structure as G″> G′.

Although SDS was used as a model anionic surfactant for this study, it is perhaps more realistic to study milder surfactants since these gels are suggested to be used in personal care products. SDS is a harsher surfactant than another anionic surfactant sodium laureth sulfate (SLES). [58,135] The anionic surfactants are cheaper than non-ionic surfactants however, often a mixture of two is used personal care products.[56] Therefore for future work, it would be interesting to analyse TOCN gels in the presence of different surfactants. Another interesting study would be to see effect of salt concentration on the alcohol gels. The concentration of salt used in this study might have been too high to understand its effect on gelation. The neutron scattering measurement of alcohol gels using 1 mm Helma cells was also difficult. The utilisation of a different cell where the gel loading is easier but also the alcohol evaporation is completely eliminated or minimised could be useful.

5.2 TOCN Films

TOCN films were deposited on silicon substrates and washed with SDS and NaCl solutions. The changes on the film thickness and toughness were measured by X-ray and neutron reflectivity. The surface modification of the substrates was achieved by aminosilanization by vapour deposition. However, this proved to be a challenge for the neutron reflectivity experiments where different sets of substrates had TOCN thickness varying from 10 to 20 nm. This could be due to the selected method of aminosilanisation and the large substrate surface making it difficult to evenly cover the surface by vapour. The majority of the planned X-ray reflectivity experiments were not successful as the beam damaged the cellulose films making it impossible to measure the reflectivity after the second measurement. On the other hand, it was possible to determine the dry cellulose film thickness by X-ray reflectivity. Although the films formed were not uniform on the surface, changes in the film layer was observed when the surface was washed with SDS and NaCl solutions during the neutron reflectivity experiments. TOCN layer was fitted with two layers where one layer was for the adsorbed surfactant head groups on the surface and the other layer for the hydrated layer closer to the substrate. The thickness of the TOCN layer increased from 20 to 23 nm when the surface was washed with d-SDS (6 *mM*), however, the thickness was changed back to the original thickness upon washing the surface with D_2O. The adsorption of SDS to the cellulose films was greater when the surfactant concentration was increased to 10 mM where the SLD of the layer increased from 2.3 to 3.0 x 10^{-6} $Å^{-2}$. There was little to no change when the surface was washed with NaCl (0.2 *M*), but the films were thicker and rougher when the surface was washed with SDS and NaCl mixture. The TOCN film thickness was at the highest when the surface was washed with high SDS concentration (10 *mM*) and NaCl (0.2 *M*) mixture.

The film deposition on silicon substrates was not easy and the films formed were rough and thick which is not ideal for a reflectivity measurement. Although, every effort was provided, the aminosilanization method needs to be further improved. The TOCN fibrils might need to be further sonicated in order to minimise the roughness of the deposited film. It would be interesting to compare the adsorption of non-ionic and cationic surfactant on TOCN which is studied with different cellulose surfaces before. [80,84,94,264]

5.3 TOCN Gels for Drug Delivery

The delivery of ibuprofen from TOCN-ethanol gel formulations at TOCN concentrations of 0.6, 1.2 and 1.8 wt % was compared to two commercially available ibuprofen alcohol gels, Ibuleve and Sainbury's gel. The ability of different formulations to deliver the active drug was measured by *in-vivo* (human volunteers) and *in-vitro* (silicone membrane and pig skin) experiments. Tape-stripping was used to quantify the drug amount and TEWL measurements allowed us to determine the SC for individual sample and normalized it for comparison. There TOCN-ethanol gels were loaded with 1 wt % ibuprofen drug whereas the commercial gels had 5 wt %. This was because 1 wt % was the maximum amount of drug that can be loaded to the TOCN gels without changing the pH or adding another component to these formulations. The concentration of TOCN present in the gel formulations had an effect on the viscosity, the delivery rate and the amount delivered across the pig skin. The formulation with the highest concentration of TOCN , formulation B (1.8 wt %) was the gel with the slowest flux around 41 µg cm^{-2} h^{-1} whereas this was almost 87 µg cm^{-2} h^{-1} for the formulation containing 1.2 wt % TOCN. The amount of ibuprofen permeated across silicone membrane was much higher compared to pig skin or human skin experiments. Overall, the results showed that the penetration of ibuprofen across the skin is achievable with formulations containing TOCN and ethanol.

There are many other interesting possible studies that could be carried out using TOCN in formulations. Since it was shown that the delivery of the ibuprofen was possible with these formulations, perhaps a more hydrophilic drug could be used to compare the penetration rates. The pH of the formulations could also be changed to measure its effect on the drug delivery. Perhaps it would be more realistic to not to occlude the skin surface during the application process as in reality the formulation is rubbed and exposed to the air.

6. References

1. Crawford, R. J., Edler, K. J., Lindhoud, S., Scott, J. L. & Unali, G. Formation of shear thinning gels from partially oxidised cellulose nanofibrils. *Green Chem.* **14,** 300–303 (2012).

2. Payen, A. Mémoire sur la composition du tissu propre des plantes et du ligneux. *C R Hebd Seances Acad Sci* **7,** 1052–1056 (1838).

3. Klemm, D. *et al.* Nanocelluloses: a new family of nature-based materials. *Angew. Chem. Int. Ed. Engl.* **50,** 5438–66 (2011).

4. Siró, I. & Plackett, D. Microfibrillated cellulose and new nanocomposite materials: a review. *Cellulose* **17,** 459–494 (2010).

5. Dufresne, A. in *Monomers, Polym. Compos. from Renew. Resour.* 401–419 (2008).

6. Henriksson, M., Berglund, L. A., Isaksson, P., Lindstrom, T. & Nishino, T. Cellulose nanopaper structures of high toughness. *Biomacromolecules* **9,** 1579–1585 (2008).

7. Ioelovich, M. Cellulose as a nanostructured polymer: A short review. *BioResources* **3,** 1403–1418 (2008).

8. Kaith, B. S., Mittal, H., Jindal, R., M., M. & Susheel, K. in *Cellul. Fibers Bio- and Nano-polymer Compos. Green Chem. Technol.* 4–28 (2011).

9. Zimmermann, T., Pöhler, E. & Geiger, T. Cellulose Fibrils for Polymer Reinforcement. *Adv. Eng. Mater.* **6,** 754–761 (2004).

10. Alves, L. *et al.* Unusual extraction and characterization of nanocrystalline cellulose from cellulose derivatives (in press). *J. Mol. Liq.* (2014).

11. Thomas, S., Paul, S. A., Pothan, L. A. & Deepa, B. in *Cellul. Fibers Bio-and Nano-polymer Compos. Green Chem. Technol.* 3–43 (Springer, 2011).

12. Herrick, F. W., Casebier, R. L., Hamilton, J. K. & Sandberg, K. R. Microfibrillated cellulose: Morphology and accessibility. *J. Appl. Polym. Sci. Appl. Polym. Symp.* **37,** 797–813 (1983).

13. Turbak, A. F., Synder, F. W. & Sandberg, K. R. Microfibrillated cellulose, a new cellulose product: Properties, uses, and commercial potential. *J. Appl. Polym. Sci. Appl. Polym. Symp.* **37,** 815–827 (1983).

14. Iwamoto, S., Abe, K. & Yano, H. The effect of hemicelluloses on wood pulp nanofibrillation and nanofiber network characteristics. *Biomacromolecules* **9,** 1022–6 (2008).

15. Isogai, A., Saito, T. & Fukuzumi, H. TEMPO-oxidized cellulose nanofibers. *Nanoscale* **3,** 71–85 (2011).

16. Fujisawa, S., Okita, Y., Fukuzumi, H., Saito, T. & Isogai, A. Preparation and characterization of TEMPO-oxidized cellulose nanofibril films with free carboxyl groups. *Carbohydr. Polym.* **84,** 579–583 (2011).

17. Habibi, Y., Lucia, L. a & Rojas, O. J. Cellulose nanocrystals: chemistry, self-assembly, and applications. *Chem. Rev.* **110,** 3479–500 (2010).

18. Alves, J. S., dos Reis, K. C., Menezes, E. G. T., Pereira, F. V. & Pereira, J. Effect of cellulose nanocrystals and gelatin in corn starch plasticized films. *Carbohydr. Polym.* **115,** 215–222 (2015).

19. Montanari, S., Roumani, M., Heux, L., & Vignon, M. R. Topochemistry of carboxylated cellulose nanocrystals resulting from TEMPO-mediated oxidation. *Macromolecules* **38,** 1665–1671 (2005).

20. Shafiei-Sabet, S., Hamad, W. Y. & Hatzikiriakos, S. G. Rheology of nanocrystalline cellulose aqueous suspensions. *Langmuir* **28,** 17124–33 (2012).

21. Henriksson, M., Henriksson, G., Berglund, L. & Lindstrom, T. An environmentally friendly method for enzyme-assisted preparation of

microfibrillated cellulose (MFC) nanofibers. *Eur. Polym. J.* **43,** 3434–3441 (2007).

22. Zhao, Y., Zhang, Y., Lindström, M. E. & Li, J. Tunicate cellulose nanocrystals: Preparation, neat films and nanocomposite films with glucomannans. *Carbohydr. Polym.* **117,** 286–296 (2015).

23. Saito, T. & Isogai, A. TEMPO-mediated oxidation of native cellulose. The effect of oxidation conditions on chemical and crystal structures of the water-insoluble fractions. *Biomacromolecules* **5,** 1983–9 (2004).

24. Saito, T., Kimura, S., Nishiyama, Y. & Isogai, A. Cellulose nanofibers prepared by TEMPO-mediated oxidation of native cellulose. *Biomacromolecules* **8,** 2485–2491 (2007).

25. Da Silva Perez, D., Montanari, S. & Vignon, M. R. TEMPO-mediated oxidation of cellulose III. *Biomacromolecules* **4,** 1417–25 (2003).

26. Saito, T., Okita, Y., Nge, T., Sugiyama, J. & Isogai, A. TEMPO-mediated oxidation of native cellulose: Microscopic analysis of fibrous fractions in the oxidized products. *Carbohydr. Polym.* **65,** 435–440 (2006).

27. Crawford, R., Scott, J. L. & Unali, G. . Structured Aqueous Detergent Compositions. *Patent* WO/2010/076292 (2010).

28. Yackel, E. A. & Kenyon, W. O. No Title. *J. Am. Chem. Soc.* **64,** 121–127 (1942).

29. Maurer, K. & Reiff, G. J. Die Oxydation der Cellulose mit Stickstoffdioxyd. *J. Makromol Chem* **1,** 27–34 (1943).

30. De Nooy, A. E. J., Besemer, A. C. & van Bekkum, H. Highly selective nitroxyl radical-mediated oxidation of primary alcohol groups in water-soluble glucans. *Carbohydr. Res.* **269,** 89–98 (1995).

31. Saito, T., Nishiyama, Y., Putaux, J.-L., Vignon, M. & Isogai, A. Homogeneous suspensions of individualized microfibrils from TEMPO-

catalyzed oxidation of native cellulose. *Biomacromolecules* **7,** 1687–1691 (2006).

32. Chang, P. S. & Robyt, J. F. Oxidation of primary alcohol groups of naturally occuring polysaccharides with 2,2,6,6-tetramethyl-1-piperidine oxoammonium ion. *J. Carbohydr. Chem.* **15,** 819–830 (1996).

33. Isogai, A. & Kato, Y. Preparation of polyuronic acid from cellulose by TEMPO-mediated oxidation. *Cellulose* **5,** 153–164 (1998).

34. Araki, J., Wada, M. & Kuga, S. Steric stabilization of a cellulose microcrystal suspension by poly(ethylene glycol) grafting. *Langmuir* **17,** 21–27 (2001).

35. Carr, M. E., J., Shen, L. L. & Hermans, J. Mass-length ratio of fibrin fibers from gel permeation and light scattering. *J. Biopolym.* **16,** 1–5 (1977).

36. Coseri, S. *et al.* Oxidized cellulose-survey of the most recent achievements. *Carbohydr. Polym.* **93,** 207–15 (2013).

37. Wan, Y. *et al.* Synthesis and characterization of hydroxyapatite–bacterial cellulose nanocomposites. *Compos. Sci. Technol.* **66,** 1825–1832 (2006).

38. Dias, G. J., Peplow, P. V & Teixeira, F. Osseous regeneration in the presence of oxidized cellulose and collagen. *J. Mater. Sci. Mater. Med.* **14,** 739–45 (2003).

39. Amit, M., Binenbaum, Y., Cohen, J. T. & Gil, Z. Effectiveness of an oxidized cellulose patch hemostatic agent in thyroid surgery: a prospective, randomized, controlled study. *J. Am. Coll. Surg.* **217,** 221–5 (2013).

40. Saferstein, L., Reginald Stilwell, L. & Whitmore, E. Calcium-modified oxidized cellulose hemostat. Patent, EP0659440 B1 (2002).

41. Banker, G. & Kumar, V. Microfibrillated oxycellulose. Patent, US 5405953 A (1995).

42. Pameijer, C. & Jensen, S. Agents and devices for providing blood clotting functions to wounds. Patent,US 20070190110 A1 (2007).

43. Mörseburg, K. & Chinga-Carrasco, G. Assessing the combined benefits of clay and nanofibrillated cellulose in layered TMP-based sheets. *Cellulose* **16,** 795–806 (2009).

44. Syverud, K., Chinga-Carrasco, G., Toledo, J. & Toledo, P. G. A comparative study of Eucalyptus and Pinus radiata pulp fibres as raw materials for production of cellulose nanofibrils. *Carbohydr. Polym.* **84,** 1033–1038 (2011).

45. Hamley, I. W. *Colloids in Introduction to Soft Matter*. (John Wiley & Sons, Ltd., 2007).

46. Mewis, J. & Wagner, N. J. in *Colloid Suspens. Rheol.* 1–34 (Cambridge University Press, 2012).

47. Biermann, C. J. in *Handb. Pulping Papermak. (Second Ed.* **i,** 421–437 (Academic Press,Inc., 1996).

48. Butt, H.-J., Cappella, B. & Kappl, M. Force measurements with the atomic force microscope: Technique, interpretation and applications. *Surf. Sci. Rep.* **59,** 1–152 (2005).

49. Bhattacharjee, S., Chen, J. Y. & Elimelech, M. DLVO interaction energy between spheroidal particles and a flat surface. *Colloids Surfaces A Physicochem. Eng. Asp.* **165,** 143–156 (2000).

50. Hunter, J. in *Found. Colloid Sci.* 533–574 (Oxford University Press, 2001).

51. Lifshitz, E. M. The theory of molecular attractive forces between solids. *Sov. Phys.* **2,** 73–83 (1956).

52. Hunter, J. in *Found. Colloid Sci.* 305–369 (Oxford University Press, 2001).

53. Tadros, T. F. in *Prod. Des. Eng. Formul. Gels Pastes* (eds. Brockel, U., Meier, W. & Wagner, G.) 75–93 (Wiley-VCH, 2013).

54. Fukuzumi, H., Tanaka, R., Saito, T. & Isogai, A. Dispersion stability and aggregation behavior of TEMPO-oxidized cellulose nanofibrils in water as a function of salt addition. *Cellulose* **21,** 1553–1559 (2014).

55. Salager, J. Surfactants: Types and Uses. *FIRP Booklet, E300-A* 1–48 (2002).

56. Holmberg, K., Bo, J. & Kronberg, B. *Surfactants and polymers in aqueous solution*. (John Wiley & Sons, Ltd., 2002).

57. Borras-Blasco, J., Lopez, A., Morant, M. J., Diez-Sales, O. & Herraez-Dominguez, M. Influence of sodium lauryl sulphate on the in vitro percutaneous absorption of compounds with different lipophilicity. *Pharm. Sci.* **5,** 15–22 (1997).

58. Tsang, M. & Guy, R. H. Effect of Aqueous Cream BP on human stratum corneum in vivo. *Br. J. Dermatol.* **163,** 954–8 (2010).

59. Song, Y., Jianrui, C. & Zheng, Q. Influence of methylcellulose on dynamic rheology of dilute wheat gliadin solution in 50%(v/v) aqueous propanol. *J. Food Eng.* **94,** 290–294 (2009).

60. Chaibundit, C. *et al.* Effect of ethanol on the gelation of aqueous solutions of Pluronic F127. *J. Colloid Interface Sci.* **351,** 190–6 (2010).

61. Fujisawa, S., Saito, T. & Isogai, A. Nano-dispersion of TEMPO-oxidized cellulose / aliphatic amine salts in isopropyl alcohol. *Cellulose* **19,** 459–466 (2012).

62. Eichhorn, S. J. *et al.* Review: current international research into cellulose nanofibres and nanocomposites. *J. Mater. Sci.* **45,** 1–33 (2009).

63. Siqueira, G., Bras, J. & Dufresne, A. Cellulosic bionanocomposites: a review of preparation, properties and applications. *Polymer (Guildf).* **2,** 728–765 (2010).

64. Sehaqui, H., Zhou, Q. & Berglund, L. A. Nanostructured biocomposites of high toughness—a wood cellulose nanofiber network in ductile hydroxyethylcellulose matrix. *Soft Matter* **7,** 7342–7350 (2011).

65. Kurihara, T. & Isogai, A. Properties of poly(acrylamide)/TEMPO-oxidized cellulose nanofibril composite films. *Cellulose* **21,** 291–299 (2013).

66. Fukuzumi, H., Saito, T., Iwata, T., Kumamoto, Y. & Isogai, A. Transparent and high gas barrier films of cellulose nanofibers prepared by TEMPO-mediated oxidation. *Biomacromolecules* **10,** 162–165 (2009).

67. Gardner, D. J., Oporto, G. S., Mills, R. & Samir, M. A. S. A. Adhesion and Surface Issues in Cellulose and Nanocellulose. *J. Adhes. Sci. Technol.* **22,** 545–567 (2008).

68. Kontturi, E., Thüne, P. C. & Niemantsverdriet, J. W. Novel method for preparing cellulose model surfaces by spin coating. *Polymer (Guildf).* **44,** 3621–3625 (2003).

69. Sczech, R. & Riegler, H. Molecularly smooth cellulose surfaces for adhesion studies. *J. Colloid Interface Sci.* **301,** 376–85 (2006).

70. Fukuzumi, H., Saito, T. & Isogai, A. Influence of TEMPO-oxidized cellulose nanofibril length on film properties. *Carbohydr. Polym.* **93,** 172–177 (2012).

71. Wu, C.-N., Saito, T., Fujisawa, S., Fukuzumi, H. & Isogai, A. Ultrastrong and high gas-barrier nanocellulose/clay-layered composites. *Biomacromolecules* **13,** 1927–32 (2012).

72. Yuan, Z. *et al.* Fabrication of cellulose self-assemblies and high-strength ordered cellulose films. *Carbohydr. Polym.* **117,** 414–421 (2015).

73. Saarikoski, E., Rissanen, M. & Seppala, J. Effect of rheological properties of dissolved cellulose/microfibrillated cellulose blend suspensions on film forming. *Carbohydr. Polym.* (2015).

74. Ong, R. C., Chung, T.-S., de Wit, J. S. & Helmer, B. J. Novel cellulose ester substrates for high performance flat-sheet thin-film composite (TFC) forward osmosis (FO) membranes. *J. Memb. Sci.* **473,** 63–71 (2015).

75. Fukuzumi, H. *et al.* Pore size determination of TEMPO-oxidized cellulose nanofibril films by positron annihilation lifetime spectroscopy. *Biomacromolecules* **12,** 4057–62 (2011).

76. Gunnars, S., Wagber, L. & Cohen Stuart, M. A. Model films of cellulose I. Method development and initial results. *Cellulose* **9,** 239–249 (2002).

77. Neuman, R. D., Berg, P. & Cleasson, J. M. Direct measurement of surface forces in papermaking and paper coating systems. *Nord. Pulp Pap. Res. J.* **8,** 96–104 (1993).

78. Holmberg, M. *et al.* Surface force studies of Langmuir–Blodgett cellulose films. *J. Colloid Interface Sci.* **186,** 369–381 (1997).

79. Homma, I., Fukuzumi, H., Saito, T. & Isogai, A. Effects of carboxyl-group counter-ions on biodegradation behaviors of TEMPO-oxidized cellulose fibers and nanofibril films. *Cellulose* **20,** 2505–2515 (2013).

80. Tucker, I., Petkov, J., Penfold, J. & Thomas, R. K. Adsorption of nonionic and mixed nonionic/cationic surfactants onto hydrophilic and hydrophobic cellulose thin films. *Langmuir* **26,** 8036–48 (2010).

81. Penfold, J. & Tucker, I. M. *Chapter 5 , Large Scale Structures*. *Neutron Scatt.* (Elsevier, 2013).

82. Tucker, I. M., Petkov, J. T., Penfold, J. & Thomas, R. K. Interaction of the anionic surfactant SDS with a cellulose thin film and the role of electrolyte and poyelectrolyte. 2 Hydrophilic cellulose. *Langmuir* **28,** 10223–9 (2012).

83. Taylor, D. J. F., Thomas, R. K. & Penfold, J. Polymer/surfactant interactions at the air/water interface. *Adv. Colloid Interface Sci.* **132,** 69–110 (2007).

84. Winnik, F. M., Regismond, S. T. A. & Goddard, E. D. Interactions of cationic surfactants with a hydrophobically modified cationic cellulose polymer: a study by fluorescence spectroscopy. *Colloids Surfaces A Physicochem. Eng. Asp.* **106,** 243–247 (1996).

85. Kundu, S. Polyelectrolyte-surfactant complexes on solid surface. *J. Colloid Interface Sci.* **344,** 547–55 (2010).

86. Caponetti, E., Martino, D. C., Floriano, M. A. & Triolo, R. Application of the small-angle neutron scattering technique to the study of solubilization mechanisms of organic molecules by micellar systems. *J. Mol. Struct.* **383,** 133–143 (1996).

87. Alila, S. *et al.* Self-aggregation of cationic surfactants onto oxidized cellulose fibers and coadsorption of organic compounds. *Langmuir* **23,** 3723–3731 (2007).

88. Lay-theng, L. Polymer–surfactant interactions: neutron scattering and reflectivity. *Curr. Opin. Colloid Interface Sci.* **4,** 205–213 (1999).

89. Penfold, J., Staples, E. & Tucker, I. The study of partitioning in mixed surfactant systems by neutron scattering techniques. *Adv. Colloid Interface Sci.* **68,** 31–55 (1996).

90. Zhang, X. L. *et al.* Adsorption behavior of hydrophobin and hydrophobin/surfactant mixtures at the solid-solution interface. *Langmuir* **27,** 10464–74 (2011).

91. Purcell, I. P. P., Lu, J. R. R., Thomas, R. K. K., Howe, A. M. M. & Penfold, J. Adsorption of Sodium Dodecyl Sulfate at the Surface of Aqueous Solutions of Poly (vinylpyrrolidone) Studied by Neutron Reflection. *Langmuir* **14,** 1637–1645 (1998).

92. Penfold, J. Instrumentation for neutron reflectivity. *Phys. B Condens. Matter* **173,** 1–10 (1991).

93. Penfold, J., Thomas, R. K. & Shen, H. Adsorption and self-assembly of biosurfactants studied by neutron reflectivity and small angle neutron scattering: glycolipids, lipopeptides and proteins. *Soft Matter* **8,** 578–591 (2012).

94. Penfold, J., Tucker, I., Petkov, J. & Thomas, R. K. Surfactant adsorption onto cellulose surfaces. *Langmuir* **23,** 8357–64 (2007).

95. Wågberg, L. *et al.* The build-up of polyelectrolyte multilayers of microfibrillated cellulose and cationic polyelectrolytes. *Langmuir* **24,** 784–95 (2008).

96. Ahola, S., Salmi, J., Johansson, L. S., Laine, J. & Osterberg, M. Model Films from Native Cellulose Nanofibrils. Preparation, Swelling, and Surface Interactions. *Biomacromolecules* **9,** 1273–1282 (2008).

97. Tucker, I. M., Petkov, J. T., Penfold, J. & Thomas, R. K. How electrolyte and polyelectrolyte affect the adsorption of the anionic surfactant SDS onto the surface of a cellulose thin film and the structure of the cellulose film. 1. Hydrophobic cellulose. *Langmuir* **28,** 10773–80 (2012).

98. Godin, B. & Touitou, E. Transdermal skin delivery: predictions for humans from in vivo, ex vivo and animal models. *Adv. Drug Deliv. Rev.* **59,** 1152–61 (2007).

99. Elias, P. M. Epidermal Lipids , Barrier Function , and Desquamation. *J. Invest. Dermatol.* **80,** 44–49 (1983).

100. Forslind, B. & Lindberg, M. in *Ski. Hair Nails Struct. Funct.* 11–23 (2004).

101. Scheuplein, R. J. & Blank, I. H. Permeability of the skin. *Physiol. Rev.* **51,** 702–747 (1971).

102. Scheuplein, R. J. Mechanism of percutaneous adsorption. *J. Invest. Dermatol.* **45,** 334–347 (1965).

103. Brown, M., Traynor, M., Martin, G. & Akomeah, F. in *Drug Deliv. Syst.* 119–140 (Humana Press, 2008).

104. Uchegbu, I. F., Sch, A. G., Cheng, W. P. & Lalatsa, A. *Fundamentals of Pharmaceutical Nanoscience*. (Springer, 2013).

105. Jain, K. K. in *Drug Deliv. Syst.* 1–50 (Humana Press, 2008).

106. Lane, M. E. Skin penetration enhancers. *Int. J. Pharm.* **447,** 12–21 (2013).

107. Netzlaff, F. *et al.* Comparison of bovine udder skin with human and porcine skin in percutaneous permeation experiments. *Altern. Lab. Anim.* **34,** 499–513 (2006).

108. Cleary, G. W. in *Top. drug bioavailability, bioequivalence penetration* 17–68 (Plenum, 1993).

109. Henzel, M. R. & Loomba, P. K. Transdermal delivery of sex steroids for hormone replacement therapy and contraception. A review of principles and practice. *J. Reprod. Med.* **48,** 525–540 (2003).

110. Kormic, C. A., Santiago-Palma, J., Moryll, N., Payne, R. & Obbens, E. A. Benefit risk assessment of transdermal fentanyl for the treatment of chronic pain. *Drug Saf.* **26,** 951–973 (2003).

111. Varvel, J. R., Shafer, S. L., Hwang, S. S., Coen, P. A. & Stanski, D. R. Absorption characteristics of transdermally administered fentanyl. *Anaesthesiology* **70,** 928 (1989).

112. Yang, S. I. *et al.* Transdermal eperisone elicits more potent and longerlasting muscle relaxation than oral operisone. *Pharmacology* **71,** 150–156 (2004).

113. Payne, R. *et al.* Quality of life and cancer pain: satisfaction and side effects with transdermal fentanyl versus oral morphine. *J. Clin. Oncol.* **16,** 1588–1593 (1998).

114. Long, C. in *Dermatological transdermal Formul.* 41–60 (Marcel Dekker Inc., 2002).

115. Bos, J. D. & Meinardi, M. M. The 500 Dalton rule for skin penetration of chemical compounds and drugs. *Exp. dermatology2* **9,** 165–169 (2000).

116. Yano, T., Nagakawa, A., Tsuji, M. & Noda, K. Skin permeability of various nonsteroidal anti-inflammatory drugs in man. *Life Sci.* **39,** 1043–1050 (1986).

117. Hogan, D. J. & Maibach, H. I. Adverse dermatologic reactions to transdermal drug delivery systems. *J. Am. Acad. Dermatol.* **22,** 811–814 (1990).

118. Carmichael, A. J. Skin sensitivity and transdermal drug delivery. A review of the problem. *Drug Saf.* **10,** 151–159 (1994).

119. Murphy, M. & Carmichael, A. J. Transdermal drug delivery systems and skin sensitivity reactions, Incidence and managemen. *Am. J. Clin. Dermatol.* **1,** 361–368 (2000).

120. Banga, A. in *Transdermal Intradermal Deliv. Ther. Agents Appl. Phys. Technol.* 6–35 (CRC Press, 2011).

121. Wester, R. C. & Maibach, H. I. in *Percutaneous Absorpt. Mech. Deliv.* 215–237 (Marcel Dekker Inc., 1989).

122. Jacobi, U. *et al.* Porcine ear skin: an in vitro model for human skin. *Ski. Res. Technol.* **13,** 19–24 (2007).

123. Holbrook, K. A. & Odland, G. F. Regional differences in the thickness (cell layers) of the human stratum corneum an ultrastructural analysis. *J. Invest. Dermatol.* **62,** 415–422 (1974).

124. Herkenne, C., Naik, A., Kalia, Y. N., Hadgraft, J. & Guy, R. H. Ibuprofen transport into and through skin from topical formulations: in vitro-in vivo comparison. *J. Invest. Dermatol.* **127,** 135–42 (2007).

125. Patel, A. *et al.* Delivery of ibuprofen to the skin. *Int. J. Pharm.* **457,** 9–13 (2013).

126. Hadgraft, J. & Valenta, C. pH, pKa and dermal delivery. *Int. J. Pharm.* **200,** 243–247 (2000).

127. Bialik, W., Walters, K. A., Brain, K. R. & Hadgraft, J. Some factors affecting the in vitro penetration of IBU through human skin. *Int. J. Pharm.* **92,** 219–223 (1993).

128. Akhter, S. A. & Barry, B. W. Absorption through human skin of ibuprofen and flurbiprofen; effect of dose variation, deposited drug films, occlusion and the penetration enhancer N-methyl-2-pyrrolidone. *J. Pharm. Pharmacol.* **37,** 27–37 (1985).

129. Trovatti, E. *et al.* Bacterial cellulose membranes applied in topical and transdermal delivery of lidocaine hydrochloride and ibuprofen: in vitro diffusion studies. *Int. J. Pharm.* **435,** 83–7 (2012).

130. Herkenne, C., Naik, A., Kalia, Y., Hadgraft, J. & Guy, R. H. Effect of Propylene Glycol on Ibuprofen Absorption into Human Skin In Vivo. *J. Pharm. Sci.* **97,** 185–197 (2008).

131. Watkinson, A. C., Brain, K. R. & Walters, K. A. in *Predict. Percutaneous Penetration* 335–341 (STS Publishing, 1993).

132. Avdeef, A., Box, K. J., Comer, J. E. A., Hibbert, C. & Tam, K. Y. pH-Metric logP 10. Determination of liposomal membrane-water partition coefficients of ionizable drugs. *Pharm. Res.* **15,** 209–215 (1998).

133. Williams, A. C. & Barry, B. W. Penetration enhancers. *Adv. Drug Deliv. Rev.* **64,** 128–137 (2012).

134. Blank, I. H. Penetration of low molecular weight alcohols into skin. *J. Invest. Dermatol.* **43,** 415–421 (1964).

135. Charbonnier, V., Morrison, B. M., Paye, M. & Maibach, H. I. Subclinical, non-erythematous irritation with an open assay model (washing): sodium lauryl sulfate (SLS) versus sodium laureth sulfate (SLES). *Food Chem. Toxicol.* **39,** 279–286 (2001).

136. Scheuplein, R. J. & Ross, L. Effects of Surfactants and Solvents on the Permeability of Epidermis. *J. Cosmet. Sci.* **21,** 853–873 (1970).

137. Barry, B. W. in *Dermatological Formul. Percutaneous Absorpt.* 296–340 (Marcel Dekker Inc., 1983).

138. Walters, K. A. in *Transdermal drug Deliv. Dev. issues Res. Initiat.* (eds. Hadgraft, J. & Guy, R. H.) 197–246 (Marcel Dekker Inc., 1989).

139. Lademann, J., Jacobi, U., Surber, C., Weigmann, H.-J. & Fluhr, J. W. The tape stripping procedure-evaluation of some critical parameters. *Eur. J. Pharm. Biopharm.* **72,** 317–23 (2009).

140. Berner, B. *et al.* Ethanol: water mutually enhanced transdermal therapeutic system: II. Skin permeation of ethanol and nitroglycerin. *J. Pharm. Sci.* **78,** 402–407 (1989).

141. Megrab, N. A., Williams, A. C. & Barry, B. W. Oestradiol permeation across human skin, silastic and snake skin membranes: the effects of ethanol/water co-solvent systems. *Int. J. Pharm.* **116,** 101–112 (1995).

142. Pershing, L. K., Lambert, L. D. & Knutson, K. Mechanism of ethanol-enhanced estradiol permeation across human skin in vivo. *Pharm. Res.* **7,** 170–175 (1990).

143. Meshali, M., Abdel-Aleem, H., Sakr, F., Nazzal, S. & El-Malah, Y. Effect of gel composition and phonophoresis on the transdermal delivery of ibuprofen: in vitro and in vivo evaluation. *Pharm. Dev. Technol.* **16,** 93–101 (2011).

144. Tupker, R. A., Pinnagoda, J. & Nater, J. P. The transient and cumulative effect of sodium lauryl sulphate on the epidermal barrier assessed by transepidermal water loss: inter-individual variation. *Acta Derm. Venereol.* **70,** 1–5 (1990).

145. Mathur, A. K., Agarwal, C., Singh, A. & Gupta, B. N. Effect of sodium lauryl sulphate and nickel alone and in combination on the skin of guinea pigs. *Toxicol. Lett.* **42,** 249–256 (1988).

146. Denda, M. Epidermal proliferative response induced by sodium dodecyl sulphate varies with environmental humidity. *Br. J. Dermatol.* **145,** 252–257 (2001).

147. Ghosh, S. & Blankschtein, D. The role of sodium dodecyl sulfate (SDS) micelles in inducing skin barrier perturbation in the presence of glycerol. *J. Cosmet. Sci.* **58,** 109–133 (2007).

148. Moore, P. N. & Puvvada, S. Challenging the surfactant monomer skin penetration model: Penetration of sodium dodecyl sulfate micelles into the epidermis. *J. Cosmet. Sci.* **54,** 29–46 (2003).

149. Chen, H. *et al.* Microemulsion-based hydrogel formulation of ibuprofen for topical delivery. *Int. J. Pharm.* **315,** 52–8 (2006).

150. Hadgraft, J., Whitefield, M. & Rosher, P. H. Skin penetration of Topical Formulations of Ibuprofen 5 %: An in vitro Comparative study. *Skin Pharmacol. Appl. Skin Physiol.* **16,** 137–142 (2003).

151. Rasool, B. K. A., Abu-gharbieh, E. F., Sahar, A., Saad, H. S. & Khan, S. A. Development and Evaluation of Ibuprofen Transdermal Gel Formulations. *Trop. J. Pharm. Res.* **9,** 355–363 (2010).

152. Stahl, J., Wohlert, M. & Kietzmann, M. The effect of formulation vehicles on the in vitro percutaneous permeation of ibuprofen. *BMC Pharmacol.* **11,** 1–5 (2011).

153. Tas, Ç., Özkan, Y., Savaser, A. & Baykara, T. In vitro release studies of chlorpheniramine maleate from gels prepared by different cellulose derivatives. *Farm.* **58,** 605–611 (2003).

154. Bruno, L., Kasapis, S. & Heng, P. W. S. Effect of polymer molecular weight on the structural properties of non aqueous ethyl cellulose gels intended for topical drug delivery. *Carbohydr. Polym.* **88,** 382–388 (2012).

155. Welin-Berger, K., Neelissen, J. a. . & Bergenståhl, B. The effect of rheological behaviour of a topical anaesthetic formulation on the release and permeation rates of the active compound. *Eur. J. Pharm. Sci.* **13,** 309–318 (2001).

156. Florence, A. & Attwood, D. in *Physicochem. Princ. Pharm.* 281–330 (Pharmaceutical Press, 2011).

157. Zhu, L., Kumar, V. & Banker, G. S. Examination of Aqueous Oxidized Cellulose Dispersions as a Potential Drug Carrier . I . Preparation and Characterization of Oxidized Cellulose- Phenylpropanolamine Complexes. **5,** 1–7 (2004).

158. Pines, E. & Cunningham, T. J. Synthetic absorbable hemostat. Patent, EP0109197 A2 (1984).

159. Dol'berg, E. B., Yasnitskii, B., Shuteeva, L. N. & Kovalev, I. P. Reaction of oxidized cellulose with medicinal compounds. II. Reaction of oxidized cellulose with isonicotinic acid hydrazide. *Zh Prikl Khim* **46,** 21–23 (1973).

160. Kaputskii, F. N., Bychkovskii, P. ., Yurkshtovich, T. L. & Nedorezov, V. L. Study of photrin sorption by monocarboxycellulose. *Colloid J.* **57,** (1995).

161. Wu, Y. S., Frijlink, H. W., Vliet, van L. J. & Voort Maarschalk, van der K. Pore shape in the sodium chloride matrix of tablets after the addition of starch as a second component. *Eur. J. Pharm. Biopharm.* **70,** 539–543 (2008).

162. Thümmler, K. *et al.* Preparation and characterization of cellulose microspheres. *Cellulose* **18,** 135–142 (2011).

163. Volkert, B., Wolf, B., Fischer, S., Li, N. & Chenhua, L. Application of modified beadcellulose as a carrier of active ingredients. *Macromol. Symp.* **280,** 130–135 (2009).

164. Wolf, B., Schmitz, W. & Schneider, H. Composites of bead cellulose andhydrophilic solubilizers. *Int. J. Pharm.* **139,** 87–94 (1996).

165. Buschle-Diller, G., Fanter, C. & Loth, F. Effect of cellulose on the pore structureof bead cellulose. *Cellulose* **2,** 179–203. (1995).

166. Ek, R., Lennholm, H., Davidson, R., Nyström, C. & Ragnarsson, G. Pore swellingin beads made of cellulose fibres and fibre fragments. *Int. J. Pharm.* **122,** 49–56 (1995).

167. Sescousse, R., Gavillon, R. & Budtova, T. Wet and dry highly porous cellulosebeads from cellulose–NaOH–water solutions: influence of the preparation con-ditions on beads shape and encapsulation of inorganic particles. *J. Mater. Sci.* **46,** 759–765 (2011).

168. Yildir, E. *et al.* Tailored beads made of dissolved cellulose--investigation of their drug release properties. *Int. J. Pharm.* **456,** 417–23 (2013).

169. Trygg, J., Yildir, E., Kolakovic, R., Sandler, N. & Fardim, P. Anionic cellulose beads for drug encapsulation and release. *Cellulose* **21,** 1945–1955 (2014).

170. Galgut, P. N. Oxidized cellulose mesh. I. Biodegradable membrane in periodontal surgery. *Biomaterials* **11,** 561–564 (1990).

171. Nerurkar, J., Jun, H. W., Price, J. C. & Park, M. O. Controlled-release matrix tablets of ibuprofen using cellulose ethers and carrageenans: effect of formulation factors on dissolution rates. *Eur. J. Pharm. Biopharm.* **61,** 56–68 (2005).

172. Almeida, I. F. *et al.* Bacterial cellulose membranes as drug delivery systems: An in vivo skin compatibility study. *Eur. J. Pharm. Biopharm.* **86,** 332–336 (2014).

173. Mohamad, N., Mohd Amin, M. C. I., Pandey, M., Ahmad, N. & Rajab, N. F. Bacterial cellulose/acrylic acid hydrogel synthesized via electron beam irradiation: accelerated burn wound healing in an animal model. *Carbohydr. Polym.* **114,** 312–20 (2014).

174. Shimotoyodome, A., Suzuki, J., Kumamoto, Y., Hase, T. & Isogai, A. Regulation of postprandial blood metabolic variables by TEMPO-oxidized cellulose nanofibers. *Biomacromolecules* **12,** 3812–8 (2011).

175. Jin, B. & Wu, W. Compositions for veterinary and medical applications. Patent, EP1663225 A4 (2009).

176. Linsky, C. B. & Cunningham, T. J. Bioresorbable fabric of oxidized regenerated cellulose, postoperative adhesion barrier. Patent, US5007916 A (1991).

177. Wiczer, S. Alcohol fuel gel. Patent, US2613142 A (1952).

178. Yiv, S. & Zana, R. Effect of Alcohol on the Properties of Micellar Systems. *J. Colloid Interface Sci.* **80,** 224–236 (1981).

179. Reekmans, S. *et al.* Influence of alcohols and alkanes on the aggregation behavior of ionic surfactants in water. *Langmuir* **6,** 628–637 (1990).

180. Zdziennicka, A. & Jańczuk, B. Behavior of Anionic Surfactants and Short Chain Alcohols Mixtures in the Monolayer at the Water–Air Interface. *J. Surfactants Deterg.* **14,** 257–267 (2011).

181. Zana, R. Aqueous surfactant-alcohol systems: A review. *Adv. Colloid Interface Sci.* **57,** 1–64 (1995).

182. Patist, A., Axelberd, T. & Shah, D. Effect of Long Chain Alcohols on Micellar Relaxation Time and Foaming Properties of Sodium Dodecyl Sulfate Solutions. *J. Colloid Interface Sci.* **208,** 259–265 (1998).

183. Rubio, D. A. R., Zanette, D., Nome, F., Catarina, S. & Bunton, C. A. Effect of 1 -Butanol on Micellization of Sodium Dodecyl Sulfate and on Fluorescence Quenching by Bromide Ion. *Langmuir* **10,** 1151–1154 (1994).

184. Zhou, M. & Rhue, R. Effect of Interfacial Alcohol Concentrations on Oil Solubilization by Sodium Dodecyl Sulfate Micelles. *J. Colloid Interface Sci.* **228,** 18–23 (2000).

185. Sansanwal, P. K. Effect of co-solutes on the physico-chemical properties of surfactant solutions. **65,** 57–64 (2006).

186. Larsen, J. W. & Tepley, L. B. Effect of aqueous alcoholic solvents on counterion-binding to CTAB micelles. *J. Colloid Interface Sci.* **49,** 113–118 (1974).

187. Rao, I. & Ruckenstein, E. Micellization behavior in the presence of alcohols. *J. Colloid Interface Sci.* **113,** (1986).

188. Reekmans, S., Luo, H., Van Der Auweraer, M. & De Schryver, F. Influence of Alcohols and Alkanes on the Aggregation Behavior of Ionic Surfactants in Water. *Langmuir* **7,** 628–631 (1990).

189. Lianos, P. & Zana, R. Surfactant-alcohol mixed-micelle formation. Cetyltrimethylammnonium bromide-1-butanol system. *Chem. Phys. Lett.* **72,** 171–175 (1979).

190. Romani, A. P., Gehlen, M. H. & Quina, F. H. The Change in the Properties of Sodium Dodecyl Sulfate Micelles upon Addition of Isomeric and Unsaturated Short-Chain Alcohols Probed by Photophysical Methods. *J. Colloid Interface Sci.* **240,** 335–339 (2001).

191. Ganguly, R., Aswal, V. K., Hassan, P. A., Gopalakrishnan, I. K. & Yakhmi, J. V. Sodium chloride and ethanol induced sphere to rod transition of triblock copolymer micelles. *J. Phys. Chem. B* **109,** 5653–5658 (2005).

192. Griffiths, P. C. *et al.* Effect of ethanol on the interaction between poly(vinylpyrrolidone) and sodium dodecyl sulfate. *Langmuir* **20,** 6904–6913 (2004).

193. Førland, G. *et al.* Influence of Alcohol on the Behavior of Sodium Dodecylsulfate Micelles. *J. Colloid Interface Sci.* **203,** 328–34 (1998).

194. Kline, S. Reduction and analysis of SANS and USANS data using IGOR Pro. *J. Appl. Crystallogr.* **39,** 895–900 (2006).

195. Feigin, L. A. & Svergun, D. I. *Principles of the Theory of X-ray and Neutron Scattering in Principles of the Theory of X-ray and Neutron Scattering in Structure Analysis by Small-Angle X-Ray and Neutron Scattering*. (1987).

196. Nallet, F., Laversanne, R. & Roux, D. Modelling X-ray or neutron scattering spectra of lyotropic lamellar phases : interplay between form and structure factors. *J. Phys. II* **3,** 487–502 (1993).

197. Heenan, R. K., Penfold, J. & King, S. M. SANS at Pulsed Neutron Sources: Present and Future Prospects. *J. Appl. Crystallogr.* **30,** 1140–1147 (1997).

198. Svergun, D. I., Koch, H. J., Timmins, P. A. & May, R. *Basics of small angle scattering in Small Angle X-Ray and Neutron Scattering from Solutions of Biological Macromolecules*. (Oxford University Press, 2013).

199. Svergun, D. I. & Koch, H. J. Small-angle scattering studies of biological macromolecules in solution. *Reports Prog. Phys.* **66,** 1735–1782 (2003).

200. Sivia, D. S. *The basics of X-ray and neutron scattering in Elementary Scattering Theory for X-ray and Neutron Users*. (Oxford University Press, 2011).

201. Munter, A. Scattering Length Density Calculator. *Date accessed 08.01.2015* at <http://www.ncnr.nist.gov/resources/sldcalc.html>

202. Munter, A. Neutron scattering lengths and cross sections. *Date accessed 18.11.2014* at <http://www.ncnr.nist.gov/resources/n-lengths/>

203. Hammouda, B. Probing nanoscale structures- the SANS toolbox. *Date accessed 08.12.2014* at <http://www.ncnr.nist.gov/staff/hammouda/the_sans_toolbox.pdf>

204. Schnablegger, H. & Singh, Y. *A practical guide to SAXS*. (Anton Paar, 2006).

205. Shibayama, M. Small-angle neutron scattering on polymer gels: phase behaviour, inhomogeneities and deformation mechanisms. *Polym. J.* **43,** 18–34 (2011).

206. Squires, G. L. *Nuclear scattering by crystals in Introduction to the theory of thermal neutron scattering*. (Cambridge University Press, 1978).

207. Borsali, R. & Pecora, R. *Small angle neutron scattering on gels in Soft Matter Characterization*. (Springer, 2008).

208. Higgins, J. & Benoit, H. *Polymers and Neutron Scattering*. (Clarendon Press, 1994).

209. Pynn, R. Neutron Scattering- A Primer. *Los Alamos Neutron Sci. Cent.* Date accessed 01.11.2014 (1990). at <http://fas.org/sgp/othergov/doe/lanl/pubs/number19.htm>

210. Hammouda, B. A tutorial on small-angle neutron scattering from polymers. *Date accessed 08.11.2014* (1995). at <http://www.ncnr.nist.gov/programs/sans/pdf/polymer_tut.pdf>

211. Grillo, I. *Small-Angle Neutron Scattering and Applications in Soft Condensed Matter*. (Springer, 2008).

212. DANSE, Small Angle Neutron Scattering Project. *Univ. Tennessee* Date accessed on 12.10.14 at <http://danse.chem.utk.edu/>

213. Guinier, A. & Fournet, G. *Small angle scattering of X-rays*. (John Wiley & Sons, Ltd., 1955).

214. Brockel, U., Meier, W. & Wagner, G. *Product Design and Engineering*. (Wiley-VCH, 2013).

215. Goodwin, J. W. & Hughes, R. W. *Rheology for Chemists: An introduction*. (Royal Society of Chemistry, 2008).

216. Larsen, R. Oscillatory Rheology. *G.I.T. aboratory J. Eur.* **11,** 68–70 (2007).

217. Leng, Y. *Materials characterization - Introduction to Microscopic and Spectroscopic Methods*. *Introd. to Microsc. Spectrosc. Methods* **17,** (John Wiley & Sons, Ltd., 2008).

218. Egerton, R. F. *The Scanning Electron Microscope*. *Phys. Princ. Electron Microsc. Introd. to TEM, SEM, AEM* (Springer, 2005).

219. Anslyn, E. & Dougherty, D. in *Mod. Phys. Org. Chem.* 140–148 (University Science Books, 2006).

220. Lu, A., Song, Y. & Boluk, Y. Electrolyte effect on gelation behavior of oppositely charged nanocrystalline cellulose and polyelectrolyte. *Carbohydr. Polym.* **114,** 57–64 (2014).

221. Agoda-Tandjawa, G., Durand, S., Gaillard, C., Garnier, C. & Doublier, J.-L. Rheological behaviour and microstructure of microfibrillated cellulose suspensions/low-methoxyl pectin mixed systems: Effect of calcium ions. *Carbohydr. Polym.* **87,** 1045–1057 (2012).

222. Pugnaloni, L. a. On the relationship between rheology and percolation in the gelation of weakly attractive colloids: Beyond 'snapshot' percolation. 4 (2004). at <http://arxiv.org/abs/cond-mat/0406713>

223. Borwankar, R. P. & Case, S. E. Rheology of emulsions, foams and gels. *Curr. Opin. Colloid Interface Sci.* **2,** 584–589 (1997).

224. Morris, K. L. *et al.* Chemically programmed self-sorting of gelator networks. *Nat. Commun.* **4,** 1480–86 (2013).

225. Agoub, A. & Morris, E. Particulate rheology and acid-induced gelation of oxidised cellulose. *Carbohydr. Polym.* **71,** 416–427 (2008).

226. Pinho, S. & Eugenia, M. Solubility of NaCl , NaBr , and KCl in Water , Methanol , Ethanol , and Their Mixed Solvent. *J. Chem. Eng. Data* **50,** 29–32 (2005).

227. Dubey, N. A Conductometric Study of Interaction between Sodium Dodecyl Sulfate and 1-Propanol , 1-Butanol , 1-Pentanol and 1-Hexanol at Different Temperatures. *J. Surf. Sci. Technol.* **24,** 139–148 (2008).

228. Lianos, P. Surfactant-alcohol mixed micelle formation. Cetyltrimethylammonium Bromide- 1-Butanol System. *Chem. Phys. Lett.* **72,** (1980).

229. Alila, S., Boufi, S., Belgacem, M. N. & Beneventi, D. Adsorption of a cationic surfactant onto cellulosic fibers I. Surface charge effects. *Langmuir* **21,** 8106–13 (2005).

230. Leung, R. & Shah, D. Dynamic Properties of Micellar Solutions I . Effects of Short-Chain Alcohols and Polymers on Micellar Stability. *J. Colloid Interface Sci.* **113,** 484–499 (1986).

231. Corti, M. & Degiorgio, V. Quasi-Elastic Light Scattering Study of Intermicellar Interactions in Aqueous Sodium Dodecyl Sulfate Solutions. *J. Phys. Chem.* **85,** 711–717 (1981).

232. Sammalkorpi, M., Karttunen, M. & Haataja, M. Ionic surfactant aggregates in saline solutions: sodium dodecyl sulfate (SDS) in the presence of excess

sodium chloride (NaCl) or calcium chloride (CaCl(2)). *J. Phys. Chem. B* **113,** 5863–70 (2009).

233. Araki, J. Electrostatic or steric? – preparations and characterizations of well-dispersed systems containing rod-like nanowhiskers of crystalline polysaccharides. *Soft Matter* **9,** 4125 (2013).

234. Comas-Rojas, H. *et al.* Interaction and film formation in polyethylenimine-cetyltrimethylammonium bromide aqueous mixtures at low surfactant concentration. *2Soft Matter* **3,** 747–753 (2007).

235. Swift, J. Human hair cuticle: biologically conspired to the owners advantage. *J. Cosmet. Sci.* **50,** 23–47 (1999).

236. Maza, A., Baucells, J., Ensenat, P. & Parra, J. Sublytic Interactions of Octylphenol Surfactants with Liposomes Modeling the Stratum Corneum Lipid Composition. *J. Colloid Interface Sci.* **184,** 155–62 (1996).

237. Kontturi, E. *et al.* Amorphous characteristics of an ultrathin cellulose film. *Biomacromolecules* **12,** 770–777 (2011).

238. Wang, W. & Vaughn, M. W. Morphology and amine accessibility of (3-aminopropyl) triethoxysilane films on glass surfaces. *Scanning* **30,** 65–77 (2008).

239. Arnold, T. *et al.* Implementation of a beam deflection system for studies of liquid interfaces on beamline I07 at Diamond. *J. Synchrotron Radiat.* **19,** 408–416 (2012).

240. IAEA. Neutron Reflectometry, A Probe for Materials Surfaces. in *Proc. a Tech. Meet. Vienna* (2004).

241. Cubitt, R. & Fragneto, G. D17 : the new reflectometer at the ILL. *Appl. Phys. A* **331,** 329–331 (2002).

242. Dalgliesh, R. M., Langridge, S., Plomp, J., de Haan, V. O. & van Well, a. a. Offspec, the ISIS spin-echo reflectometer. *Phys. B Condens. Matter* **406,** 2346–2349 (2011).

243. Arnold, O. *et al.* Mantid—Data analysis and visualization package for neutron scattering and μ SR experiments. *Nucl. Instruments Methods Phys. Res. Sect. A Accel. Spectrometers, Detect. Assoc. Equip.* **764,** 156–166 (2014).

244. Russell, T. P. On the reflectivity of polymers: Neutrons and X-rays. *Phys. B Condens. Matter* **221,** 267–283 (1996).

245. Parratt, L. G. Surface Studies of Solids by Total Reflectin of X-Rays. *Phys. Rev.* **95,** (1954).

246. Wasbrough, M. J. Nanostructured hydrogel films for encapsulation and release . (2011).

247. Dai, Y. *et al.* A comparative study of Langmuir surfactant films: Grazing incidence x-ray off-specular scattering vs. x-ray specular reflectivity. *J. Appl. Phys.* **110,** 102213 (2011).

248. Salah, F., Harzallah, B. & van der Lee, a. Data reduction practice in X-ray reflectometry. *J. Appl. Crystallogr.* **40,** 813–819 (2007).

249. Gibaud, a., Vignaud, G. & Sinha, S. K. The correction of geometrical factors in the analysis of X-ray reflectivity. *Acta Crystallogr. Sect. A Found. Crystallogr.* **49,** 642–648 (1993).

250. Nelson, A. Co-refinement of multiple-contrast neutron/X-ray reflectivity data using MOTOFIT. *J. Appl. Crystallogr.* **39,** 273–276 (2006).

251. Wavemetrics Curve Fitting. *http://www.wavemetrics.com/products/igorpro/dataanalysis/curvefitting.htm* Accessed on 02.01.2013

252. Daniel, J. *et al.* in *At. Force Microsc. Process Eng. Introd. to AFM Improv. Process. Prod.* 3–22 (Elsevier, 2009).

253. Hansma, P. K. *et al.* Tapping mode atomic force microscopy in liquids. *Appl. Phys. Lett.* **64,** 1738 (1994).

254. Suri, C. R. & Mishra, G. C. Activating piezoelectric crystal surface by silanization for microgravimetric immunobiosensor application. *Biosens. Bioelectron.* **11,** 1199–205 (1996).

255. Wang, Y.-P., Lee, Y.-C., Hong, Y.-J. & Yew, T.-R. A novel method for soluble hydrophilic anthracene derivative self-assembled on APTES in air. *Org. Electron.* **null,** (2012).

256. Choi, S.-H. & Zhang Newby, B. Suppress polystyrene thin film dewetting by modifying substrate surface with aminopropyltriethoxysilane. *Surf. Sci.* **600,** 1391–1404 (2006).

257. Jafarzadeh, M., Ab Rahman, I. & Sipaut, C. S. Synthesis of silica–polypyrrole core–shell nanocomposite using in situ γ-aminopropyltriethoxysilane (APTES)-modified nanosilica. *Synth. Met.* **162,** 466–476 (2012).

258. Tan, G., Zhang, L., Ning, C., Liu, X. & Liao, J. Preparation and characterization of APTES films on modification titanium by SAMs. *Thin Solid Films* **519,** 4997–5001 (2011).

259. Kim, J., Seidler, P., Wan, L. S. & Fill, C. Formation, structure, and reactivity of amino-terminated organic films on silicon substrates. *J. Colloid Interface Sci.* **329,** 114–9 (2009).

260. Doong, R. *et al.* Effect of anionic and nonionic surfactants on sorption and micellar solubilization of monocyclic aromatic compounds. *Water Sci. Technol.* **34,** 327–334 (1996).

261. Vandenberg, E. T. *et al.* Structure of 3-Aminopropyl Triethoxy Silane on Silicon Oxide Preparation of APTES Surfaces. *J. Colloid Interface Sci.* **147,** (1991).

262. Penfold, J., Staples, E., Tucker, I. & Thomas, R. K. Adsorption of mixed anionic and nonionic surfactants at the hydrophilic silicon surface. *Langmuir* **18,** 5755–5760 (2002).

263. Penfold, J., Tucker, I., Staples, E. & Thomas, R. K. Manipulation of the adsorption of ionic surfactants onto hydrophilic silica using polyelectrolytes. *Langmuir* **20,** 7177–7182 (2004).

264. Torn, L. H., Koopal, L. K., de Keizer, A. & Lyklema, J. Adsorption of nonionic surfactants on cellulose surfaces: adsorbed amounts and kinetics. *Langmuir* **21,** 7768–75 (2005).

265. Singh, S. K. & Notley, S. M. Adsorption of Nonionic Surfactants (CnEm) at the Silica - Water and Cellulose - Water Interface. *J. Phys. Chem. B* **114,** 14977–14982 (2010).

266. Paria, S., Manohar, C. & Khilar, K. C. Adsorption of anionic and non-ionic surfactants on a cellulosic surface. *Colloids Surfaces A Physicochem. Eng. Asp.* **252,** 221–229 (2005).

267. Nicoli, S., Bunge, A. L., Delgado-Charro, M. B. & Guy, R. H. Dermatopharmacokinetics: Factors influencing drug clearance from the stratum corneum. *Pharm. Res.* **26,** 865–871 (2009).

268. Ghanbarzadeh, S., Khorrami, A. & Arami, S. Nonionic surfactant-based vesicular system for transdermal drug delivery. *Drug Deliv.* **7544,** 1–7 (2013).

269. Gaur, P. K., Bajpai, M., Mishra, S. & Verma, A. Development of ibuprofen nanoliposome for transdermal delivery : Physical characterization , in vitro / in vivo studies , and anti-inflammatory activity. *Artif. Cells, Nanomedicine, Biotechnol.* 1–6 (2014). doi:10.3109/21691401.2014.953631

270. Yong, C. S. *et al.* Improved solubility and in vitro dissolution of Ibuprofen from poloxamer gel using eutectic mixture with menthol. *Drug Deliv.* **10,** 179–183 (2003).

271. Wisniewski, S. J. & Gemborys, M. Method for percutaneous delivery of ibuprofen using hydroalcoholic gel. (1992).

272. Herkenne, C., Naik, A., Kalia, Y. N., Hadgraft, J. & Guy, R. H. Dermatopharmacokinetic prediction of topical drug bioavailability in vivo. *J. Invest. Dermatol.* **127,** 887–94 (2007).

273. Watkinson, R. M. *et al.* Influence of ethanol on the solubility, ionization and permeation characteristics of ibuprofen in silicone and human skin. *Skin Pharmacol. Physiol.* **22,** 15–21 (2009).

274. Gracin, S. & Rasmuson, C. Solubility of Phenylacetic Acid , p -Hydroxyphenylacetic Acid , p -Aminophenylacetic Acid , p -Hydroxybenzoic Acid , and Ibuprofen in Pure Solvents. 1379–1383 (2002).

275. Manrique, J. & Martínez, F. Solubility of Ibuprofen in Some Ethanol + Water Cosolvent Mixtures at Several Temperatures. **26,** 344–354 (2007).

276. Wang, S., Song, Z., Wang, J., Dong, Y. & Wu, M. Solubilities of Ibuprofen in Different Pure Solvents. 5283–5285 (2010).

277. Kumar, L. & Verma, R. In vitro evaluation of topical gel prepared using natural polymer. *Int. J. Drug Deliv.* **2,** 58–63 (2010).

278. Rhee, Y.-S., Chang, S.-Y., Park, C.-W., Chi, S.-C. & Park, E.-S. Optimization of ibuprofen gel formulations using experimental design technique for enhanced transdermal penetration. *Int. J. Pharm.* **364,** 14–20 (2008).

279. Lindhoud, S., Colver, P., Scott, J. L., Edler, K. J. & Kingdom, U. Gel formation of C6-partially oxidised cellulose fibrils and salts. 1–19

280. Mack Correa, M. C. *et al.* Molecular interactions of plant oil components with stratum corneum lipids correlate with clinical measures of skin barrier function. *Exp. Dermatol.* **23,** 39–44 (2014).

281. Anderson, R. L. & Cassidy, J. M. Variations in physical dimensions and chemical composition of human stratum corneum. *J. Invest. Dermatol.* **61,** 30–32 (1973).

282. Schwindt, D. a, Wilhelm, K. P. & Maibach, H. I. Water diffusion characteristics of human stratum corneum at different anatomical sites in vivo. *J. Invest. Dermatol.* **111,** 385–9 (1998).

283. Alberti, I., Kalia, Y. N., Naik, a, Bonny, J. & Guy, R. H. Effect of ethanol and isopropyl myristate on the availability of topical terbinafine in human stratum corneum, in vivo. *Int. J. Pharm.* **219,** 11–9 (2001).

284. Russell, L. M., Wiedersberg, S. & Delgado-Charro, M. B. The determination of stratum corneum thickness: an alternative approach. *Eur. J. Pharm. Biopharm.* **69,** 861–70 (2008).

285. Kalia, Y. N. *et al.* Normalization of Stratum Corneum Barrier Function and Transepidermal Water Loss In Vivo. *Pharm. Res.* **17,** 1148–1150 (2000).

286. McMaster, M. *HPLC: A Practical User's Guide*. *HPLC A Pract. User's Guid.* (Wiley-VCH, 2006). at <http://onlinelibrary.wiley.com.ezp1.bath.ac.uk/book/10.1002/0470079096>

287. Ahuja, S. & Rasmussen, H. *HPLC Method Development for Pharmaceuticals*. (Elsevier, 2007).

288. Biox Aquaflux Technical Information. at <http://www.biox.biz/Technical/CondenserMethod.php>

289. Alberti, I., Kalia, Y., Naik, A. & Guy, R. H. Assessment and prediction of the cutaneous bioavailability of topical terbinafine, in vivo, in man. *Pharm. Res.* **18,** 1472–1475 (2001).

290. Shah, V., Flynn, G., Yacobi, A., Maibach, H. & Bon, C. et al. Bioequivalence of topical dermatological dosage forms- methods of evaluation of bioequivalence. *Pharm. Res.* **15,** 167–171 (1998).

291. Kalia, Y. N., Pirot, F. & Guy, R. H. Homogeneous Transport in a Heterogeneous Membrane : Water Diffusion Across Human Stratum Corneum In Vivo. *Biophys. J.* **71,** 2692–2700 (1996).

292. Franz, T. J. Percutaneous absorption on the relevance of in vitro data. *J. Invest. Dermatol.* **64,** 190–195 (1975).

293. Silva, N. H. C. S. *et al.* Bacterial cellulose membranes as transdermal delivery systems for diclofenac: in vitro dissolution and permeation studies. *Carbohydr. Polym.* **106,** 264–9 (2014).

294. Shahzad, Y., Khan, Q., Hussain, T. & Shah, S. N. H. Influence of cellulose derivative and ethylene glycol on optimization of lornoxicam transdermal formulation. *Int. J. Biol. Macromol.* **61,** 26–32 (2013).

295. Bartosova, L. & Bajgar, J. Transdermal Drug Delivery. 4671–4677 (2012).

296. Dias, M. *et al.* Topical delivery of caffeine from some commercial formulations. *Int. J. Pharm.* **182,** 41–47 (1999).

297. Ng, S.-F., Rouse, J. J., Sanderson, F. D. & Eccleston, G. M. The relevance of polymeric synthetic membranes in topical formulation assessment and drug diffusion study. *Arch. Pharm. Res.* **35,** 579–93 (2012).

298. Ng, S.-F., Rouse, J., Sanderson, D. & Eccleston, G. A Comparative Study of Transmembrane Diffusion and Permeation of Ibuprofen across Synthetic Membranes Using Franz Diffusion Cells. *Pharmaceutics* **2,** 209–223 (2010).

299. Todo, H., Oshizaka, T., Kadhum, W. R. & Sugibayashi, K. Mathematical model to predict skin concentration after topical application of drugs. *Pharmaceutics* **5,** 634–51 (2013).

300. Irwin, W. J., Sanderson, F. D. & Li Wan Po, a. Percutaneous absorption of ibuprofen and naproxen: Effect of amide enhancers on transport through rat skin. *Int. J. Pharm.* **66,** 243–252 (1990).

301. Servier Medical Art Image Bank (with permission). *Date accessed 14.12.2014* at <http://www.servier.com/Powerpoint-image-bank>

302. Glatter, O. & Kratky, O. in *Small angle X-ray Scatt.* 3–53 (Academic Press,Inc., 1982).

303. LOQ Instrument Web Page. Date accessed 03.02.2015 at <http://www.isis.stfc.ac.uk/instruments/loq/loq2470.html>

304. Riviere, J. C. in *Handb. Surf. Interface Anal. Methods Probl.* 210–240 (CRC Press, 2009).

305. Imae, T., Kanaya, T., Furusaka, M. & Torikai, N. in *Neutrons Soft Matter* 115–147 (John Wiley & Sons, Ltd., 2011).